UNIVERSITY OF CANTERBURY

MASTER'S THESIS

Executive Function and CADASIL in MRI Brain Scans

Author:
Rebecca Meng-Jou LEE

Supervisors:
Dr Steven MARSH
Dr Tracy MELZER
Dr Campbell LE HERON

A thesis submitted in fulfillment of the requirements for the degree of Master of Science

in

Medical Physics
School of Physical and Chemical Sciences

April 29, 2020

UNIVERSITY OF CANTERBURY

Abstract

Master of Science in Medical Physics

Executive Function and CADASIL in MRI Brain Scans

by Rebecca Meng-Jou LEE

Cerebral autosomal dominant arteriopathy with subcortical infarcts and leukoencephalopathy (CADASIL) is a hereditary and debilitating small vessel disease. One of the main features of CADASIL is progressive executive dysfunction, specifically problems in working memory, that ultimately leads to dementia. Due to the early-onset nature of the disease (symptomatic around 45 years old), CADASIL is often seen as a 'pure' model for small vessel diseases.

In this thesis, I investigated working memory in CADASIL using a novel behavioral task that dissociated components of the working memory process. I also used structural and perfusion magnetic resonance imaging (MRI) to examine any differences associated with CADASIL. Finally, I investigated whether changes in the imaging metrics can predict working memory performance in CADASIL, both globally and within specific regions of interest, selected a priori.

Nineteen CADASIL patients with nineteen healthy controls matched for age and sex ratio participated in this study. They completed a battery of neuropsychological assessments, including the novel behavioral task designed specifically to measure spatial working memory. The participants also completed an MRI brain scanning session on a 3T machine that included T1 structural imaging to measure grey matter volume and arterial spin labelling (ASL) perfusion imaging to quantify cerebral blood flow.

From the behavioral task, I found significant decreases in spatial working memory in the CADASIL group, but their spatial binding ability appeared intact. The MR imaging modalities were analyzed using a general linear model for comparisons between the healthy controls and the CADASIL patients. Relative to the healthy controls, CADASIL patients showed significant grey matter atrophy in the medial and lateral frontal, and temporal regions, as well as extensive hypoperfusion encompassing the frontal, pre-frontal, anterior-occipital, parietal, and temporal lobes. Regions of grey matter atrophy and hypoperfusion included the dorsolateral prefrontal cortex, believed to be highly involved in spatial working memory, which suggested an association between brain integrity and behavioral metrics. Results presented in this thesis suggest a tight relationship between brain integrity and spatial working memory in the context of CADASIL. Furthermore, brain changes observed in CADASIL may help explain the observed deficits in one aspect of executive function - spatial working memory. These findings may contribute to a more complete understanding of executive function in CADASIL and may also help inform common features present in other small vessel diseases.

Acknowledgements

My profound gratitude first goes to Dr Tracy Melzer, Dr Campbell Le Heron, and Dr Steven Marsh for being such amazing supervisors, sharing this journey with my sparkly notebook and me. Their continuous motivation, and their infinite wisdom and patience are awe-inspiring.

I would also like to thank my friends and colleagues at the New Zealand Brain Research Institute (NZBRI) for providing great laughs and advice, and for creating a friendly and enjoyable environment to work in every day.

To my friends at home back in Auckland, thank you for your continuous support an island away, and keeping me in the loop through memes, snaps, and weekly calls. To friends in Christchurch, thank you for helping me settle into a new city so quickly. Special thanks go to Ethan, Amber, Dylan, and Nick for the weekly DnDnD nights, even when Nissa and Blendaeth keeps accidentally nearly killing the party.

Finally, I would like to thank my family for their unconditional love, support, and encouragement. Without the knowledge of having mum (Lily) and dad (Albert) behind me, I would not have had the confidence and courage to do this.

Contents

List of Figures

List of Tables

List of Abbreviations

ACC	**A**nterior **C**ingulate **C**ortex
ACE	**A**ddenbrooke's **C**ognitive **E**xamination
AIC	**A**kaike **I**nformation **C**riteria
ASL	**A**rterial **S**pin **L**abelling
BF	**B**lood **F**low
BV	**B**lood **V**olume
CADASIL	**C**erebral **A**utosomal **D**ominant **A**rteriopathy with **S**ubcortical **I**nfarcts and **L**eukoencephalopathy
CBF	**C**erebral **B**lood **F**low
CI	**C**onfidence **I**nterval
CSF	**C**erebro**s**pinal **F**luid
CT	**C**omputed **T**omography
DLPFC	**D**orsol**a**teral **Pre**f**r**ontal **C**ortex
DTI	**D**iffusion **T**ensor **I**maging
FLAIR	**F**luid-**A**ttenuated **I**nversion **R**ecovery
GLM	**G**eneral **L**inear **M**odel
GM	**G**rey **M**atter
GOM	**G**ranular **O**smiophilic **M**aterial
HC	**H**ealthy **C**ontrols
ICV	**I**ntracranial **V**olume
MCC	**M**id**c**ingulate **C**ortex
MMSE	**M**ini-**M**ental **S**tate **E**xamination
MNI	**M**ontreal **N**eurological **I**nstitute
MoCA	**Mo**ntreal **C**ognitive **A**ssessment
MRI	**M**agnetic **R**esonance **I**maging
PCA	**C**ADASIL **Pa**tients
PCC	**P**osterior **C**ingulate **C**ortex
PET	**P**ositron **E**mission **T**omography
ROI	**R**egions **o**f **I**nterest
SPECT	**S**ingle **P**hoton **E**mission **C**omputed **T**omography
SVD	**S**mall **V**essel **D**isease
TFCE	**T**hreshold-**F**ree **C**luster **E**nhancement
TIA	**T**ransient **I**schemic **A**ttack
VBM	**V**oxel **B**ased **M**orphometry
VEPCASL	**V**essel **E**ncoding **P**seudo-**C**ontinuous **A**rterial **S**pin **L**abelling
WMH	**W**hite **M**atter **H**yperintensity

Chapter 1

Introduction

1.1 Introduction

Cerebral Autosomal Dominant Arteriopathy with Subcortical Infarcts and Leukoencephalopathy (CADASIL) is a unique non-amyloid small vessel disease (SVD) and is considered to be the most common form of hereditary vascular dementia and cause of stroke (Mascalchi et al., 2017). Chromosome 19p13 carries the NOTCH3 gene, which is mutated in CADASIL patients, and thus results in the degeneration of vascular smooth muscle cells and production of granular osmiophilic material (GOM). This is one of the main pathological hallmarks of CADASIL as the GOM is deposited within the arteries and in the brain's basal membrane (Schoemaker et al., 2019), as displayed in Figure 1.1.

FIG. 1.1. Punch skin biopsy demonstrating granular osmiophilic material (GOM) deposits on, and embedded in, the membranous infoldings of vascular smooth muscle cells (curved arrows). Some GOM are scattered in the extracellular interstitial tissue of the small cutaneous arteriolar wall (straight arrows). A capillary with endothelial cells and erythrocytes is seen in the left upper corner (ultrathin section, x16750). Image and caption retrieved from Filley et al. (1999).

In CADASIL, the NOTCH3 gene located on chromosome 19 (shown in Figure 1.2) usually undergoes missense mutations, thus adding or deleting a cysteine amino acid, and resulting in an odd number of cysteines. This mutation is often encoded in the earlier exons of the gene, especially in exon 4, which leads to deposition of GOM and damage to epidermal growth factor (EGF) receptors, preventing cell to cell communication (Chavoshi Tarzjani et al., 2018). This in turn presents as smooth muscle degeneration, ultimately resulting in vascular degeneration.

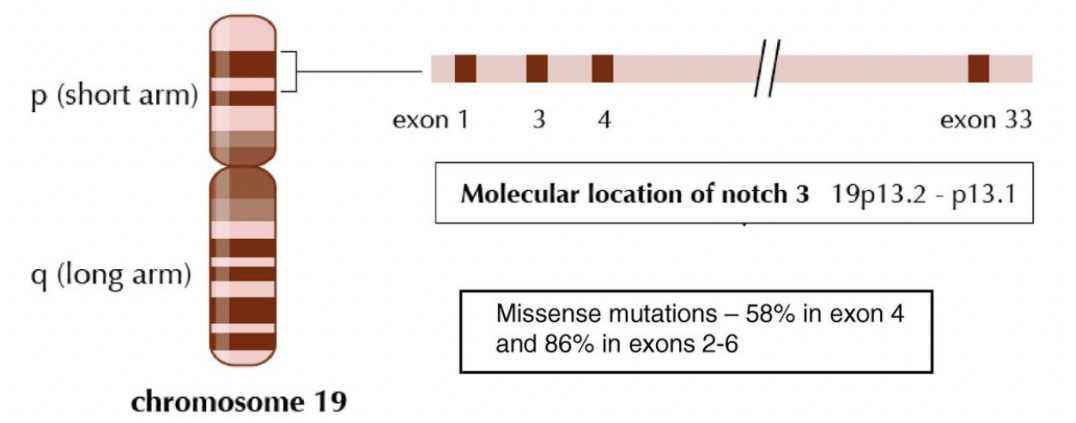

FIG. 1.2. CADASIL is a small vessel disease that results from many mutations in the NOTCH3 gene located on chromosome 19. This gene has 33 exons; the majority of mutations occur in exons 2-6 and are mostly missense mutations. Image and caption retrieved from Baird (2010).

The radiological hallmark of CADASIL is white matter hyperintensities (WMH) that can be clearly seen on T2-weighted MRI fluid-attenuated inversion recovery (FLAIR) imaging. This is thought to be a consequence of vascular smooth muscle cell degeneration, and can usually be seen in both symptomatic and asymptomatic gene carriers before the age of 35, thus allowing for early diagnosis in people who undergo MRI, as symptoms are often not noticed until around the age of 45 (Chabriat et al., 1995). Figure 1.3 displays an example of varying levels of WMHs seen with differing levels of disease.

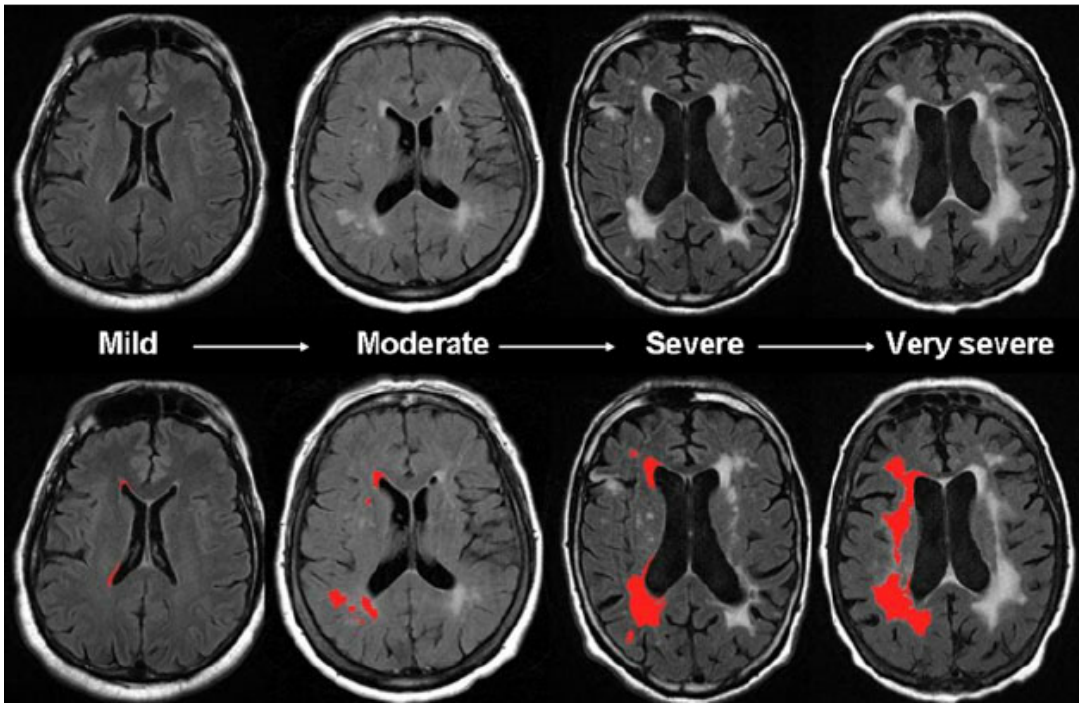

FIG. 1.3. Severity of MRI-detected white matter hyperintensities (WMH), where red indicates regions of WMH. Total burden of white matter disease varies significantly amongst symptomatic and asymptomatic CADASIL patients. Image and caption retrieved from Chutinet and Rost (2014).

Classical symptoms include migraine with aura, transient ischemic attacks (TIA), recurrent strokes, progressive cognitive impairment, and neuropsychiatric disorders such as irritability, depression and apathy (Chabriat et al., 1995). CADASIL also leads to premature mortality, with the average age at death between 65 and 70 years old, although disease severity and progression will, of course, vary between individual patients (Chabriat et al., 1995; Opherk et al., 2004).

The long-term prognosis for CADASIL is relatively poor, with many patients ultimately dying prematurely. Towards the later years of life, patients will often experience severe physical and mental dysfunction, with frank dementia eventuating in many cases. This means that they need constant care and attention, with no hope of improvement. The burden and emotional turmoil of the caregivers and family members is consequential and must not be overlooked. The premature deaths of the patients are mostly not from CADASIL itself, but from complications which arise with the disease. Leading causes include pneumonia, pulmonary embolism (PE), and asphyxia. Pulmonary embolism is a fairly common complication as most patients will have become completely immobile before death (Opherk et al., 2004).

Importantly, because CADASIL has an earlier age of onset than most other neurodegenerative and small vessel diseases, comorbid conditions from age-related pathologies are rarer. Therefore, CADASIL can be used as a "pure" model of the vastly more common sporadic SVD, which often co-occurs with, for example, Alzheimer's disease (Di Donato et al., 2017; Dichgans, 2009; Jouvent et al., 2007), allowing investigation of the effects of small vessel diseases independent from co-existent pathologies.

However, there has been little research on how changes in cognition relate to the radiological changes observed in patients with CADASIL. Therefore this thesis hopes to study the disease from a combined cognition and imaging perspective - specifically with volumetric and perfusion magnetic resonance imaging (MRI) - and establish a link between cognitive impairments associated with CADASIL, and the radiological changes that are so prominent in this condition.

1.2 Magnetic Resonance Imaging in CADASIL

Magnetic resonance imaging (MRI) of the brain is a non-invasive imaging modality that uses strong magnets, radiofrequency waves, and tunable parameters, to generate images of the body's organs. It is commonly used for diagnosing and evaluating CADASIL patients, and for tracking the progression of the disease thereafter (Stojanov et al., 2015). Various MRI protocols are used to better understand different aspects of the disease and its effect on the patients as all the individuals have slightly differing clinical presentations.

1.2.1 T2-Weighted FLAIR Imaging

By 35 years old, all NOTCH3 mutation carriers are expected to have detectable abnormalities via MRI. The most obvious imaging hallmark is the presence of white matter hyperintensities (WMHs) shown through T2-weighted FLAIR imaging. Fluid attenuation inversion recovery (FLAIR) is an MRI technique used to null signal from cerebrospinal fluid (CSF). This is similar to T2-weighted images, which normally presents bright grey matter and dim white matter, however, unlike T2-weighted, the CSF in FLAIR is normally dark instead of bright. This is due to a longer inversion time (TI) that nulls the CSF signal. Therefore WMH, especially in the anterior temporal lobe, is a primary MRI marker for CADASIL as it is consistently found in all symptomatic and asymptomatic patients with CADASIL (Chutinet and Rost, 2014; De Guio et al., 2015; Duchesnay et al., 2018; Stojanov et al., 2015).

WMHs are commonly found in the general aging population as well, but are especially found with abundance in individuals with vascular risk factors (e.g. hypertension), and forms of dementia (Chutinet and Rost, 2014; Dadar et al., 2019). For CADASIL patients, WMHs are more frequently found in the periventricular areas of the brain (Dadar et al., 2019; Schoemaker et al., 2019). Additionally CADASIL patients consistently show the presence of WMH in the anterior temporal lobe, which can be a useful clinical sign (Schoemaker et al., 2019; Van Den Boom et al., 2003).

WMHs are a diagnostic and prognostic biomarker of cerebrovascular diseases, such as CADASIL, and are generally interpreted as a measure of vascular pathology. They are a marker of many potential SVD causes, such as metabolic abnormalities - e.g. chronic hypoperfusion and blood brain barrier alterations (Chutinet and Rost, 2014; Dadar et al., 2019; McAleese et al., 2016; Bohnen and Albin, 2011). As a result, this makes the study of CADASIL immensely valuable as it allows us to study how WMHs affect cognitive function of people, in a younger cohort, relatively free from the large confounding effects of age. It has been reported that white matter lesions are associated with cognitive impairment. Such burden can be assessed by the size

and quantity of lesions in various neuroanatomical locations (Bohnen and Albin, 2011). Individuals with increased WMHs also have a greater risk of stroke, vascular cognitive impairment, and ultimately dementia (Chutinet and Rost, 2014).

WMHs in CADASIL

Several studies have documented that patients with CADASIL have a significantly higher volume of WMHs than cognitively normal individuals. As WMHs are known to adversely impact cognitive function of individuals with CADASIL, those with higher WMH volumes also show a significantly higher risk of cognitive decline and conversion to dementia (Dadar et al., 2019; Dichgans, 2009; Tosto et al., 2014; Yoshita, Fletcher, and DeCarli, 2005). In particular, cognitive decline was reportedly isolated to independent domains: memory, conceptualization, visuospatial skills, and executive dysfunction (Chutinet and Rost, 2014). It was also found that age was positively associated with the increased volume and effect of WMHs on executive dysfunction, suggesting greater cognitive defects with increased age, but education was negatively associated, suggesting that those with more years of education were less prone to cognitive defects (Dadar et al., 2019). Stojanov et al. (2015) reported that WMH lesions in CADASIL tend to be symmetrical and bilateral, with particular preference for regions around the anterior temporal lobe.

Greater clinical severity of CADASIL is associated with brain atrophy and an increasing number of lacunar infarcts. Thus patients with higher loads of lacunar lesions may have lower brain and WM volumes, with reduced capacity to develop extensive WMH (De Guio et al., 2015). Therefore, particularly when considering cognitive decline, other imaging markers may be more closely associated with progressive underlying pathology. More advanced neuroimaging techniques, such as diffusion tensor imaging (DTI), are required to address this issue, and can even further facilitate looking at the microstructural integrity of WMHs, and how it acts to affect the brain (Schoemaker et al., 2019).

1.2.2 Diffusion Tensor Imaging

Diffusion tensor imaging (DTI) is a sensitive MRI technique which can be used to infer microstructural tissue integrity. As an advanced MR imaging technique, DTI can be used for tractography mapping - a 3D modelling to visualize specific white matter tracts - and for providing further information on the microstructural integrity of white matter (Basser et al., 2000; Molko et al., 2001; Schoemaker et al., 2019; Stojanov et al., 2015). The NOTCH3 gene mutation can lead to demyelination and ultimately to neurodegeneration, with accompanying changes in DTI metrics (Chabriat et al., 1999; Stojanov et al., 2015). These imaging findings have been corroborated by microscopic examinations establishing demyelination, axonal loss, and gliosis in the WM of the brain in CADASIL patients (Chabriat et al., 1999; Mascalchi et al., 2017; Mori and Zhang, 2006).

Studies have shown that a patient's cognitive scores are closely related to DTI metrics in both the white matter and subcortical grey matter that appears 'normal' on T2 FLAIR images (Chabriat et al., 1999; Dichgans, 2009; Molko et al., 2001). This

presents the idea that the extent of microstructural tissue damage is clinically relevant as it further contributes to cognitive decline.

Mean diffusivity (MD) and fractional anisotropy (FA) are DTI metrics which are used to infer the health of, and damage to, white matter (Alexander et al., 2007). DTI has consistently shown increased MD and decreased FA in patients with CADASIL, most likely due to the aforementioned demyelination (Chabriat et al., 1999; Jouvent et al., 2007; Mascalchi et al., 2017). Regions of decreased FA were shown in another study to correlate with the extensive T2 hyperintensity, as well as the severity of the microstructural damage (Mascalchi et al., 2017). Whole-brain analyses employing tract based spatial statistics (TBSS) have been used to map the voxel-wise distribution of the microstructural changes revealed by DTI in the WM of the brain (Mascalchi et al., 2017).

Studies using regions of interest (ROI) analyses and histogram measurements of diffusion indices have demonstrated progressively widespread microstructural tissue damage caused by CADASIL, in particular the microstructural integrity of the basal nuclei and the thalamus (Mascalchi et al., 2017; Schoemaker et al., 2019). DTI may be able to be used to monitor the disease progression amongst patients (Chabriat et al., 1999).

1.2.3 Volumetric MRI

T1-weighted structural MRI of the brain is a non-invasive MR technique used to identify and measure volumetric and structural brain information, such as the grey matter volume changes associated with a pathological process or clinical syndrome, and atrophy.

One of the main uses for volumetric analysis of the brain is to identify patterns of atrophy associated with a particular disease process. In CADASIL, structural MRI has specifically identified atrophy in the medial temporal lobe as a classical biomarker, and this may serve as a measure of disease severity (Anstey and Maller, 2003; Bottino et al., 2002; Opherk et al., 2006; Shen et al., 2011). An example of atrophy on a T1-weighted image is presented in Figure 1.4.

Grey matter atrophy rate in CADASIL patients are found to be three times higher than a normally aging brain, thus suggesting that the CADASIL patients are predisposed to cognitive impairments (Jouvent et al., 2007; Peters et al., 2006). Studies have found decreased grey matter volume in CADASIL patients in both cortical and subcortical areas. This includes the parietal, occipital, and temporal lobes, as well as in the middle temporal gyrus, and in the caudate nucleus (Lambert et al., 2015; Su et al., 2019).

Volumetric MRI is one of the imaging modalities used in this study in an effort to relate grey matter atrophy to changes in cognition caused by CADASIL.

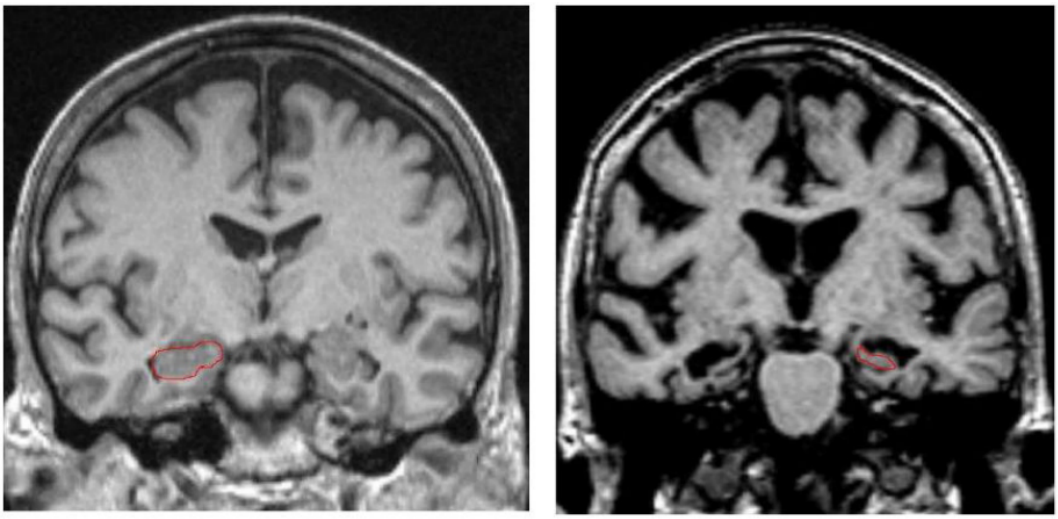

FIG. 1.4. Hippocampal atrophy of an Alzheimer's disease patient. On the left, the hippocampus outlined in red shows no atrophy in both hemispheres. On the right, the hippocampus presents with severe atrophy in both hemispheres. Image and caption retrieved from Shen et al. (2011).

1.2.4 Perfusion MRI

Perfusion MRI is used to image fluids that pass through the patients' blood vessels. Typical metrics include blood volume (BV), blood flow (BF), mean transit time (MTT), and the time to peak (TTP) (Calamante, 2013). Perfusion MRI is split into three main types of techniques: dynamic susceptibility contrast (DSC), dynamic contrast-enhancing imaging (DCE), and arterial spin labelling (ASL) (Calamante, 2013; Sourbron and Buckley, 2013). DSC and DCE are similar in that they both require a Gadolinium (Gd) contrast agent to be injected into the patient (Sourbron and Buckley, 2013). Most other methods of measuring perfusion also require exogenous contrast agents, such as PET, SPECT, and CT. Using contrast-enhancing MRI, Gavazzi et al. (2019) reported decreased vasoreactivity seen in their CADASIL group compared to healthy controls in an almost symmetrical manner in the anterior cingulate cortex (ACC), the insula, the thalamus, and the lower brain stem (dorsal pontomedullary junction). They also reported no regions of hyperperfusion in the CADASIL group compared to their healthy controls.

Furthermore, both Su et al. (2019) and Tatsch et al. (2003) used cerebral glucose metabolism (CMR_{Glc}) measured by ^{18}F-fluorodeoxyglucose positron emission tomography (^{18}F-FDG PET) as a measure of metabolism, which is known to be highly correlated to perfusion (Cha et al., 2013; Tuominen et al., 2004). Su et al. (2019) and Tatsch et al. (2003) report extensive hypometabolism in cortical and subcortical grey matter regions, such as the thalamus, hippocampus, caudate, and putamen, suggesting severely reduced perfusion.

ASL is a non-invasive technique that does not rely on an exogenous contrast agent or radiation (Grade et al., 2015; Moreton et al., 2015). Instead it uses magnetically labelled blood as an endogenous tracer, which allows for repeated scans and high

reproducibility. This makes ASL a desirable method for determining brain perfusion (Alsop et al., 2015). However despite this, and the potential drawbacks of other modalities listed above, very little work has examined perfusion deficits in CADASIL patients using ASL MRI.

A study by Moreton et al. (2018) investigated vasoreactivity in CADASIL patients using hypercapnia and functional ASL. Hypercapnia is used to look at non-neuronal vasodilation, which was believed to be disrupted in CADASIL. They showed a correlation between perfusion, and the number of lacunae and brain atrophy caused by CADASIL, suggesting impaired cerebral vasoreactivity - the ability for vessels to react (contract or expand) in order to maintain cerebral blood flow (CBF) and blood pressure. A pattern of greater disability, depression, and impaired processing speed with worsening cerebral vasoreactivity was also observed, which are oftentimes later symptoms of CADASIL patients.

Perfusion MRI is the second imaging modality used in this thesis.

1.2.5 Functional MRI

So far, all techniques previously discussed have been varying forms of structural and perfusion MRI. These are different to functional MRI (fMRI) - a technique that infers changes in brain metabolism via alterations in blood flow and blood oxygenation levels, which change as brain cells expend energy (Glover, 2011; Logothetis et al., 2001). fMRI has been increasingly popular for research aiming to establish the functions of different regions of the cortex, as it is non-invasive and does not expose patients to ionizing radiation (Huettel, Song, and McCarty, 2008). The primary form of fMRI used by neuroscientists is the blood oxygen level dependent (BOLD) contrast that maps the hemodynamic response (Logothetis et al., 2001).

Given that the primary pathology in CADASIL is a small vessel disease, it is likely that vasoreactivity in these patients will be abnormal. Furthermore, the accumulation of damage associated with this may lead to impaired cognitive functions, mood and personality changes, and, in the long term, ultimately result in dementia (Gavazzi et al., 2019; Moreton et al., 2018). A recent study has examined some of these issues, using functional MRI and a behavioural task (Go/No go task) - a standard measure of executive function (see section 1.3.1) - in which CADASIL patients were reported to have a decreased BOLD effect in regions involved in executive functioning, including the anterior cingulate cortex (ACC), the insula, the thalamus, the dorsal pontomedullary junction, and the left cerebellar hemisphere. The authors believed that this reflected an altered hemodynamic response likely secondary to underlying neuronal dysfunction, presumably related to the characteristic small vessel changes previously mentioned. However, there are limitations to this, such as the use of medications which can suppress neural activity, and therefore go undetected on fMRI (Gavazzi et al., 2019).

1.3 Neurocognition

Cognitive decline occurs commonly in CADASIL, where dementia (meaning cognition has declined to the point a person can no longer function independently) is commonly diagnosed towards the end stage of the disorder. Oftentimes, cognitive decline for CADASIL patients includes alterations in executive functions and working memory, processes classically thought to rely on frontal-subcortical connections.

In our society, sporadic cerebral small vessel disease is the most common cause of vascular cognitive impairment (Duering et al., 2011). Various cognitive tests can be used to assist in the diagnosis of a patient's mental state, such as the Addenbrooke's Cognitive Examination (ACE), the Mini-Mental State Examination (MMSE), and the Montreal Cognitive Assessment (MoCA). However, although important, all of these are relatively non-specific assessments, and are best viewed as screening tools rather than tapping into specific underlying cognitive processes. One limitation of the MMSE in particular is minimal focus on executive functions, a group of inter-related cognitive functions that are often impaired in people with SVD, including CADASIL.

Of the three aforementioned cognitive tests, MoCA provides a more complete cognitive screening tool than the MMSE as it includes some executive function testing. This covers broader cognitive functions and is therefore a more thorough and desirable evaluation (Nasreddine et al., 2005; Smith, Gildeh, and Holmes, 2007).

1.3.1 Executive Functions

Small vessel diseases are consistently reported to be associated with increasing the risk of cognitive impairment, in particular impaired executive functioning (executive dysfunction) and processing speed (Jiménez-Balado et al., 2019; Lohner et al., 2017). Executive functions are a set of neurological processes that are necessary for the cognitive control of behaviour. This includes inhibition and interference control, working memory, and cognitive flexibility. They make it possible to concentrate, think before acting, resist temptations, and mentally hold information to manipulate thoughts and ideas, such as facing novel challenges (Diamond, 2013). This study primarily focuses on the working memory aspect of executive functions, and its relationship with SVDs.

A key aspect of executive function, working memory, is the ability to perceptually hold information in mind and mentally work with it, e.g. relating previous memories/knowledge and using that information to solve a future problem; a quintessential example is performing long division in your head (Diamond, 2013). Imaging studies show working memory relies, in particular, on the dorsolateral prefrontal cortex whereas memory maintenance for a reasonable number of items only relies on the ventrolateral prefrontal cortex. This allows for irrelevant thoughts and stimuli to be disregarded, selectively focusing on information held in mind or on stimuli in the surrounding environment (Diamond, 2013). Therefore, reasoning and creativity would not be possible without working memory as they require the ability to disassemble and recombine ideas. Working memory declines with age for multiple potential reasons, making the older population more susceptible to interference and distraction, thus slowing their processing speed. One method to test for working

memory is by asking the subjects to reorder items verbally listed to them e.g. from smallest to largest (Diamond, 2013).

An aspect of working memory is the ability to bind components of a memory trace, e.g. the location and order of objects. Fallon, Zokaei, and Husain (2016) suggested that whilst spatial working memory is conventionally thought to be supported by the dorsolateral prefrontal cortex (DLPFC), the spatial binding support to working memory may rely more on medial temporal lobe regions, such as the hippocampus. Therefore, this thesis studied whether executive dysfunction in CADASIL affected the spatial working memory, the ability for spatial binding of information, or both. This is particularly important in CADASIL as small vessel diseases often tend to impair executive functions, thus contributing to clinical burden.

Executive function, as a whole, can be assessed using cognitive tests, such as those mentioned above. However, most of the tasks set for these tests do not address an individual's executive functions in a context-specific situation, but there are also behavioural examinations that allow for the testing of specific aspects of executive functions. It must also be noted that there is no set gold standard assessment, such as it is for all cognitive tests (Chan et al., 2008). Furthermore, executive function is heavily affected by the individual's age, hence making it harder to study for later-onset neurodegenerative diseases. However, with CADASIL being a SVD, it can be used as a "pure" study for other forms of subcortical ischemic vascular dementia (SIVD), where cognition may be impacted by multiple underlying pathologies (Dichgans, 2009; Peters et al., 2005). Studies have shown that CADASIL seems to preserve the individual's memory encoding process, even though the recall is affected, unlike in Alzheimer's where there is no evidence for the preservation of the encoding process. CADASIL patients also experience ideational apraxia. This is a neurological disorder wherein the individual loses their ability to conceptualize and execute complex motor actions, including planning and error monitoring impairments, and is especially seen amongst patients who have previously experienced strokes (Amberla et al., 2004; Peters et al., 2005).

1.4 Thesis Objectives

The work presented in this thesis focuses on the following three areas:

1. To investigate working memory in CADASIL using a novel behavioral task that dissociates components underlying the working memory process, i.e. spatial working memory and spatial binding of information. I hypothesised CADASIL patients would perform worse than the healthy controls in the behavioral task.

2. To investigate structural and perfusion differences associated with CADASIL using MR imaging. Again, my hypothesis was that CADASIL patients will have more grey matter atrophy and less grey matter perfusion, with frontal and subcortical dominance in these deficits.

3. To investigate whether these changes in the imaging metrics predict the working memory performance in CADASIL, both globally and within specific regions of interest. I hypothesised that GM atrophy and perfusion would be associated with working memory performance in regions crucial for this normal process, including dorsolateral prefrontal cortex (DLPFC), but that dissociable behavioral components (working memory and spatial binding) would be associated with changes in different neural regions - specifically DLPFC and hippocampus, respectively.

Chapter 2

Methods

In this chapter I will describe the data acquisition, processing, and analysis methods used in the behavioral and MR studies whose results are presented in Chapters 3, 4, and 5.

2.1 Participants

Nineteen CADASIL subjects (PCAs) and nineteen healthy controls (HCs) were recruited for this study. The CADASIL subjects were recruited from two regional specialist centres in Cambridge and Oxford, UK. The age- and gender-matched healthy controls were recruited through a local database in Oxford, UK. Those with physical disabilities that prevented the patients from squeezing a hand-held dynamometer, or those who had large vessel strokes were excluded (Le Heron et al., 2018). Three out of the nineteen patients had a history of lacunar stroke but were included as this is an intrinsic feature of CADASIL and sporadic SVD (Chabriat et al., 2009; Pantoni, 2010).

Nineteen participants and nineteen controls completed the behavioral experiments and MRI scanning. However, three of the nineteen patients were excluded from MRI scanning: one patient was not scanned due to severe claustrophobia, another was excluded due to significant movement artefacts on MRI rendering the image uninterpretable, and the third patient developed a cortical stroke during the one-month period between the behavioral test and imaging (Le Heron et al., 2018). This resulted in a final imaging cohort of 16 CADASIL participants and 16 healthy controls.

2.2 Diagnostic Criteria and Cognitive Assessment

Cognitive levels were formally assessed using the Addenbrooke's Cognitive Examination (ACE III) (Hsieh et al., 2013). Further neuropsychological testing was conducted for executive function, attention, working memory and processing speed, memory, and visuospatial function (Le Heron et al., 2018). These included a digit span working memory task (Groth-Marnat, 2012), the Trail-Making Tasks parts A and B (Tombaugh, 2004), and a design fluency task (Tucha et al., 2012). Quality of life was determined using the Cantril ladder (Cantril, 1965) where participants rated

their overall quality of life on a visual scale ranging from 1 to 10 and the WHO-5 Well-Being Index (Topp et al., 2015). Demographics are presented in Table 2.1.

TABLE 2.1. Demographics

Measure	Control (HC) n = 19	CADASIL (PCA) n = 19	P-value
Age	54.5 (11.2) (range: 29 – 70)	54.3 (10.3) (range: 33 – 70)	N/A
Gender, female/male	12/7 (0.50)	13/6 (0.48)	N/A
Education (years)	17.5 (2.4)	15.6 (2.9)	**0.03**
ACE III, range 0 – 100	96.6 (2.4)	92.3 (5.3)	**0.003**
Digit span	12.8 (1.9)	6.05 (0.78)	**< 0.0001**
Trail-making part A	N/A	30.0 (15.7)	N/A
Trail-making part B	N/A	86.7 (54.3)	N/A
Trail-making part A & B	N/A	56.7 (41.4)	N/A
Design fluency	30.7 (6.6)	25.4 (9.3)	0.051
Quality of life: CANTRIL, range 0 – 10	8.1 (1.6)	6.6 (2.2)	**0.017**
ICV (cm^3)*	1467.1 (110.9)	1434.6 (136.9)	0.47
Mean GM CBF (ml/100g/min)*	36.3 (8)	25.5 (8.6)	**0.0009**
Median WMH Volume (cm^3) *^	115.3 [87.2 - 152.0]	123.4 [89.8 - 233.7]	0.073#

Values are mean (standard deviation), except for WMH volume, which is reported as median [range]. P-values are the results of a two-sample t-test for the difference in means between the CADASIL group and the healthy controls; bold values represent $p < 0.05$. ICV = Intracranial volume; CBF = Cerebral Blood Flow; WMH = White Matter Hyperintensity.
*Data for ICV and CBF from 16 HC and 16 PCA.
^Data for mean WMH volume in HC are inflated. BIANCA was maximized to identify WMHs in the PCA group. These same parameters were applied to the control group, but produced an overestimated WMH volume in the control group.
#Because WMHs are not normally distributed, I present a non-parametric Wilcoxon test.

2.2.1 Dalmatian Task

Each subject was administered the Dalmatian task to test their working memory and spatial misbinding, using a touch-screen computer. Participants were instructed to remember the spatial location and order of sequentially presented dots on the screen. Six conditions, corresponding to the number of dots presented (1, 2, 3 ..., 6) were used. Each dot was displayed for 1.5 seconds, with no gap between the dot disappearing and the appearance of the next dot. At the start of each trial, participants were informed how many dots would be in the forthcoming sequence. At the end of the sequence the screen went black, and participants then touched the screen at the remembered locations, in the order that they had been presented. 30 trials in total were administered, with order of conditions pseudo-randomised. Conditions were identical (i.e. same dot location) for all participants. Prior to starting the experiment, participants completed two practice trials, with verbal feedback about their performance.

Two primary metrics were recorded from the task: repaired error distance and error distance. Repaired error distance was the distance on the screen between where the participants clicked and the closest dot to that, irrespective of the chronological order the dots appeared in Figure 2.1. Error distance was defined as the distance on the screen between where the participants tapped and where the dot previously appeared, in chronological order for conditions > 1. Thus the repaired error distance measured participants' spatial working memory only (for location), whereas error distance measured each participants' spatial working memory and spatial binding ability of the dots (correct order of conditions 1-6) to their respective locations. As the difference between the two should give a measure of spatial binding ability, I also looked at the subtracted error distance, defined as the repaired error distance subtracted from the error distance (subtracted = error - repaired error).

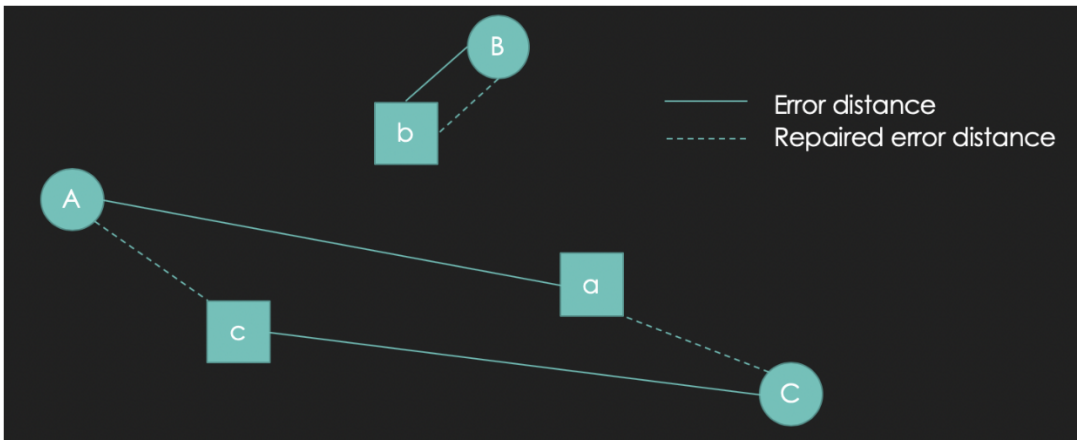

FIG. 2.1. Example of the Dalmatian task, measuring repaired error and error distances for condition = 3 dots. The capital letters an example of the positions from the task, the lower case letters an example of where a patient may have tapped the screen.

I created three values from each of the two outcome metrics - error and repaired error - from the Dalmatian task to link with MRI-derived brain measures: condition 6, mean, and mean difference. I chose to use just the condition 6 behavioral results

(with 6 dots) for each subject as it was the most difficult in the designed task, and should therefore be able to show the greatest difference between the subjects.

I also looked at the mean values to represent the average performance across all the 6 conditions. This was calculated as the average of the (repaired) error distances of all six conditions for each subject (Equation 2.1).

$$\text{mean} = (\Sigma\,(\text{conditions 1 to 6}))\ /\ 6 \qquad \textbf{Eq. 2.1.}$$

Finally, I also considered the mean difference model, which showed the within-subject performance, looking at how the conditions change. This was calculated from subtracting the mean of conditions 1-3 from the mean of conditions 4-6 (Eq. 2.2).

$$\text{mean difference} = \Sigma\,(\text{conditions 4 to 6}) - \Sigma\,(\text{conditions 1 to 3}) \qquad \textbf{Eq. 2.2.}$$

This resulted in six metrics: repaired error distance and error distance quantified by only during condition 6, the mean, and the mean difference.

2.2.2 BIANCA Mask

White matter hyperintensity on T2 FLAIR images can appear hypointense on T1-weighted MR images, similar to the signal intensity seen within GM; this can lead to mis-classification errors in which WMHs are classified as GM during the segmentation procedure. In order to correctly analyse grey matter properties for the purpose of this study, a white matter lesion template created from brain intensity abnormality classification algorithm (BIANCA) in FSL (Griffanti et al., 2016) was used to mask the white matter hyperintensities. BIANCA WMH masks were created previously by Dr Le Heron as part of an earlier study with these same participants (Le Heron et al., 2018). Using these BIANCA WMH masks, areas defined as WMH on the BIANCA masks were used to fill WMH areas on the T1-weighted image with a distribution of normal WM signal from surrounding, unaffected white matter, which was within a normal white matter intensity range. These T1-weighted images with the corrected white matter were then used in my study as 'input' images to undergo further image processing, described below. It is important to note that the lesion masks (understandably) did not 100% cover the white matter hyperintensities. This approach gave confidence that the GM segments were valid, however, it was at the cost of the WM segments being a random distribution of WM; due to this, WM segments were not analysed here. Figure 2.2 shows white matter hyperintensities in CADASIL patients (images A and C), compared to a healthy control (image D). Image B shows a BIANCA mask created for the same CADASIL patient as image A.

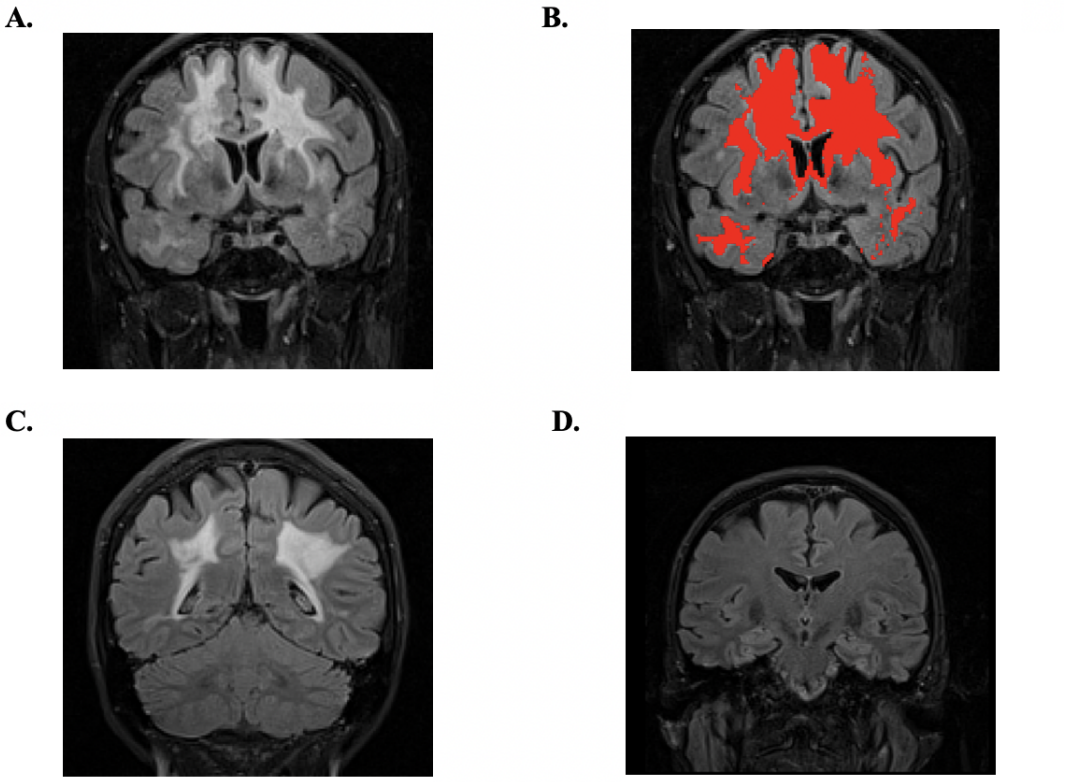

FIG. 2.2. (**A** and **C**) Coronal sections of T2 FLAIR MR images of two different CADASIL patients. The white matter hyperintensities are obvious and extensive. (**B**) Same patient image as **A**, but with a BIANCA mask applied, as indicated in red. (**D**) T2 FLAIR MR image of a healthy control subject with normal signal intensity in white matter areas, suggesting no white matter hyperintensities.

2.3 T1 Imaging Acquisition

The structural T1-weighted images (TE/TR = 1.94/2000 ms, TI = 880 ms, flip angle = 8 deg, acquisition matrix = 256×256×208, FOV = 256 mm, slice thickness = 1 mm) were acquired with a Magnetization Prepared Rapid Gradient Echo (MPRAGE) acquisition on a 3T Siemens Magnetom Verio syngo MR B17 scanner (Siemens Healthcare, Erlangen, Germany) using a 12-channel head coil between January 2015 and June 2017. The subjects were instructed to lie as still as possible (Le Heron et al., 2018).

2.4 T1 Imaging and Pre-Processing

The following describes the process I used during image processing, including a description of the iterations, errors, and remedies I encountered in producing high quality processed data for analysis.

2.4.1 Initial T1 Processing Steps

At the beginning of this thesis, I was provided with partially pre-processed T1 MRI images for all subjects, so I continued pre-processing from this point. However, I was unsure exactly what steps and parameters had been used, so ultimately decided to start from the beginning and process all images myself. I used FSL-VBM (version 1.1, Douaud et al. (2007), `https://fsl.fmrib.ox.ac.uk/fsl/fslwiki/FSLVBM`) to segment (into grey matter, white matter, and cerebral spinal fluid), and normalize the T1 images to MNI152 (Montreal Neurologic Institute) standard space . A crucial step in this process is accurate removal of non-brain tissue (i.e., skull and scalp). In the brain extraction (BET) stage, I used the '-N' option to account for the raw images including the subjects' necks, which needed to be excluded. Then I tried to create a GM template of my images and register them to the MNI152 standard space using non-linear registration (FNIRT). After observing the erroneous results of this step, I quickly learned that a non-linear warp required a linear affine registration as a starting point. I then took a step back and performed an affine registration to MNI space in all subjects, and visually inspected all results. When I went through each of my subjects' template results, many were not well registered, especially those of the CADASIL patients. Specifically, the CADASIL patients had greater regions of WMHs, which resulted in inappropriate segmentation and normalization. On T1-weighted images, signal from areas of extensive WMHs appear very similar to the signal seen in grey matter. In these cases, the segmentation algorithm may misclassify WMHs as GM. This was the case with this processing stream. I tried again, this time applying the affine registration first before the non-linear registration, but the results were still sub-optimal. These results suggested that I needed to consider the extensive WMHs prior to segmenting and normalizing the images.

For my second attempt, I started by using FSL (version 6.0.1, Smith et al. (2004)) to reorient the raw T1 images to match the orientation of the standard MNI152 template images, using 'fslreorient2std', followed by 'robustfov' to crop the neck and lower head from the images (Jenkinson et al., 2012). To separate the intensities of the GM from the WMH, I used a lesion filling tool (Battaglini, Jenkinson, and De Stefano, 2012). This utilized the BIANCA masks (Griffanti et al., 2016) to make lesion templates of where the WMHs were and replaced the signal of those areas with a distribution of signal from normal-appearing white matter. The resulting images were what was used in my study as the new 'input' images.

For my final attempt with FSL, I ran VBM again with the new raw images. However, I still observed quality issues in the final normalized (non-linear) GM segments. For example, some CADASIL subjects were missing parts of the cortex and had warped ventricles. As a final attempt to produce usable GM segments, I used an alternative approach: CAT12 (version 12.6, `http://www.neuro.uni-jena.de/cat/`), a toolbox of SPM12 (version 7487, `https://www.fil.ion.ucl.ac.uk/spm/software/spm12/`) (see below).

2.4.2 Final T1 Pre-Processing Steps Employed in this Thesis

Based on the pre-processing outlined above, the final pre-processing was as follows: In FSL (version 6.0.1, Smith et al. (2004)), raw T1-weighted images were reoriented to match the orientation of the standard template images (MNI152, using 'fslreorient2std'), cropped to remove the neck and lower head ('robustfov') (Battaglini, Jenkinson, and De Stefano, 2012; Jenkinson et al., 2012) and WMHs (as defined by BIANCA masks) were filled. I used CAT12 for all further processing steps.

Whole brain voxel-based morphometry (VBM) of the 'input' T1 imaging data was performed using the CAT12 toolbox (version 12.6, `http://www.neuro.uni-jena.de/cat/`) in SPM12 (version 7487, `https://www.fil.ion.ucl.ac.uk/spm/software/spm12/`). VBM provides an automated quantitative analysis of the distribution of white matter and grey matter by establishing voxel-for-voxel correspondence across subjects. VBM consists of four main steps: spatial normalization and registration, tissue segmentation, modulation and smoothing, and statistical analysis (Salmenpera and Duncan, 2005; Memarian et al., 2013; Martinkovic et al., 2014).

'Input' images were bias corrected, spatially normalized via DARTEL (using the MNI-registered template provided within CAT12), modulated to compensate for the effect of spatial normalization, and classified into grey matter (GM), white matter (WM), and cerebrospinal fluid (CSF), all within the same generative model. As only grey matter segments could be analysed (WMHs had been filled with a distribution of normal-appearing white matter signal, and therefore did not reflect original values), I only smoothed the grey matter images with a Gaussian filter (FWHM = 8mm). All images were visually inspected at each stage of processing. The final step was to perform voxel-wise statistical comparisons of grey matter volume across the two groups, HC and PCA (Ashburner and Friston (2000), Good et al. (2001), Memarian et al. (2013), and Martinkovic et al. (2014); `http://www.neuro.uni-jena.de/cat/`). This is further explained in the 'Statistical Analysis' section below.

A grey matter (GM) mask was created from the segmented T1-weighted images in order to restrict analyses to GM and exclude any residual non-GM tissue inclusion. A mean image of each subjects' smoothed GM was created, and a threshold of 0.15 was applied to remove false positives. I then binarized the image to finalize the grey matter mask.

2.5 ASL Imaging Acquisition

Vessel encoding pseudo-continuous arterial spin labelling (VEPCASL) is a method of using magnetic resonance imaging (MRI) to map vascular territories and cerebral blood flow (CBF) in the brain. Unlike conventional ASL, VEPCASL has a more efficient signal-to-noise ratio (SNR) and provides vessel-selective information, so it can therefore estimate CBF with greater accuracy (Okell et al., 2013).

All scans were acquired in the same session as the T1 images. The ASL perfusion imaging protocol included a 1.4 s duration VEPCASL pulse train which cycled through eight different vessel-encodings: four left-right, and four anterior-posterior.

Two repetitions of these encodings were acquired for each of six nominal post-labelling delays (PLDs) (0.25, 0.5, 0.75, 1.0, 1.25, and 1.5 s) with a repetition time of 4.186 s, to give a total of 96 volumes in 6.5 minutes. Images were acquired with a 2D multi-slice echo-planar imaging readout (voxel size = $3.4\times3.4\times5$ mm, matrix size = 64×64, 6/8ths partial Fourier, echo time = 14 ms, 24 slices acquired in ascending order). It took 1085 ms to acquire all the slices, meaning the average effective PLDs across the brain were 0.79, 1.04, 1.29, 1.54, 1.79, and 2.04 s. Calibration scans were acquired with both head and body coils for signal reception to allow for correction of coil non-uniformity and quantification of absolute CBF, with an M0 repetition time of 10 s (Okell et al., 2019).

2.6 ASL Image Processing

In this study, I used Oxford ASL suite (OXASL version 0.1.6, `https://oxasl.readthedocs.io/en/latest/index.html`) to create quantified perfusion maps in all subjects. OXASL is a package for performing Bayesian analysis on multi-delay ASL data and is capable of tracking perfusion from each individual blood vessel in the brain.

Alongside the VEPCASL data and post-labelling delays provided, structural data (T1-weighted) and calibration data (M0) were also supplied. Structural data allowed for better brain extraction and presented the output in both native and structural space, whereas calibration data was necessary to enable quantification of the perfusion map. This is paramount in cross-subject comparisons. Calibration data is based around the M0 images, taking into account the different repetition time used to create the M0 image compared to the other images. I also corrected for partial volume, using the white and grey matter segmentations from the structural data to model their respective contributions separately. This was weighted accordingly with the tissue proportions in each voxel.

The quantified perfusion output was co-registered to the T1 images and normalized to MNI space using the deformation fields produced during the structural processing. These images were then smoothed with a Gaussian filter (FWHM = 10mm). All images were visually inspected at each stage of processing.

2.7 Statistical Analysis

2.7.1 Dalmatian Task

The repaired error distance and error distance data were analyzed using repeated measures ANOVA to test for a difference between the healthy controls (HC) and the CADASIL patients (PCA) in regard to the respective conditions (1-6 dots), and the rate of increased error distance across those conditions, in addition to any interaction between group and condition. Significance was set at a p-value of < 0.05.

2.7.2 Whole-brain MRI Analyses

Whole brain data (both T1 and ASL) were analyzed using randomise (Winkler et al., 2014) to carry out non-parametric, voxel-wise cross-subject statistics using 10000 permutations, and threshold-free cluster enhancement (TFCE) to correct for multiple comparisons across the space (TFCE-corrected $p<0.05$).

Structural Images

The smoothed, modulated, normalized GM segments were analyzed thrice using randomize.

Model 1: I tested for group differences in GM volume between the HC and PCA groups, with age, sex, and intracranial volume (ICV) as covariates.

Model 2: I used multiple regression to test for any association between repaired error distance and GM volume, with age, sex, ICV, and group as covariates (note, an additional model with an interaction between group and GM volume was also fit).

Model 3: This model was the same as Model 2, only here I investigated the relationship between error distance and GM volume.

Perfusion Images

All ASL perfusion analyses were restricted to grey matter using the mask produced in structural processing. I applied the same analysis strategy as with the whole-brain structural analysis. Smoothed, normalized perfusion images were analyzed using randomise.

Model 1: I tested for a group differences in GM perfusion between the HC and PCA groups, with age and sex as covariates. An additional model also included voxel-wise GM volume as an additional covariate. Specifically, I tested whether HC>PCA and PCA>HC.

Model 2: I used multiple regression to test for any association between repaired error distance and GM perfusion, with age, sex, and group as covariates (note, an additional model with an interaction between group and GM perfusion was also fit). An additional model also included voxel-wise GM volume as an additional covariate.

Model 3: This model was the same as Model 2, only here I investigated the relationship between error distance and GM perfusion.

2.7.3 Region of Interest Analysis

Finally, I performed a region of interest (ROI) analysis comparing the perfusion of healthy controls and CADASIL patients in predetermined regions. The ROIs include the hippocampus, amygdala, orbitofrontal cortex (OFC), anterior cingulate cortex (ACC), midcingulate cortex (MCC), posterior cingulate cortex (PCC), caudate, putamen, thalamus, and the dorsolateral prefrontal cortex (DLPFC - comprised of superior, middle, and inferior frontal gyri). These regions were defined anatomically using the Harvard/Oxford cortical and subcortical GM atlases (available with FSL). Mean GM volume and perfusion were extracted from these ROIs, selected a priori. ROI analyses were performed in R using 'ANCOVA' (version 3.6.1, `https://www.r-project.org/`).

For each of the MR metrics (GM volume and GM perfusion), two models were explored.

Model 1: I investigated the relationship between the behavioral metric (repaired error distance or error distance) and MR metric (GM volume or GM perfusion) across all subjects (Eq. 2.3).

$$\text{Behavioral metric} \sim \text{Age} + \text{Sex} + \text{MR metric} \qquad \textbf{Eq. 2.3.}$$

Model 2: I investigated whether the association between behaviour and MRI differed between the HC and PCA groups by including both group and group-by-MR metric interaction terms (Eq 2.4).

$$\text{Behavioral metric} \sim \text{Age} + \text{Sex} + \text{MR metric} * \text{Group} \qquad \textbf{Eq. 2.4.}$$

For both models, values of $p < 0.05$ were considered significant.

Chapter 3

Behavioral Results

This chapter presents the behavioral results gathered from administration of the Dalmatian task, designed to provide fine-grained measures of spatial working memory, and particularly to dissociate putative prefrontal cortex and hippocampal contributions to this function in CADASIL.

3.1 Repaired Error Distance

Repaired error distance is defined as the distance on the screen between where the participants clicked and the closest dot to that, irrespective of the chronological order the dots appeared in. Thus, repaired error distance measures a person's spatial working memory, without requiring additional temporal binding of the items (1st item was in x location, 2nd item was in y location etc.).

Both CADASIL patients (PCA) and healthy control (HC) groups showed a significant increase in repaired error distance as condition difficulty increased (more items to remember), and this was significantly different between the groups [$F(1) = 6.0$, $p = 0.02$]. Figure 3.1 also clearly shows that CADASIL subjects were no different from the healthy controls in the easy conditions (conditions 1-3), but as the conditions became harder (conditions 4-6), the CADASIL patients started doing worse than the controls, thus creating the significant group-by-condition interaction term [$F(5) = 2.6$, $p = 0.03$].

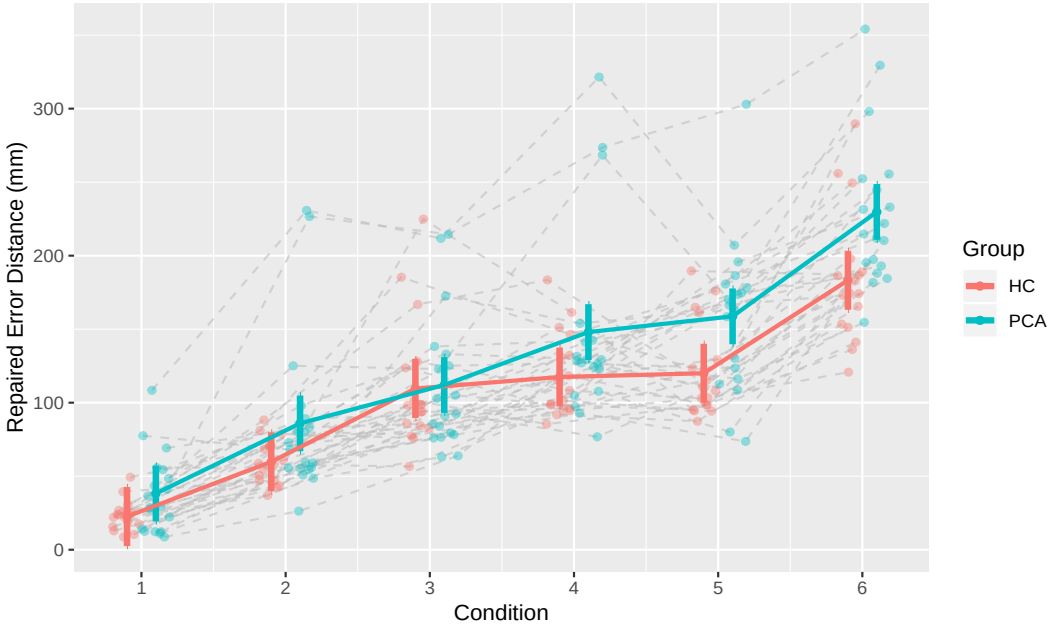

FIG. 3.1. Estimated mean repaired error distance with 95% CI, co-varying for age and sex. Repaired error distance progressively increased as the task became harder [F(5) = 153.5, p < 0.001], with significant differences between the two groups [F(1) = 6.0, p = 0.02]. A monotonic increase was seen as condition difficulty increased; repaired error distance also increased. Evidence showed this relationship was significantly different between the groups [F(5) = 2.6, p = 0.03]. The statistical values are from repeated measures ANOVAs.

As there was an interaction term between the groups and conditions, I used the Tukey test to present a post-hoc analysis to test for the first 3 conditions versus condition 4-6 (easy vs hard) by group (Fig 3.2).

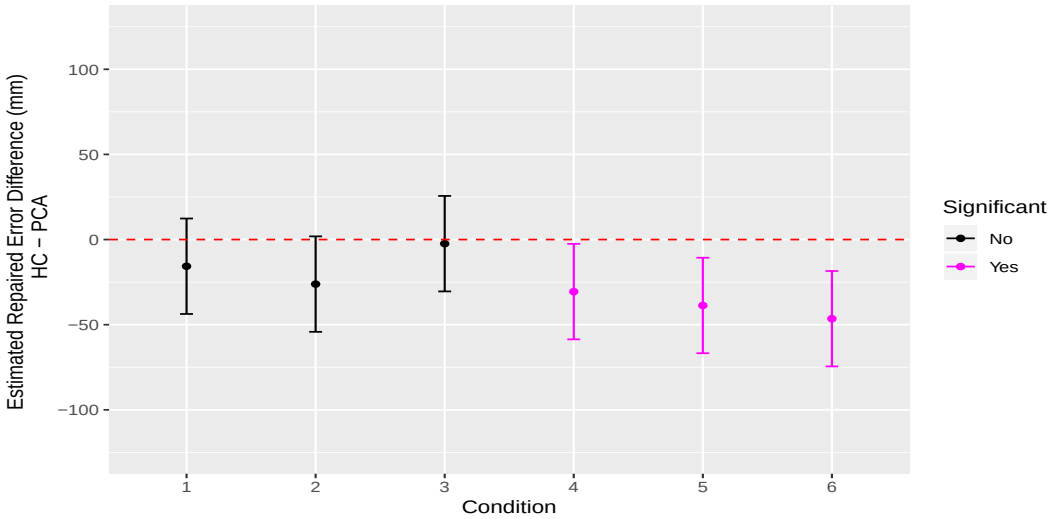

FIG. 3.2. Post-hoc Tukey test comparing repaired error difference estimates between the healthy control group (HC) and the CADASIL patients' group (PCA) across the 6 conditions. The uncertainty bars correspond to 95% confidence intervals. Mean estimates of repaired error distances were significantly different (p < 0.05) across conditions 4, 5, and 6 (pink).

3.2 Error Distance

Error distance is defined as the distance on the screen between where the participants clicked and where the dot previously appeared, in chronological order for conditions 2-6. It measures both the subjects' spatial working memory (for location) and spatial binding ability - two processes which may depend on dissociable neural regions (dorsolateral prefrontal cortex and hippocampus) (Fallon, Zokaei, and Husain, 2016).

Both PCA and HC groups showed a significant increase in error distance as the conditions increased in difficulty [$F(5) = 102.7$, $p < 0.001$] (Fig 3.3), but this was not significantly different between the groups [$F(1) = 2.6$, $p = 0.1$]. There were also no significant effects of group-by-condition interactions [$F(5) = 0.99$, $p = 0.4$]. Due to this, I did not carry out a post-hoc analysis for error distance.

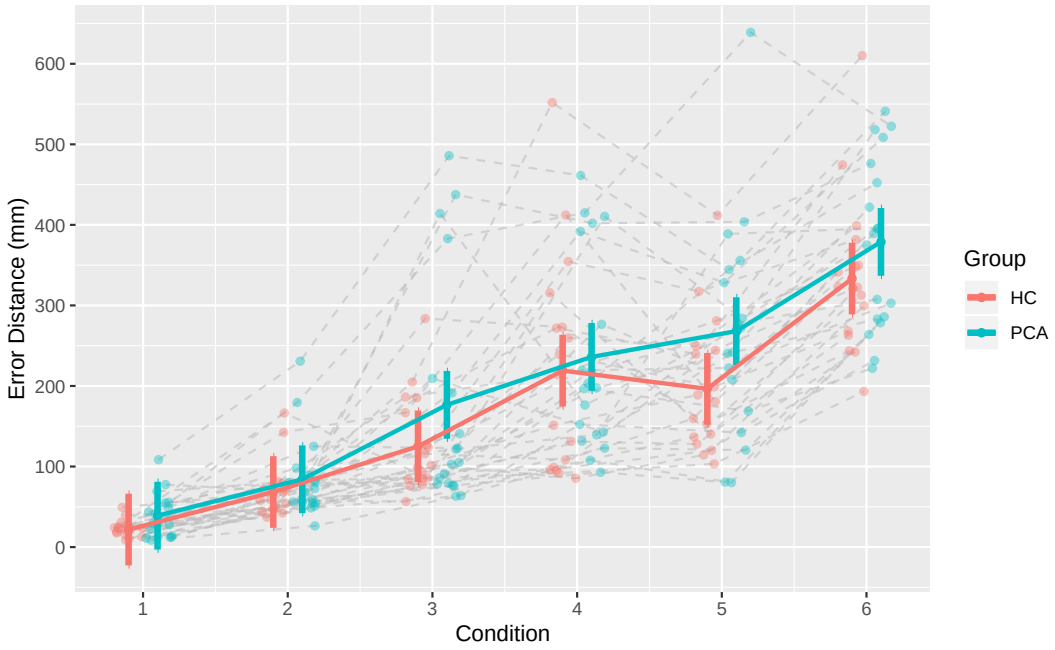

FIG. 3.3. Estimated mean error distance with 95% CI, co-varying for age and sex. Error distance progressively increased across the greater conditions [$F(5) = 102.7$, $p < 0.001$], but had insignificant group effect [$F(1) = 2.6$, $p = 0.1$]. A monotonic increase was seen as condition difficulty increased; error distance also increased. There was no evidence of interaction between the groups [$F(5) = 0.99$, $p = 0.4$]. The statistical values are from repeated measures ANOVAs.

3.3 Subtracted Error Distance

The subtracted error distance is defined as the repaired error distance subtracted from the error distance (subtracted = error – repaired error). Previous literature suggests that the error distance measures both working memory (prefrontal cortex) and spatial misbinding (hippocampus), and repaired error distance measures only the

working memory in the prefrontal cortex, so theoretically, the subtracted error distance should only account for the spatial misbinding in the hippocampus (Fallon, Zokaei, and Husain, 2016).

However, although both PCA and HC groups showed a significant increase in subtracted error distance as the conditions increased and became harder ($F(5) = 30.6$, $p < 0.001$), there was no significant difference between the two groups ($F(1) = 0.3$, $p = 0.6$), nor interaction between group and condition ($F(5) = 1.4$, $p = 0.2$) (Fig 3.4).

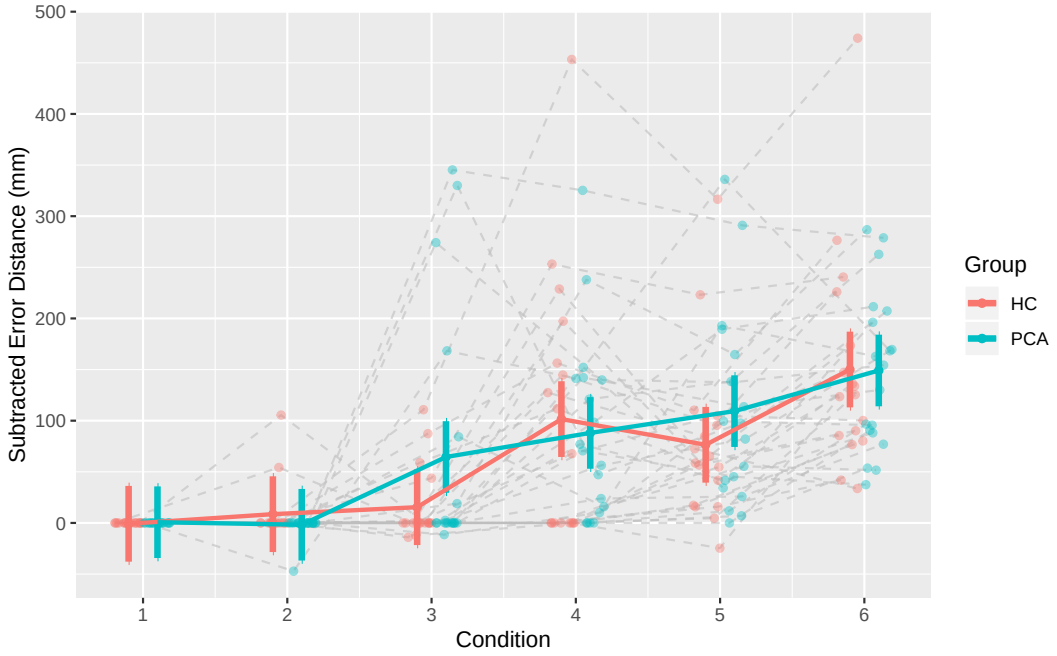

FIG. 3.4. The subtracted error distances were shown to progressively increase across the greater conditions ($F(5) = 30.6$, $p < 0.001$), but with no significant difference between the two groups ($F(1) = 0.3$, $p = 0.6$). A monotonic increase was seen as condition difficulty increased; the subtracted error distances also increased. There was no evidence of interaction between the groups ($F(5) = 1.4$, $p = 0.2$). The statistical values are from repeated measures ANOVAs.

3.4 Summary of Behavioral Results

The CADASIL group had significantly greater repaired error distances relative to the healthy controls, which suggests that CADASIL patients were comparatively more impaired on the Dalmatian task, mainly driven by poorer recollection of item locations. In contrast, the CADASIL group was not significantly worse than the healthy controls at binding item location to temporal order of presentation, a process putatively relying more on medial temporal lobe structures. This suggests that impairments in spatial working memory in CADASIL may be predominantly associated with dysfunction of the dorsolateral prefrontal cortex (DLPFC), a hypothesis I explore in the upcoming chapters. The subtracted error distance results suggest a lesser involvement of spatial binding, and as such, I will not continue to analyse subtracted error distance in the following chapters.

3.5 Behavioral Metrics Used for MR Analysis

In order to analyse any relationships and interactions the behavioral metrics (repaired error and error distances) may have with the MR metrics (GM volume and GM perfusion), I needed to reduce the 6 behavioral metrics each participant had from the 6 conditions in the Dalmatian task into a single behavioral metric.

There were three viable methods to create values from the Dalmatian task to link with the MRI-derived brain measures: condition 6, mean, and mean difference. A priori, I was unsure which would be better, so I investigated all three.

3.5.1 Condition 6

For each subject, condition 6 behavioral results (with 6 dots) was the most difficult in the Dalmatian task and should therefore show the greatest difference between the groups. Based on this, I chose to use condition 6 as my primary variable, for both repaired error distance (Fig 3.5) and error distance (Fig 3.6).

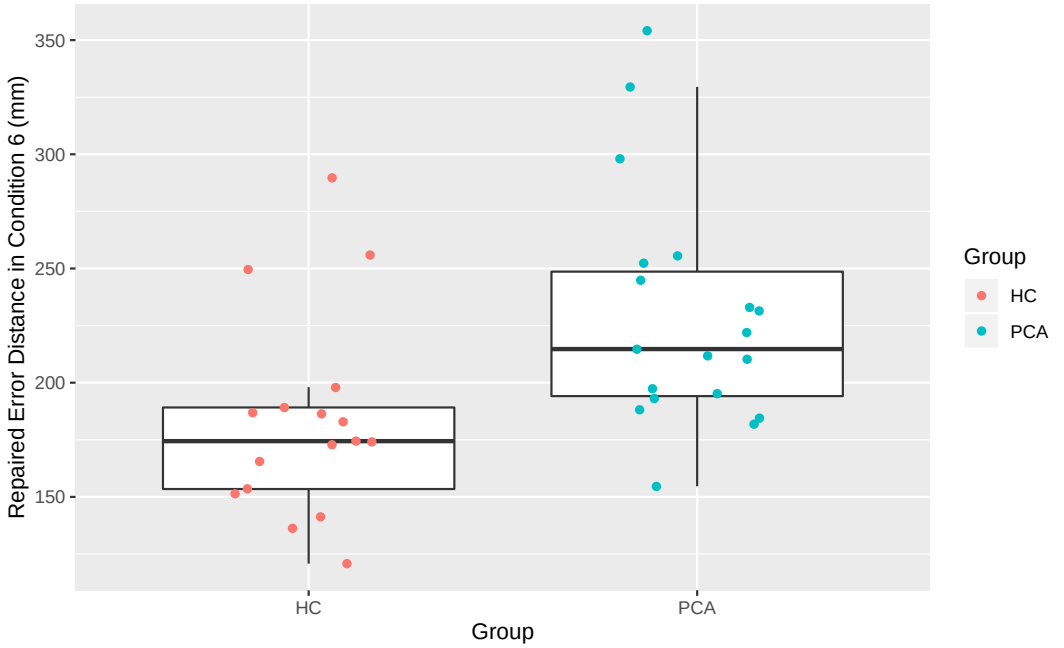

FIG. 3.5. Repaired error distance in condition 6 compared between the healthy controls (HC) and the CADASIL patients (PCA).

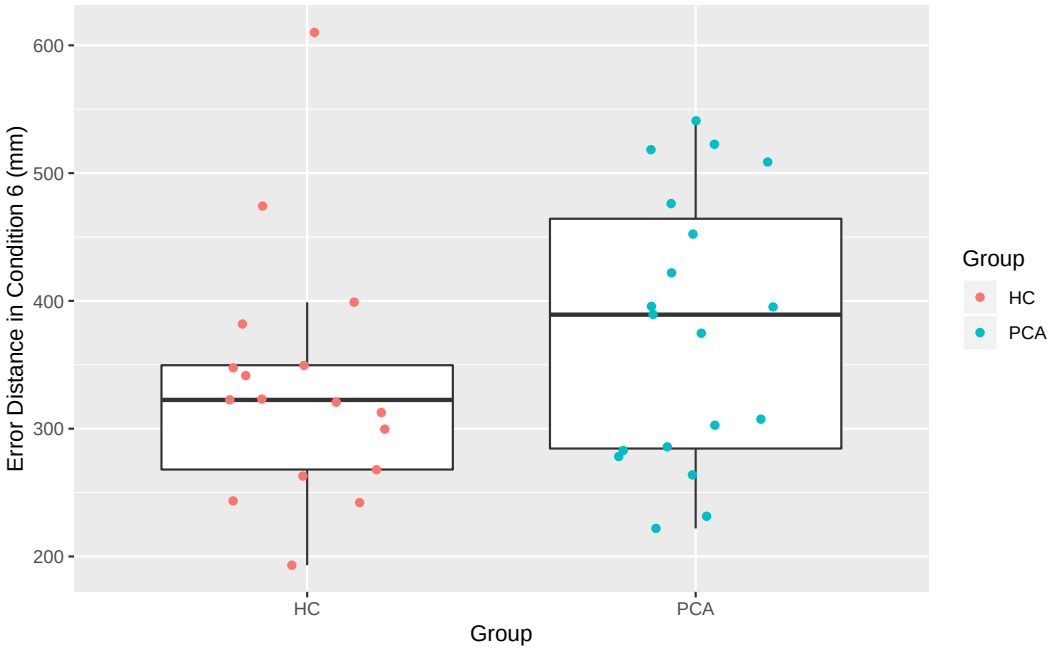

FIG. 3.6. Error distance in condition 6 compared between the healthy controls (HC) and the CADASIL patients (PCA).

3.5.2 Mean Distance

I also considered the average performance across all 6 conditions for each subject as a single measure for the behavioral metric. This was calculated for both repaired error distance (Fig 3.7) and error distance (Fig 3.8).

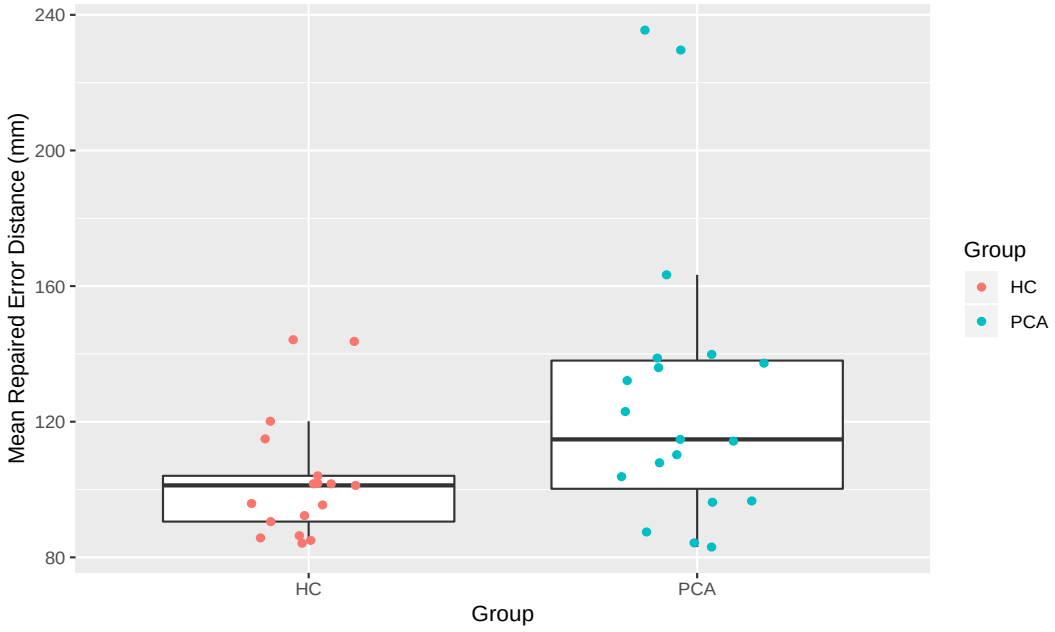

FIG. 3.7. Mean repaired error distance compared between the healthy controls (HC) and the CADASIL patients (PCA).

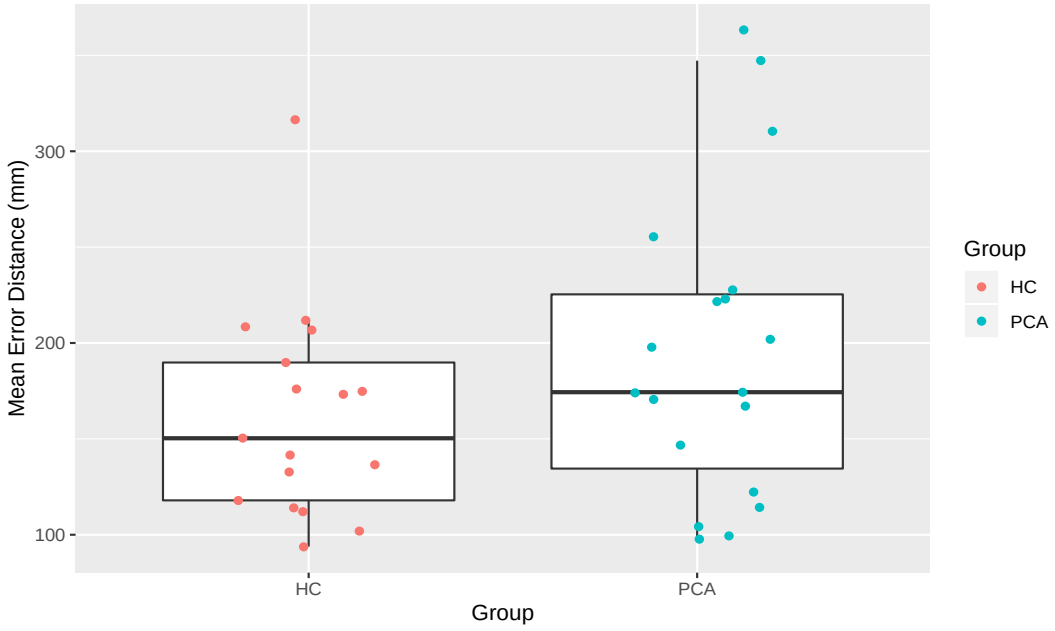

FIG. 3.8. Mean error distance compared between the healthy controls (HC) and the CADASIL patients (PCA).

3.5.3 Mean Difference Distance

From the repaired error distance post hoc analysis, conditions 1-3 had no significant difference between healthy controls and CADASIL patients, whereas conditions 4-6 showed significant difference between the two groups. Therefore, I also decided to look at the mean difference between conditions 1-3 and 4-6 as a single behavioral metric. This metric differed from the other two, by, for each subject, measuring how much worse they performed on the harder conditions compared to the easier conditions. This was calculated for both repaired error distance (Fig 3.9) and error distance (Fig 3.10).

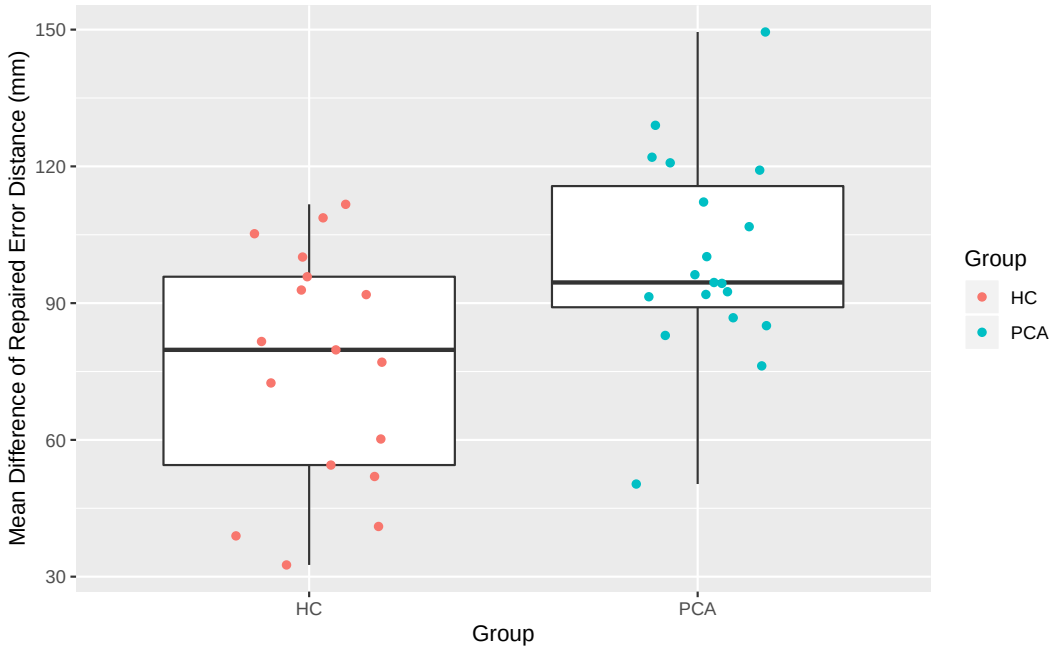

FIG. 3.9. Mean difference of repaired error distance compared between the healthy controls (HC) and the CADASIL patients (PCA).

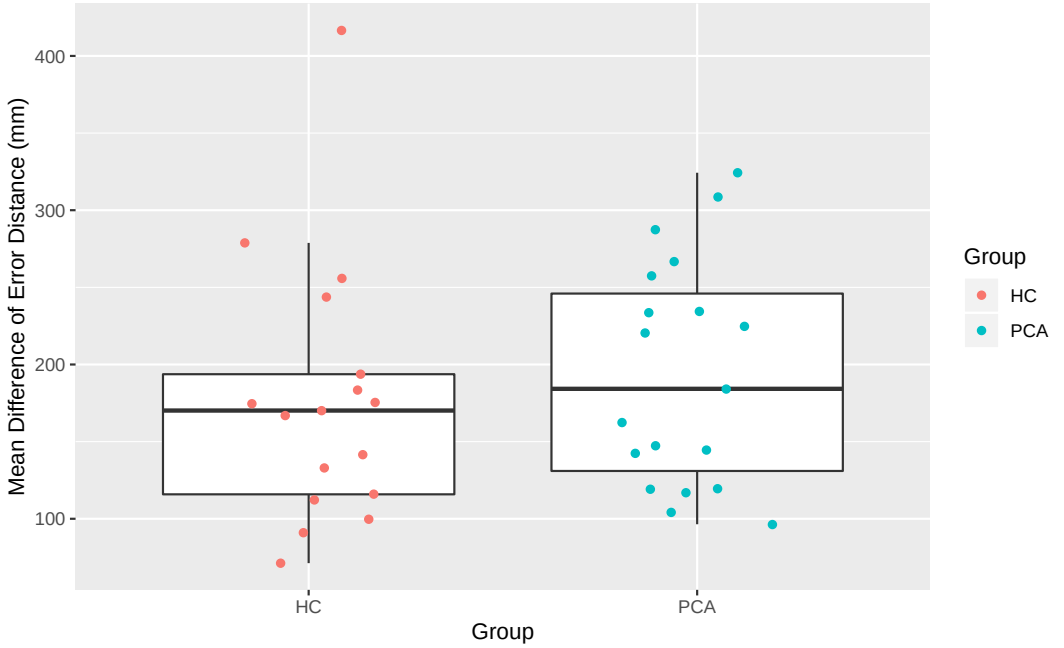

FIG. 3.10. Mean difference of error distance compared between the healthy controls (HC) and the CADASIL patients (PCA).

3.6 Summary of Behavioral Metric Findings Used for MR Analysis

Of the three methods – condition 6 only, mean across conditions, and mean difference between conditions 1-3 and 4-6 – I decided to use condition 6 as the primary variable in this thesis to represent repaired error and error distances in the MR analyses as it was the most difficult condition in the Dalmatian task, and should show the greatest difference between the CADASIL patients and healthy controls. The results from mean across conditions and mean difference between conditions 1-3 and 4-6 will still be reported, but not graphically represented. Table 3.1 shows a summary of the three methods.

TABLE 3.1. Summary of the three behavioral metrics used for MR analysis.

		Estimate	Standard Error	df	t-value	p-value
Condition 6	**Repaired**	-47.6	15.4	32	-3.1	0.004
	Error	-47.0	31.6	32	-1.5	0.15
Mean	**Repaired**	-26.7	10.9	32	-2.5	0.02
	Error	-36.5	22.8	32	-1.6	0.12
Mean Difference	**Repaired**	-24.7	7.9	32	-3.1	0.004
	Error	-18.4	24.4	32	-0.8	0.46

Estimate is the difference between the healthy control and CADASIL group (HC - PCA). A positive estimate means that the control group had a larger value; a negative estimate means that the CADASIL group had a larger value. df = degrees of freedom.

Chapter 4

T1 Structural MRI Results

In this chapter, I report the results from the volumetric T1-weighted images, focusing on grey matter (GM) volumes in patients with CADASIL compared to the healthy controls, and the association between this metric and a fine-grained behavioural measure of executive functioning. I also studied five regions of interest (ROI), selected a priori: anterior and midcingulate cortex, middle frontal gyrus, hippocampus, caudate, and putamen.

4.1 Whole Brain Grey Matter Atrophy

Differences between CADASIL patients and healthy controls were analysed using a general linear model (GLM). Group comparisons of GM volume co-varied for age, sex, and intracranial volume (ICV) (Equation 4.1).

$$\text{GM volume} \sim \text{Age} + \text{Sex} + \text{ICV} + \text{Group} \qquad \textbf{Eq. 4.1.}$$

Voxel-based morphometry (VBM) analysis revealed decreased GM volume in the CADASIL group compared to the healthy controls. The pattern of reduced GM volume in the CADASIL group was not widespread across the brain, but instead particularly involved the medial and lateral frontal, and temporal regions in a strikingly symmetrical manner. Specific regions of GM atrophy are reported in Figure 4.1 and Table 4.1 (all results were TFCE-corrected $p < 0.05$). Additionally, there was a small area surrounding the left putamen that showed larger GM volume in the CADASIL group compared to the healthy controls.

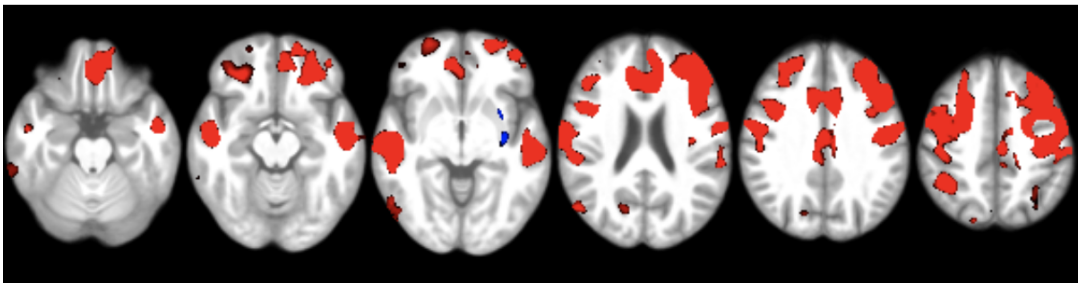

FIG. 4.1. Red indicates regions with significantly smaller grey matter volume (i.e. greater atrophy) in CADASIL patients (PCA) relative to healthy controls (HC). Blue indicates regions with significantly larger grey matter volume in PCAs than in HCs. All comparisons are $p < 0.05$ corrected for multiple comparisons using threshold free cluster enhancement (TFCE), displayed in radiological convention (the left side of the image represents the right side of the brain). Slices displayed: z = -21, -14, -4, 22, 34, 50 mm.

TABLE 4.1. Regions of decreased GM volume in CADASIL patients compared with healthy controls that survived a TFCE-corrected statistical threshold of $p < 0.05$.

Cluster	MNI Space (mm)			p-value	Cluster Size (voxels)	z-value	Anatomical Region
	x	y	z				
1	-3	39	-30	0.01	61889	3.72	Left frontal medial cortex
2	33	48	9	0.04	1010	3.43	Right frontal pole
3	27	36	-12	0.03	844	3.72	Right frontal pole / frontal orbital cortex
4	16.5	-73.5	42	0.02	613	3.72	Right lateral occipital cortex
5	33	-90	6	0.03	407	3.72	Right occipital pole / lateral occipital cortex
6	66	-46.5	-18	0.04	247	3.54	Right inferior temporal gyrus
7	-30	-52.5	46.5	0.04	143	3.72	Left superior parietal lobule
8	-45	-61.5	7.5	0.05	88	3.72	Left middle temporal gyrus
9	3	-73.5	52.5	0.05	18	3.43	Right precuneus cortex

MNI = Montreal Neurological Institute; x, y, z = coordinates at the clusters' maximum. Anatomical regions were identified with the Harvard/Oxford cortical and subcortical atlases.

4.2 Voxel-wise Grey Matter Atrophy in Relation to Behavioral Metrics

The correlation between GM volume and behavioral metrics (repaired error distance and error distance) were analysed for the whole population (CADASIL patients and healthy controls) using a general linear model (GLM) (Eq. 4.2).

$$\text{GM volume} \sim \text{Age} + \text{Sex} + \text{ICV} + \text{Behavioral metric} \qquad \textbf{Eq. 4.2.}$$

I present results for behavioral metrics from the most difficult condition only (condition 6). The mean difference across conditions had very similar results, but the mean difference between conditions 1-3 and 4-6 did not show any significant regions.

Voxel-based morphometry (VBM) analysis revealed a negative association between GM volume and condition 6 of repaired error distance (i.e. GM volume decreased as repaired error distance increased (worsening working memory)). The pattern of association was concentrated on two clusters; one centred on the right frontal pole, another on the left occipital pole and lateral occipital cortex. Specific regions of association are reported in Figure 4.2 and Table 4.2 (all results were corrected TFCE-corrected $p < 0.05$).

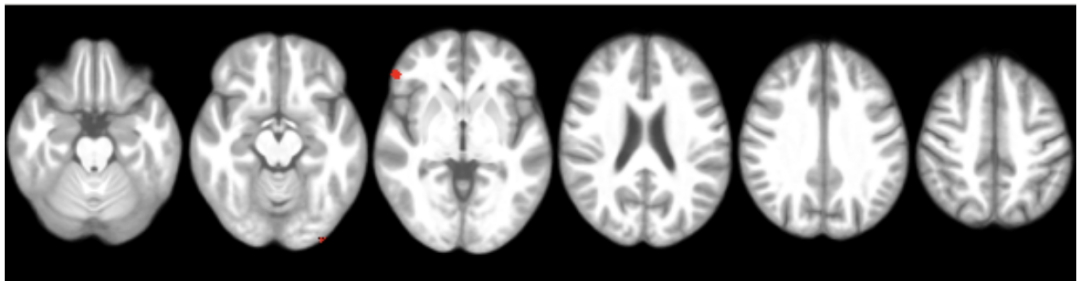

FIG. 4.2. Red indicates regions with significant association between reduced GM volume in the whole population and condition 6 repaired error distance increases (i.e. worsening working memory). All comparisons are $p < 0.05$ corrected for multiple comparisons using threshold free cluster enhancement (TFCE), displayed in radiological convention (the left side of the image represents the right side of the brain). Slices displayed: z = -21, -14, -2, 22, 34, 50 mm.

TABLE 4.2. Regions of decreased GM volume with increased condition 6 repaired error distance (i.e. worsening working memory) for our whole population that survived a TFCE-corrected statistical threshold of $p < 0.05$.

Cluster	MNI Space			p-value	k-value	z-value	Anatomical Region
	x	y	z				
1	24	107	44	0.04	91	3.72	Right frontal pole
2	82	20	39	0.04	83	3.72	Left occipital pole / lateral occipital cortex

MNI = Montreal Neurological Institute; x, y, z = coordinates at the clusters' maximum; k-value = number of voxels / size of the respective clusters.

I then used GLM to explore whether the association between GM volume and the behavioral metrics differed between the HC and PCA groups. Again, I used three different models in analysing the behavioral data: the most difficult condition only (condition 6), mean across conditions, and mean difference between conditions 1-3 and 4-6.

No areas survived correction for multiple comparisons ($p < 0.05$, threshold free cluster enhancement corrected), indicating no significant difference in association between grey matter volume and any of the behavioral measures between groups.

4.3 Region of Interest Analysis

Here I present a region of interest analysis, selected a priori, using two models. These regions are involved in executive function and spatial memory, and are also known to be affected by CADASIL (Amberla et al., 2004; Fallon, Zokaei, and Husain, 2016).

Model 1: First, I investigated the relationship between behavioural metric and GM volume across all subjects. Using a linear regression, the behavioural metric (repaired error and error distance) was modelled as a function of age, sex, and GM volume (Eq. 4.3). In Figures 4.5 to 4.14, the relationship between GM volume and behavioral metric is represented by the black dashed lines.

$$\text{Behavioral metric} \sim \text{Age} + \text{Sex} + \text{GM volume} \qquad \textbf{Eq. 4.3.}$$

Model 2: In order to determine whether the association between behaviour and MRI differed between the HC and PCA groups, both group (HC/PCA) and group-by-GM volume interaction terms were added to Model 1 (Eq. 4.4). In Figures 4.5 to 4.14, the relationship between GM volume and behavioural metric within each group is represented by the red (HC) and blue (PCA) coloured lines.

$$\text{Behavioral metric} \sim \text{Age} + \text{Sex} + \text{GM volume} * \text{Group} \qquad \textbf{Eq. 4.4.}$$

All figures show the behavioral data from the most difficult condition only (condition 6), but I also report results from the other models: mean across conditions and mean difference between conditions 1-3 and 4-6. Parameter estimates from one-way ANCOVAs are reported; $p<0.05$ was considered significant. In addition, the Akaike Information Criteria (AIC) is reported for each model as a measure of model fit. A smaller AIC suggests a better model fit.

Figures 4.3 and 4.4 are a visual representation of the cortical and subcortical regions of interest, selected a priori: anterior and midcingulate gyrus, middle frontal gyrus, hippocampus, caudate, and putamen.

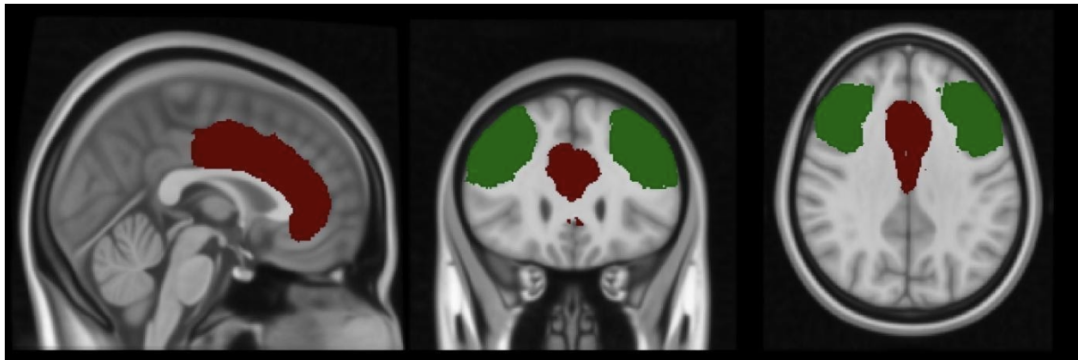

FIG. 4.3. Cortical regions of interest (ROI), in MNI-normalized space, selected a priori, displayed in radiological convention (the left side of the image represents the right side of the brain). Red = Anterior and midcingulate cortex (ACC and MCC); green = middle frontal gyrus.

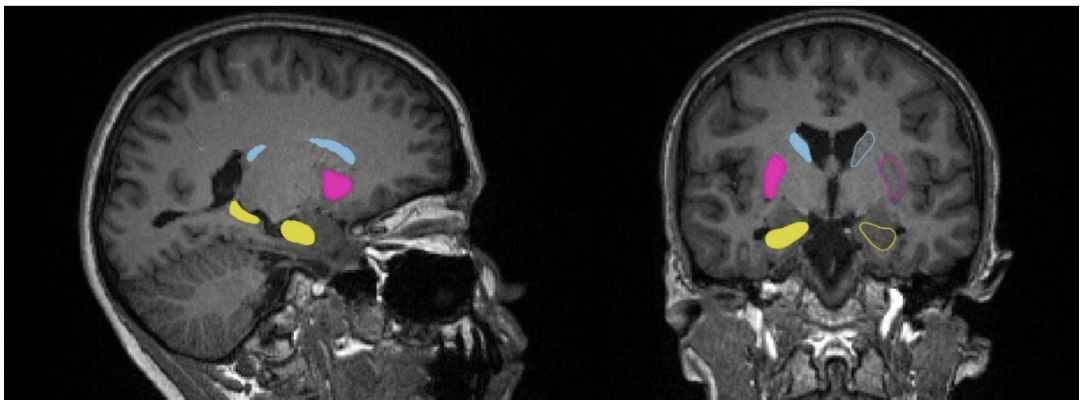

FIG. 4.4. Subcortical regions of interest (ROI), in subject space, selected a priori, displayed in radiological convention (the left side of the image represents the right side of the brain). Yellow = hippocampus; blue = caudate; pink = putamen.

4.3.1 Repaired Error Distance

4.3.1.1. Anterior cingulate cortex (ACC) and midcingulate cortex (MCC), condition 6

Figure 4.5 reports the relationship between the cingulate cortex and repaired error distance. In model 1, I observed a significant association between repaired error distance and grey matter volume [F(1) = 4.7, p = 0.04]. In model 2, I observed no significant difference in GM volume between the groups [F(1) = 1.9, p = 0.2], no significant association between repaired error distance and GM volume [F(1) = 0.6, p = 0.5], and no interaction between group and GM volume [F(1) = 0.3, p = 0.6]. Model 1 AIC = 329.7; Model 2 AIC = 331.1.

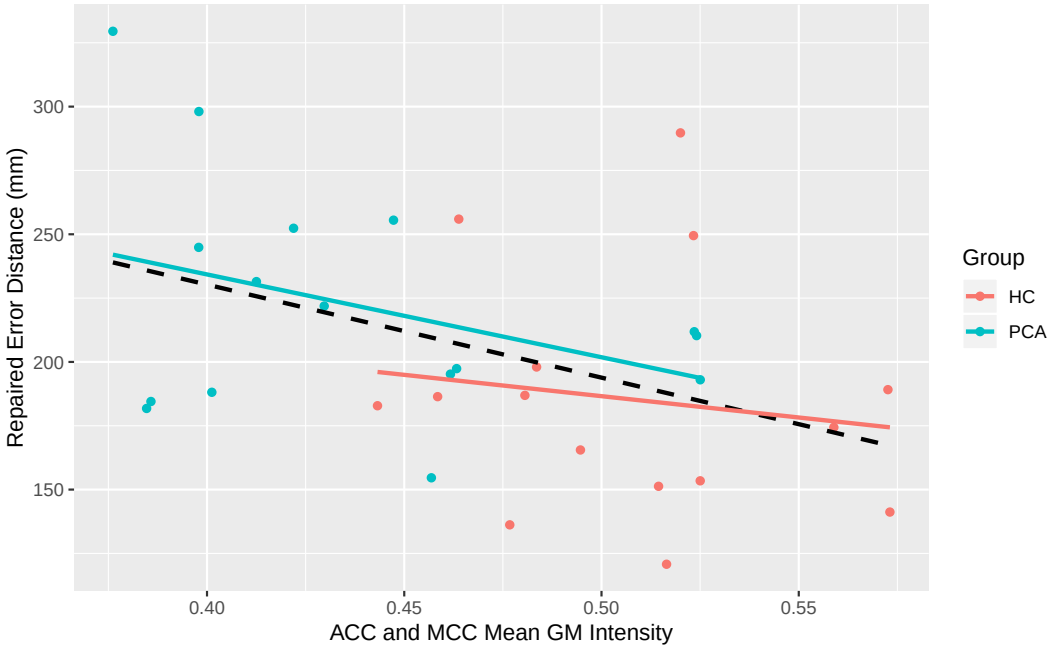

FIG. 4.5. Scatter plot of the GM volume in the combined ACC and MCC for each subject in relation to repaired error distances at condition 6. The black dashed line is the line of best fit across all the subjects combined. Coloured lines indicate the line of best fit within each group (red for HC and blue for PCA).

Mean model
I also carried out a one-way ANCOVA on mean repaired error distance. In model 1, I observed no significant association between repaired error distance and grey matter volume [F(1) = 4.1, p = 0.05]. In model 2, I observed no significant difference in GM volume between the groups [F(1) = 0.5, p = 0.5], no significant association between repaired error distance and GM volume [F(1) = 1.2, p = 0.3], and no interaction between group and GM volume [F(1) = 2.0, p = 0.2]. Model 1 AIC = 300.8; Model 2 AIC = 301.8.

Mean difference model
One-way ANCOVA was also performed for the mean difference model. In model 1, I observed no significant association between repaired error distance and grey matter

volume [F(1) = 2.9, p = 0.1]. In model 2, I observed no significant difference in GM volume between the groups [F(1) = 4.0, p = 0.06], no significant association between repaired error distance and GM volume [F(1) = 0.002, p = 0.97], and no interaction between group and GM volume [F(1) = 0.2, p = 0.7]. Model 1 AIC = 294.4; model 2 AIC = 298.4.

4.3.1.2. Middle frontal gyrus, condition 6

Figure 4.6 reports the relationship between the middle frontal gyrus and repaired error distance. In model 1, I observed a significant association between repaired error distance and grey matter volume [F(1) = 8.4, p = 0.007]. In model 2, I observed no significant difference in GM volume between the groups [F(1) = 0.5, p = 0.5], no significant association between repaired error distance and GM volume [F(1) = 2.2, p = 0.2], and no interaction between group and GM volume [F(1) = 1.4, p = 0.2]. Model 1 AIC = 326.3; Model 2 AIC = 328.0.

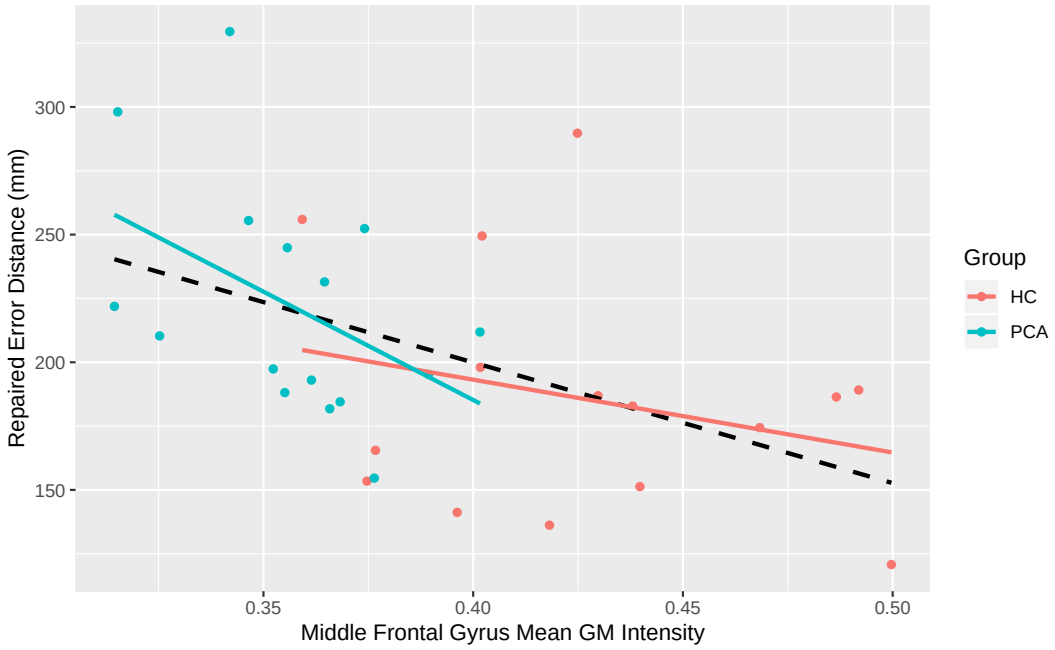

FIG. 4.6. Scatter plot of the GM volume in the middle frontal gyrus for each subject in relation to repaired error distances at condition 6. The black dashed line is the line of best fit across all the subjects combined. Coloured lines indicate the line of best fit within each group (red for HC and blue for PCA).

Mean model

I also carried out a one-way ANCOVA on mean repaired error distance. In model 1, I observed a significant association between repaired error distance and grey matter volume [F(1) = 6.3, p = 0.02]. In model 2, I observed no significant difference in GM volume between the groups [F(1) = 0.01, p = 0.9], and no significant association between repaired error distance and GM volume [F(1) = 3.1, p = 0.09], however there was an interaction between group and GM volume [F(1) = 6.5, p = 0.02]. Model 1 AIC = 298.6; Model 2 AIC = 295.5.

Mean difference model
One-way ANCOVA was also performed for the mean difference model. In model 1, I observed no significant association between repaired error distance and grey matter volume [F(1) = 1.2, p = 0.3]. In model 2, I observed a significant difference in GM volume between the groups [F(1) = 7.7, p = 0.01], but no significant association between repaired error distance and GM volume [F(1) = 1.5, p = 0.2], and no interaction between group and GM volume [F(1) = 0.7, p = 0.4]. Model 1 AIC = 296.2; Model 2 AIC = 291.3.

4.3.1.3. Hippocampus, condition 6

Figure 4.7 reports the relationship between the hippocampus and repaired error distance. In model 1, I observed no significant association between repaired error distance and grey matter volume [F(1) = 0.3, p = 0.6]. In model 2, I observed a significant difference in GM volume between the groups [F(1) = 6.5, p = 0.02], but no significant association between repaired error distance and GM volume [F(1) = 0.8, p = 0.4], and no interaction between group and GM volume [F(1) = 0.02, p = 0.9]. Model 1 AIC = 334.3; Model 2 AIC = 331.1.

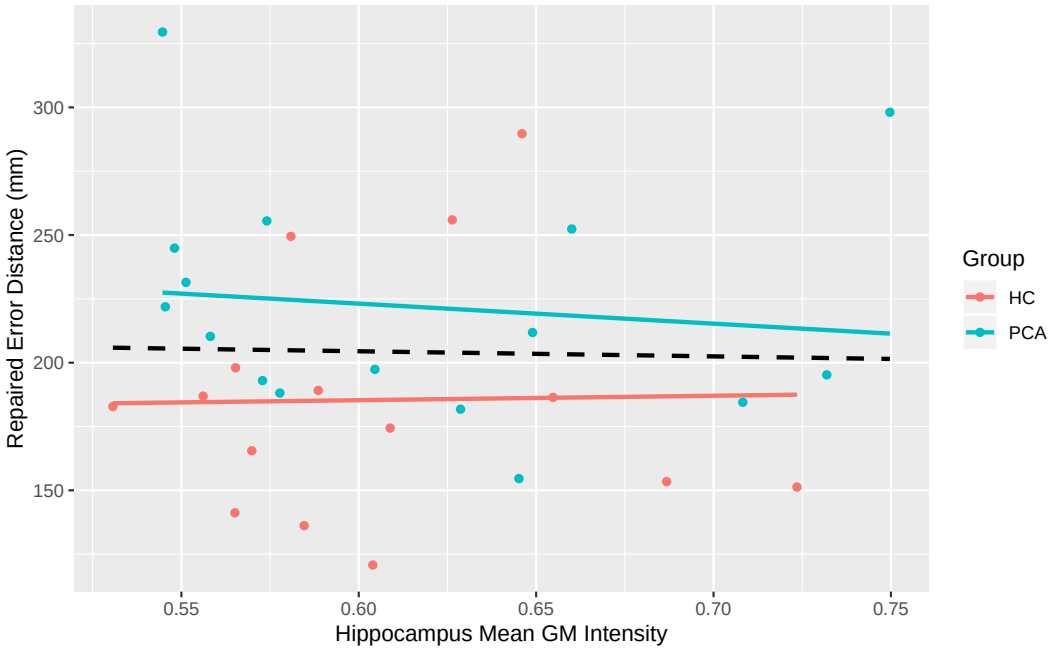

FIG. 4.7. Scatter plot of the GM volume in the hippocampus for each subject in relation to repaired error distances at condition 6. The black dashed line is the line of best fit across all the subjects combined. Coloured lines indicate the line of best fit within each group (red for HC and blue for PCA).

Mean model
I also carried out a one-way ANCOVA on mean repaired error distance. In model 1, I observed no significant association between repaired error distance and grey matter volume [F(1) = 0.006, p = 0.9]. In model 2, I observed no significant difference in GM volume between the groups [F(1) = 3.1, p = 0.09], and no significant association

between repaired error distance and GM volume [F(1) = 0.01, p = 0.9], and no interaction between group and GM volume [F(1) = 0.04, p = 0.8]. Model 1 AIC = 305.1; Model 2 AIC = 305.4.

Mean difference model
One-way ANCOVA was also performed for the mean difference model. In model 1, I observed no significant association between repaired error distance and grey matter volume [F(1) = 0.2, p = 0.6]. In model 2, I observed a significant difference in GM volume between the groups [F(1) = 8.0, p = 0.009], but no significant association between repaired error distance and GM volume [F(1) = 0.7, p = 0.4], and no interaction between group and GM volume [F(1) = 0.9, p = 0.4]. Model 1 AIC = 297.3; Model 2 AIC = 291.9.

4.3.1.4. Caudate, condition 6

Figure 4.8 reports the relationship between the caudate and repaired error distance. In model 1, I observed no significant association between repaired error distance and grey matter volume [F(1) = 2.6, p = 0.1]. In model 2, I observed no significant difference in GM volume between the groups [F(1) = 3.8, p = 0.06], no significant association between repaired error distance and GM volume [F(1) = 0.2, p = 0.6], and no interaction between group and GM volume [F(1) = 3.6, p = 0.07]. Model 1 AIC = 331.8; Model 2 AIC = 327.8.

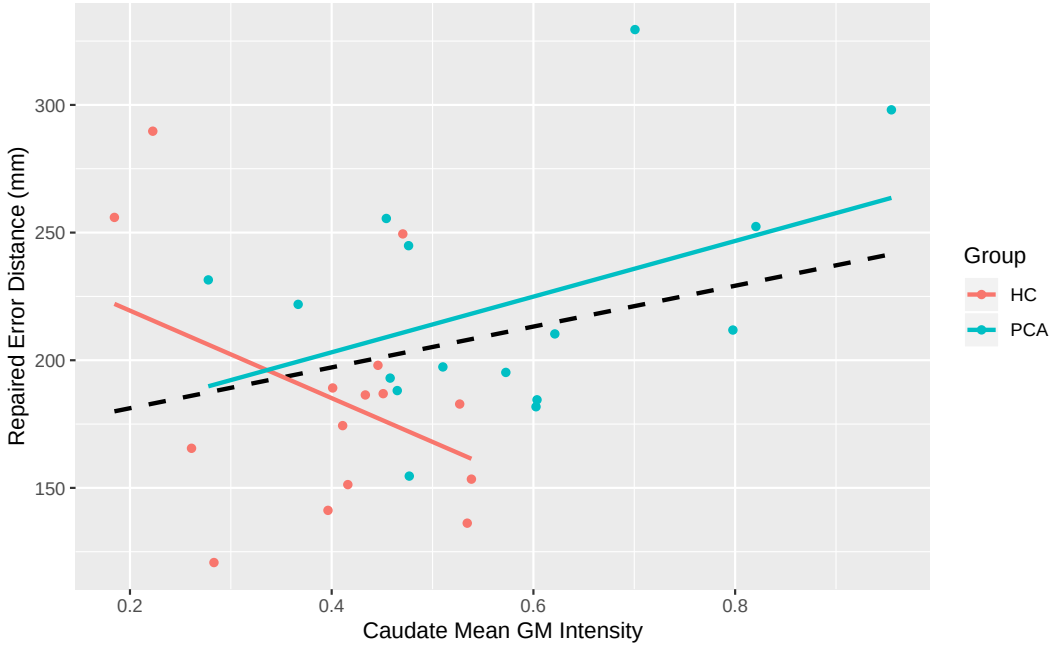

FIG. 4.8. Scatter plot of the GM volume in the caudate for each subject in relation to repaired error distances at condition 6. The black dashed line is the line of best fit across all the subjects combined. Coloured lines indicate the line of best fit within each group (red for HC and blue for PCA).

Mean model
I also carried out a one-way ANCOVA on mean repaired error distance. In model 1, I observed a significant association between repaired error distance and grey matter volume [F(1) = 4.8, p = 0.04]. In model 2, I observed no significant difference in GM volume between the groups [F(1) = 0.7, p = 0.4], and no significant association between repaired error distance and GM volume [F(1) = 2.0, p = 0.2], and no interaction between group and GM volume [F(1) = 0.3, p = 0.6]. Model 1 AIC = 300.0; Model 2 AIC = 302.9.

Mean difference model
One-way ANCOVA was also performed for the mean difference model. In model 1, I observed no significant association between repaired error distance and grey matter volume [F(1) = 2.2, p = 0.1]. In model 2, I observed a significant difference in GM volume between the groups [F(1) = 5.0, p = 0.04], but no significant association between repaired error distance and GM volume [F(1) = 0.04, p = 0.8], and no interaction between group and GM volume [F(1) = 1.2, p = 0.3]. Model 1 AIC = 295.1; Model 2 AIC = 292.3.

4.3.1.5. Putamen, condition 6

Figure 4.9 reports the relationship between the putamen and repaired error distance. In model 1, I observed no significant association between repaired error distance and grey matter volume [F(1) = 0.7, p = 0.4]. In model 2, I observed a significant difference in GM volume between the groups [F(1) = 5.1, p = 0.03], but no significant association between repaired error distance and GM volume [F(1) = 0.02, p = 0.9], and no interaction between group and GM volume [F(1) = 0.2, p = 0.6]. Model 1 AIC = 333.8; Model 2 AIC = 331.9.

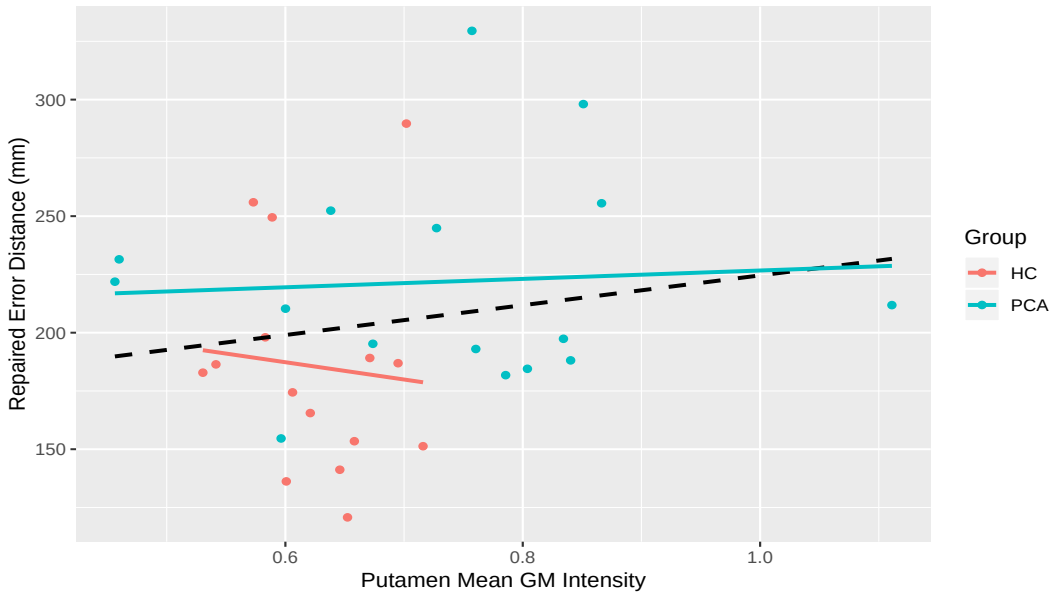

FIG. 4.9. Scatter plot of the GM volume in the putamen for each subject in relation to repaired error distances at condition 6. The black dashed line is the line of best fit across all the subjects combined. Coloured lines indicate the line of best fit within each group (red for HC and blue for PCA).

Mean model
I also carried out a one-way ANCOVA on mean repaired error distance. In model 1, I observed no significant association between repaired error distance and grey matter volume [F(1) = 0.6, p = 0.4]. In model 2, I observed no significant difference in GM volume between the groups [F(1) = 2.5, p = 0.1], and no significant association between repaired error distance and GM volume [F(1) = 0.002, p = 0.96], and no interaction between group and GM volume [F(1) = 0.2, p = 0.7]. Model 1 AIC = 304.4; Model 2 AIC = 305.3.

Mean difference model
One-way ANCOVA was also performed for the mean difference model. In model 1, I observed no significant association between repaired error distance and grey matter volume [F(1) = 2.3, p = 0.1]. In model 2, I observed a significant difference in GM volume between the groups [F(1) = 4.9, p = 0.04], but no significant association between repaired error distance and GM volume [F(1) = 0.3, p = 0.6], and no interaction between group and GM volume [F(1) = 0.07, p = 0.8]. Model 1 AIC = 295.0; Model 2 AIC = 293.4.

4.3.2 Error Distance

4.3.2.1. Anterior cingulate cortex (ACC) and midcingulate cortex (MCC), condition 6

Figure 4.10 reports the relationship between the cingulate cortex and error distance. In model 1, I observed no significant association between error distance and grey matter volume [F(1) = 1.1, p = 0.3]. In model 2, I observed no significant difference in GM volume between the groups [F(1) = 0.4, p = 0.5], no significant association between error distance and GM volume [F(1) = 0.1, p = 0.7], and no interaction between group and GM volume [F(1) = 0.004, p = 0.95]. Model 1 AIC = 377.1; Model 2 AIC = 380.6.

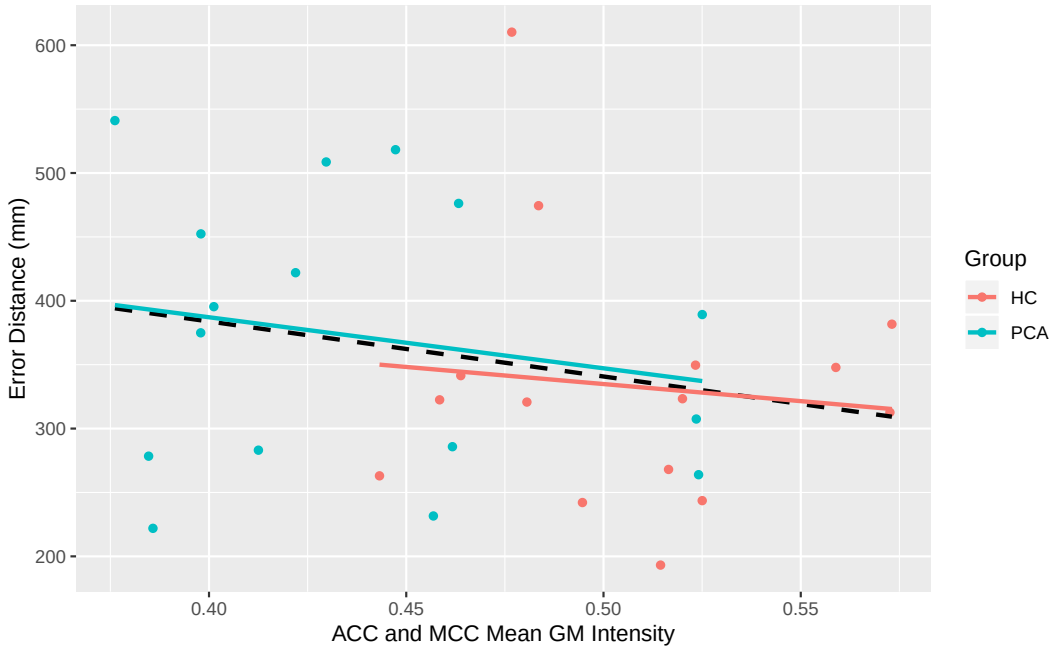

FIG. 4.10. Scatter plot of the GM volume in the ACC and MCC for each subject in relation to error distances at condition 6. The black dashed line is the line of best fit across all the subjects combined. Coloured lines indicate the line of best fit within each group (red for HC and blue for PCA).

Mean model
I also carried out a one-way ANCOVA on mean error distance. In model 1, I observed no significant association between error distance and grey matter volume [F(1) = 1.3, p = 0.3]. In model 2, I observed no significant difference in GM volume between the groups [F(1) = 0.1, p = 0.7], no significant association between error distance and GM volume [F(1) = 0.3, p = 0.6], and no interaction between group and GM volume [F(1) = 0.4, p = 0.6]. Model 1 AIC = 353.4; Model 2 AIC = 356.8.

Mean difference model
One-way ANCOVA was also performed for the mean difference model. In model 1, I observed no significant association between error distance and grey matter volume [F(1) = 0.02, p = 0.9]. In model 2, I observed no significant difference in GM volume

between the groups [F(1) = 0.09, p = 0.8], no significant association between error distance and GM volume [F(1) = 0.009, p = 0.9], and no interaction between group and GM volume [F(1) = 0.006, p = 0.9]. Model 1 AIC = 358.6; Model 2 AIC = 362.5.

4.3.2.2. Middle frontal gyrus, condition 6

Figure 4.11 reports the relationship between the middle frontal gyrus and error distance. In model 1, I observed a significant association between error distance and grey matter volume [F(1) = 5.5, p = 0.03]. In model 2, I observed no significant difference in GM volume between the groups [F(1) = 0.5, p = 0.5]. There was a significant association between error distance and GM volume [F(1) = 4.3, p = 0.05], but no interaction between group and GM volume [F(1) = 0.4, p = 0.5]. Model 1 AIC = 372.5; Model 2 AIC = 375.5.

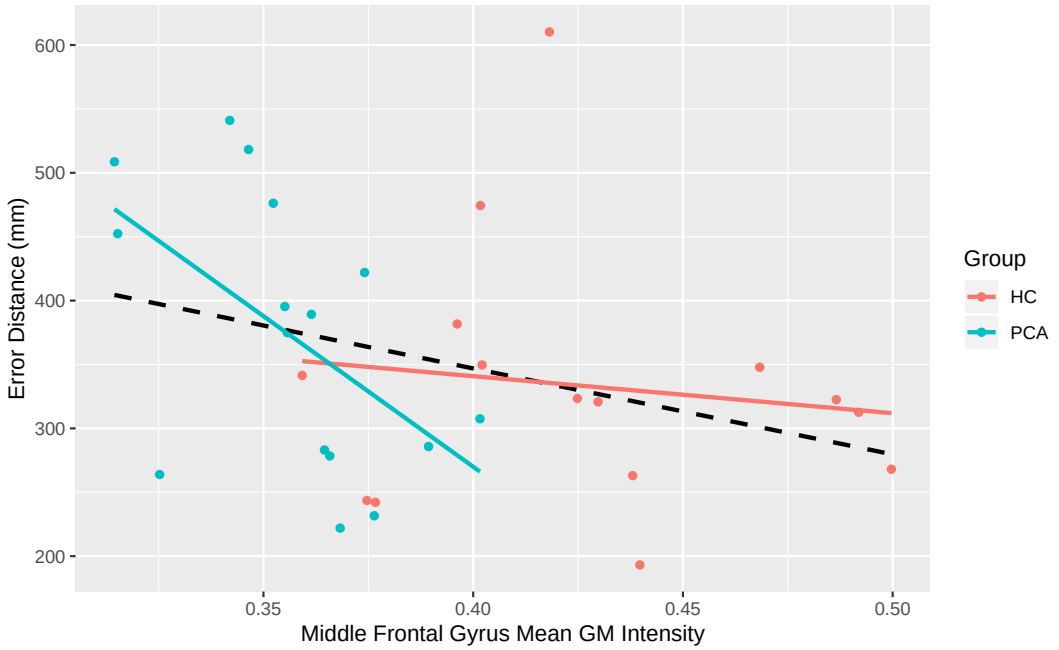

FIG. 4.11. Scatter plot of the GM volume in the middle frontal gyrus for each subject in relation to error distances at condition 6. The black dashed line is the line of best fit across all the subjects combined. Coloured lines indicate the line of best fit within each group (red for HC and blue for PCA).

Mean model
I also carried out a one-way ANCOVA on mean error distance. In model 1, I observed a significant association between error distance and grey matter volume [F(1) = 4.5, p = 0.04]. In model 2, I observed no significant difference in GM volume between the groups [F(1) = 0.5, p = 0.5], no significant association between error distance and GM volume [F(1) = 4.0, p = 0.06], and no interaction between group and GM volume [F(1) = 2.5, p = 0.1]. Model 1 AIC = 350.1; Model 2 AIC = 250.6.

Mean difference model
One-way ANCOVA was also performed for the mean difference model. In model 1, I observed no significant association between error distance and grey matter volume

[F(1) = 1.2, p = 0.3]. In model 2, I observed no significant difference in GM volume between the groups [F(1) = 0.5, p = 0.5], no significant association between error distance and GM volume [F(1) = 1.5, p = 0.2], and no interaction between group and GM volume [F(1) = 0.2, p = 0.7]. Model 1 AIC = 357.3; Model 2 AIC = 360.5.

4.3.2.3. Hippocampus, condition 6

Figure 4.12 reports the relationship between the hippocampus and error distance. In model 1, I observed no significant association between error distance and grey matter volume [F(1) = 0.6, p = 0.5]. In model 2, I observed no significant difference in GM volume between the groups [F(1) = 1.5, p = 0.2], no significant association between error distance and GM volume [F(1) = 0.8, p = 0.4], and no interaction between group and GM volume [F(1) = 0.01, p = 0.9]. Model 1 AIC = 377.6; Model 2 AIC = 379.8.

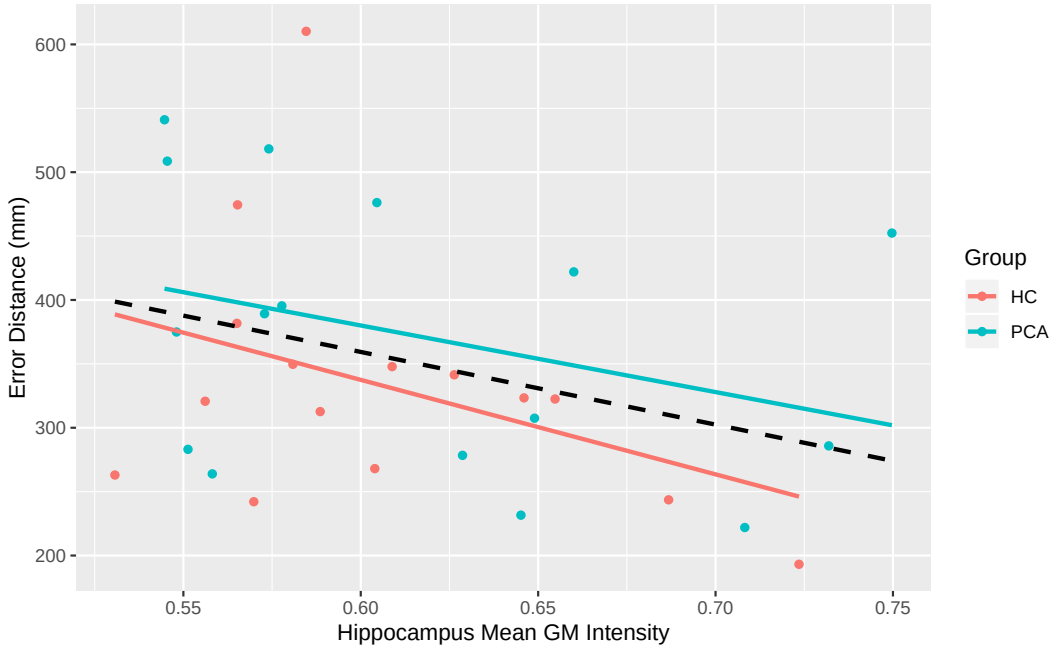

FIG. 4.12. Scatter plot of the GM volume in the hippocampus for each subject in relation to error distances at condition 6. The black dashed line is the line of best fit across all the subjects combined. Coloured lines indicate the line of best fit within each group (red for HC and blue for PCA).

Mean model

I also carried out a one-way ANCOVA on mean error distance. In model 1, I observed no significant association between error distance and grey matter volume [F(1) = 0.004, p = 0.9]. In model 2, I observed no significant difference in GM volume between the groups [F(1) = 0.96, p = 0.3], no significant association between error distance and GM volume [F(1) = 0.002, p = 0.96], and no interaction between group and GM volume [F(1) = 0.0, p = 0.98]. Model 1 AIC = 354.8; Model 2 AIC = 357.7.

Mean difference model
One-way ANCOVA was also performed for the mean difference model. In model 1, I observed no significant association between error distance and grey matter volume [F(1) = 0.7, p = 0.4]. In model 2, I observed no significant difference in GM volume between the groups [F(1) = 0.2, p = 0.7], no significant association between error distance and GM volume [F(1) = 0.7, p = 0.4], and no interaction between group and GM volume [F(1) = 0.0, p = 0.99]. Model 1 AIC = 357.9; Model 2 AIC = 361.7.

4.3.2.4. Caudate, condition 6

Figure 4.13 reports the relationship between the caudate and error distance. In model 1, I observed no significant association between error distance and grey matter volume [F(1) = 1.1, p = 0.3]. In model 2, I observed no significant difference in GM volume between the groups [F(1) = 0.5, p = 0.5], no significant association between error distance and GM volume [F(1) = 0.3, p = 0.6], and no interaction between group and GM volume [F(1) = 0.0, p = 0.995]. Model 1 AIC = 377.0; Model 2 AIC = 380.5.

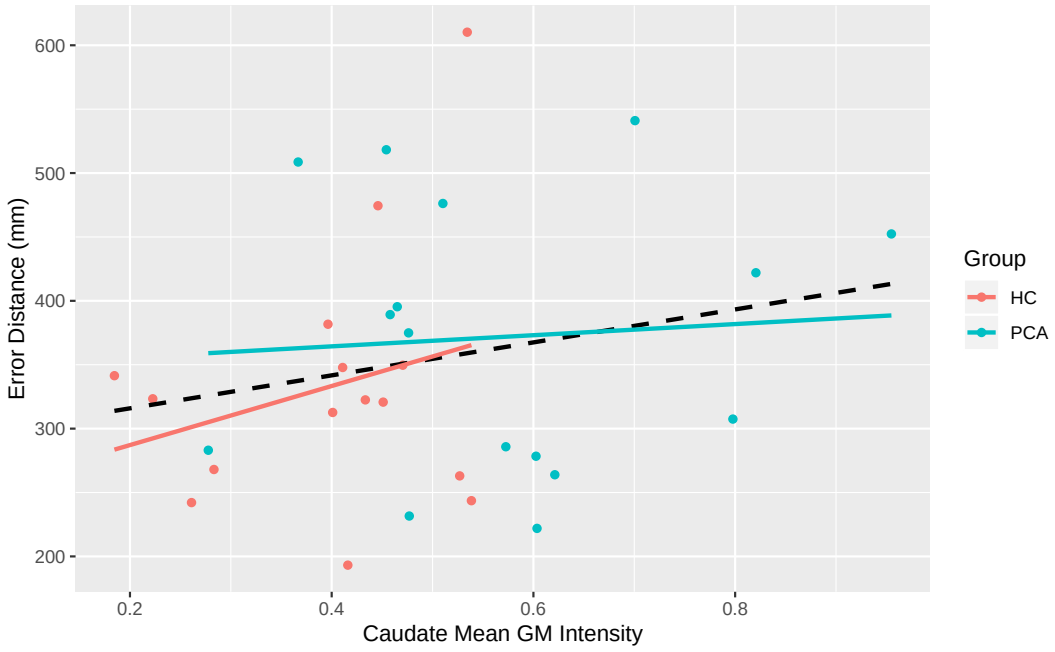

FIG. 4.13. Scatter plot of the GM volume in the caudate for each subject in relation to error distances at condition 6. The black dashed line is the line of best fit across all the subjects combined. Coloured lines indicate the line of best fit within each group (red for HC and blue for PCA).

Mean model
I also carried out a one-way ANCOVA on mean error distance. In model 1, I observed no significant association between error distance and grey matter volume [F(1) = 1.6, p = 0.2]. In model 2, I observed no significant difference in GM volume between the groups [F(1) = 0.2, p = 0.7], no significant association between error distance and GM volume [F(1) = 0.7, p = 0.4], and no interaction between group and GM volume [F(1) = 0.1, p = 0.7]. Model 1 AIC = 353.1; Model 2 AIC = 356.7.

Mean difference model
One-way ANCOVA was also performed for the mean difference model. In model 1, I observed no significant association between error distance and grey matter volume [F(1) = 0.06, p = 0.8]. In model 2, I observed no significant difference in GM volume between the groups [F(1) = 0.05, p = 0.8], no significant association between error distance and GM volume [F(1) = 0.008, p = 0.9], and no interaction between group and GM volume [F(1) = 0.01, p = 0.9]. Model 1 AIC = 358.6; Model 2 AIC = 362.5.

4.3.2.5. Putamen, condition 6

Figure 4.14 reports the relationship between the putamen and error distance. In model 1, I observed no significant association between error distance and grey matter volume [F(1) = 0.4, p = 0.5]. In model 2, I observed no significant difference in GM volume between the groups [F(1) = 0.9, p = 0.4], no significant association between error distance and GM volume [F(1) = 0.02, p = 0.9], and no interaction between group and GM volume [F(1) = 0.07, p = 0.8]. Model 1 AIC = 377.8; Model 2 AIC = 380.7.

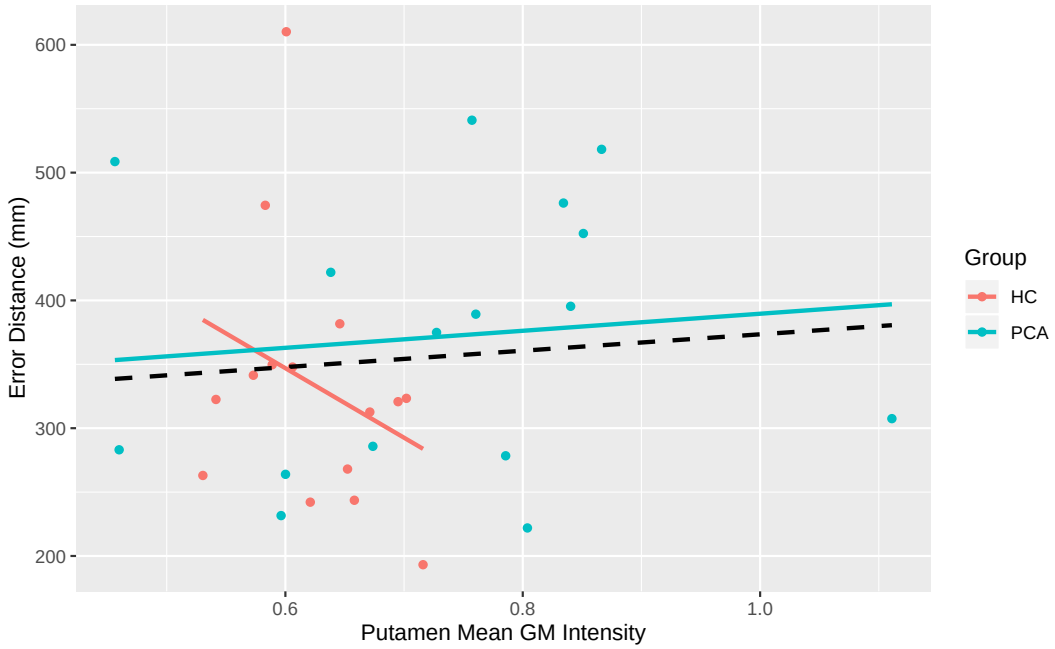

FIG. 4.14. Scatter plot of the GM volume in the putamen for each subject in relation to error distances at condition 6. The black dashed line is the line of best fit across all the subjects combined. Coloured lines indicate the line of best fit within each group (red for HC and blue for PCA).

Mean model
I also carried out a one-way ANCOVA on mean error distance. In model 1, I observed no significant association between error distance and grey matter volume [F(1) = 0.7, p = 0.4]. In model 2, I observed no significant difference in GM volume

between the groups [F(1) = 0.5, p = 0.5], no significant association between error distance and GM volume [F(1) = 0.2, p = 0.7], and no interaction between group and GM volume [F(1) = 0.01, p = 0.9]. Model 1 AIC = 354.0; Model 2 AIC = 357.4.

Mean difference model
One-way ANCOVA was also performed for the mean difference model. In model 1, I observed no significant association between error distance and grey matter volume [F(1) = 0.1, p = 0.8]. In model 2, I observed no significant difference in GM volume between the groups [F(1) = 0.04, p = 0.8], no significant association between error distance and GM volume [F(1) = 0.03, p = 0.9], and no interaction between group and GM volume [F(1) = 0.0, p = 0.99]. Model 1 AIC = 358.5; Model 2 AIC = 362.5.

4.4 Summary of Grey Matter Volume Findings

The CADASIL group had lower grey matter volume across symmetrical cortical and subcortical areas relative to healthy controls. At the voxel level, I observed only two small regions showing significant relationship between GM volume and behavioral metrics (one centred at the right frontal pole, the other at the left occipital pole and lateral occipital cortex). Regionally, the anterior and midcingulate cortex (ACC and MCC) and the middle frontal gyrus showed significant behavioral correlation with GM volume in model 1, whereas the hippocampus and putamen showed significant group correlation with GM volume in model 2. The middle frontal gyrus showed significant group-by-GM volume interactions in the mean model.

Generally, an AIC difference that is greater than two is taken to have substantial support that one model fits better than another (Burnham and Anderson, 2002). The AIC in this GM volume study suggested one of the models was better than the other, however this was not always in a consistent direction (i.e. for some regions model 1 had a higher AIC and did better, whilst model 2 was better for others). This therefore suggests that adding group as a factor does not necessarily improve the model, and may thus allude that the behavioral metrics (repaired error and error distance), GM volume, and group are all interlinked and tightly correlated.

Chapter 5

Perfusion MRI Results

In this chapter, I used vessel encoding pseudo-continuous arterial spin labelling (VEPCASL) to study perfusion in CADASIL patients compared to the healthy controls. I also examined whether perfusion was associated with a fine-grained behavioural measure of executive functioning. Finally, similar to the previous chapter, I studied five regions of interest (ROI), selected a priori: anterior and midcingulate cortex, middle frontal gyrus, hippocampus, caudate, and putamen. Unlike how the previous chapter examined grey matter volume changes, cerebral perfusion studies how blood flow differs between the CADASIL brain and healthy brain. Despite perfusion being closely related to underlying brain metabolism, very little is known about perfusion changes in CADASIL.

5.1 Voxel-wise Whole Brain Perfusion

Comparison of global cerebral perfusion between CADASIL patients and healthy controls were analysed using a general linear model (GLM), co-varying for age, sex, and GM volume (Equation 5.1).

$$\text{GM perfusion} \sim \text{Age} + \text{Sex} + \text{GM volume} + \text{Group} \qquad \textbf{Eq. 5.1.}$$

Voxel-based analysis revealed extensive decreased perfusion in the CADASIL patient group compared to the healthy controls. A single widespread cluster ($p < 0.05$, threshold free cluster enhancement corrected) encompassing the frontal, pre-frontal, anterior-occipital, parietal, and temporal lobes was identified (Figure 5.1). No clusters of significant hyperperfusion in the CADASIL group compared to healthy controls were found.

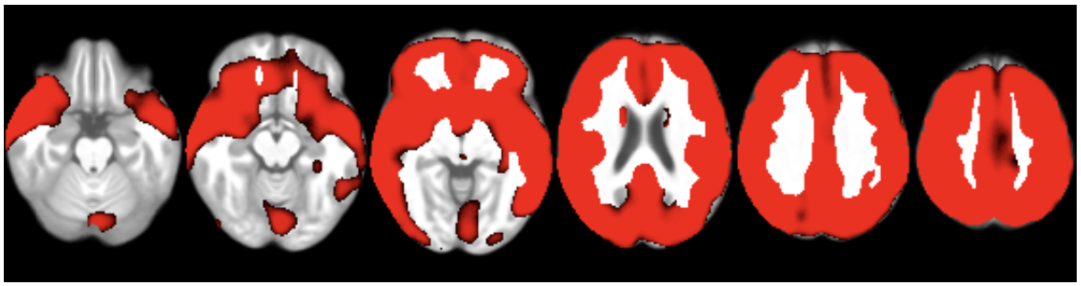

FIG. 5.1. Red indicates regions with significantly lower perfusion in CADASIL patients (PCA) than in healthy controls (HC). All results were family-wise error corrected for multiple comparisons using TFCE ($p<0.05$), displayed in radiological convention (the left side of the image represents the right side of the brain). Slices displayed: z = -21, -14, -4, 22, 34, 50 mm.

5.2 Voxel-wise Perfusion with Relation to Behavioral Metrics

The correlation between GM perfusion and behavioral metrics (repaired error distance and error distance) was analysed for the whole population (CADASIL patients and healthy controls) using a general linear model (GLM) (Eq. 5.2).

$$\text{GM perfusion} \sim \text{Age} + \text{Sex} + \text{GM volume} + \text{Behavioral metric} \qquad \textbf{Eq. 5.2.}$$

I then explored whether the association between GM perfusion and the behavioral metrics differed between the HC and PCA groups. I used three different models in analysing the behavioral data: the most difficult condition only (condition 6), mean across conditions, and mean difference between conditions 1-3 and 4-6.

No areas survived correction for multiple comparisons ($p < 0.05$, threshold free cluster enhancement corrected), indicating (1) no significant association between cerebral blood flow (CBF) and any of the behavioral measures, and (2) no difference in this association between the two groups.

5.3 Region of Interest Analysis

Presentation of regions of interest analysis, selected a priori follows, using two models. These regions are involved in executive function and spatial memory, and are also known to be affected by CADASIL (Fallon, Zokaei, and Husain, 2016).

Model 1: First, I investigated the relationship between behavioral metric and GM perfusion across all subjects. Using a linear regression, the behavioral metric (repaired error and error distance) was modelled as a function of age, sex, and GM perfusion (Eq. 5.3). In Figures 5.2 to 5.11, the relationship between GM perfusion and behavioral metric is represented by the black dashed lines.

$$\text{Behavioral metric} \sim \text{Age} + \text{Sex} + \text{GM perfusion} \qquad \textbf{Eq. 5.3.}$$

Model 2: In order to determine whether the association between behaviour and MRI differed between the HC and PCA groups, both group (HC/PCA) and group-by-GM perfusion interaction terms were added to Model 1 (Eq. 5.4). In Figures 5.2 to 5.11, the relationship between GM perfusion and behavioral metric within each group is represented by the red (HC) and blue (PCA) coloured lines.

$$\text{Behavioral metric} \sim \text{Age} + \text{Sex} + \text{GM perfusion} * \text{Group} \qquad \textbf{Eq. 5.4.}$$

All figures show the behavioral data from the most difficult condition only (condition 6), but I also report results from the other models: mean across conditions and mean difference between conditions 1-3 and 4-6. Parameter estimates from one-way ANCOVAs are reported; $p<0.05$ was considered significant. In addition, the Akaike Information Criteria (AIC) is reported for each model as a measure of model fit. A smaller AIC suggests a better model fit.

5.3.1 Repaired Error Distance

5.3.1.1. Anterior cingulate cortex (ACC) and midcingulate cortex (MCC), condition 6

Figure 5.2 reports the relationship between the cingulate cortex and repaired error distance. In model 1, I observed no significant association between repaired error distance and grey matter perfusion [F(1) = 3.2, p = 0.09]. In model 2, I observed no significant difference in GM perfusion between the groups [F(1) = 2.9, p = 0.1], no significant association between repaired error distance and GM perfusion [F(1) = 0.2, p = 0.6], and no interaction between group and GM perfusion [F(1) = 0.001, p = 0.97]. Model 1 AIC = 331.2; Model 2 AIC = 331.9.

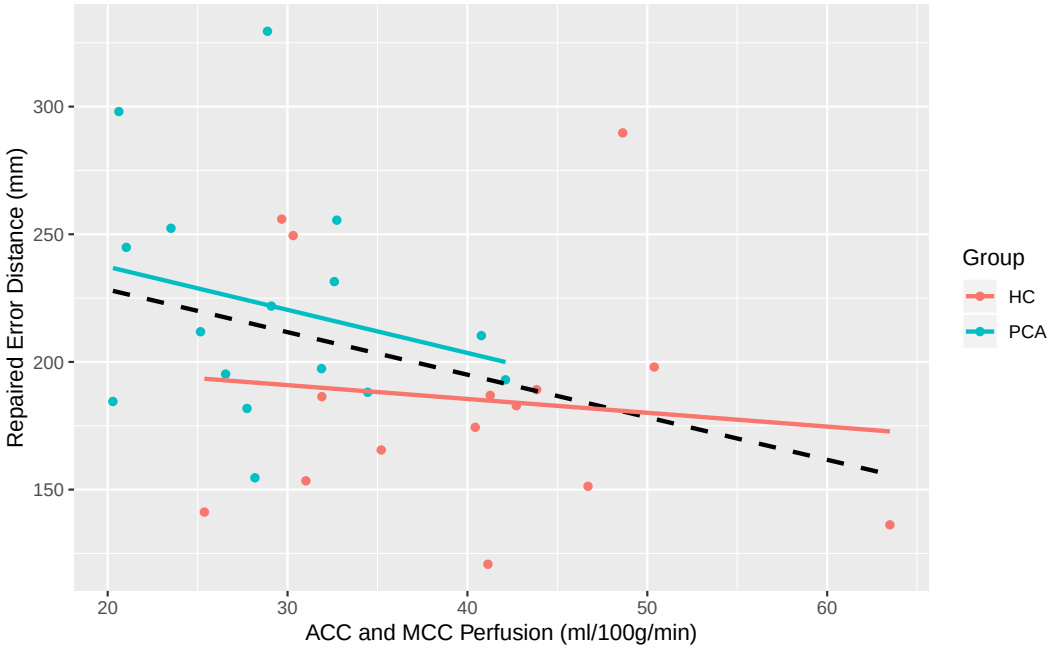

FIG. 5.2. Scatter plot of perfusion in the combined ACC and MCC for each subject in relation to repaired error distances at condition 6. The black dashed line is the line of best fit across all the subjects combined. Coloured lines indicate the line of best fit within each group (red for HC and blue for PCA).

Mean model

I also carried out a one-way ANCOVA on mean repaired error distance. In model 1, I observed no significant association between repaired error distance and grey matter perfusion [F(1) = 3.8, p = 0.06]. In model 2, I observed no significant difference in GM perfusion between the groups [F(1) = 0.8, p = 0.4], no significant association between repaired error distance and GM perfusion [F(1) = 1.1, p = 0.3], and no interaction between group and GM perfusion [F(1) = 1.2, p = 0.3]. Model 1 AIC = 301.1; Model 2 AIC = 302.7.

Mean difference model
One-way ANCOVA was also performed for the mean difference model. In model 1, I observed no significant association between repaired error distance and grey matter perfusion [F(1) = 3.8, p = 0.06]. In model 2, I observed no significant difference in GM perfusion between the groups [F(1) = 3.6, p = 0.07], no significant association between repaired error distance and GM perfusion [F(1) = 0.3, p = 0.6], and no interaction between group and GM perfusion [F(1) = 0.6, p = 0.4]. Model 1 AIC = 293.5; Model 2 AIC = 292.7.

5.3.1.2. Middle frontal gyrus, condition 6

Figure 5.3 reports the relationship between the middle frontal gyrus and repaired error distance. In model 1, I observed a significant association between repaired error distance and grey matter perfusion [F(1) = 4.2, p = 0.049]. In model 2, I observed no significant difference in GM perfusion between the groups [F(1) = 1.8, p = 0.2], no significant association between repaired error distance and GM perfusion [F(1) = 0.2, p = 0.7], and no interaction between group and GM perfusion [F(1) = 0.2, p = 0.7]. Model 1 AIC = 330.1; Model 2 AIC = 331.8.

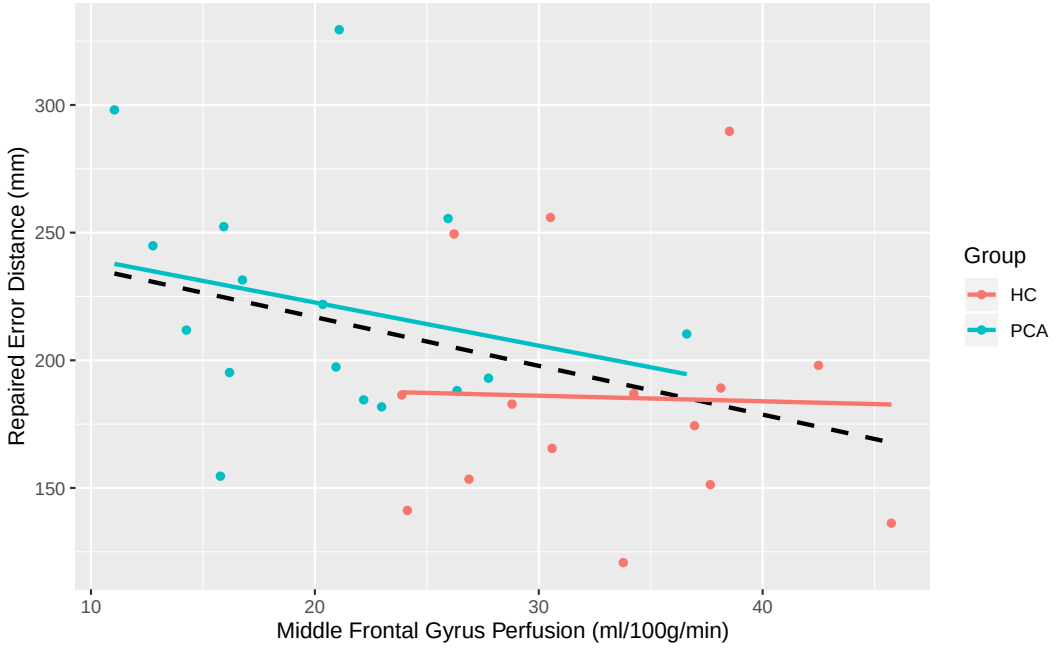

FIG. 5.3. Scatter plot of perfusion in the middle frontal gyrus for each subject in relation to repaired error distances at condition 6. The black dashed line is the line of best fit across all the subjects combined. Coloured lines indicate the line of best fit within each group (red for HC and blue for PCA).

Mean model
I also carried out a one-way ANCOVA on mean repaired error distance. In model 1, I observed no significant association between repaired error distance and grey matter perfusion [F(1) = 6.9, p = 0.01]. In model 2, I observed no significant difference in GM perfusion between the groups [F(1) = 0.0, p = 0.99], no significant association

between repaired error distance and GM perfusion [F(1) = 3.2, p = 0.09], and no interaction between group and GM perfusion [F(1) = 2.4, p = 0.1]. Model 1 AIC = 298.1; Model 2 AIC = 299.2.

Mean difference model
One-way ANCOVA was also performed for the mean difference model. In model 1, I observed a significant association between repaired error distance and grey matter perfusion [F(1) = 5.6, p = 0.03]. In model 2, I observed no significant difference in GM perfusion between the groups [F(1) = 2.1, p = 0.2], no significant association between repaired error distance and GM perfusion [F(1) = 0.4, p = 0.6], and no interaction between group and GM perfusion [F(1) = 2.0, p = 0.2]. Model 1 AIC = 291.7; Model 2 AIC = 291.0.

5.3.1.3. Hippocampus, condition 6

Figure 5.4 reports the relationship between the hippocampus and repaired error distance. In model 1, I observed no significant association between repaired error distance and grey matter perfusion [F(1) = 2.2, p = 0.1]. In model 2, I observed a significant difference in GM perfusion between the groups [F(1) = 4.4, p = 0.046], but no significant association between repaired error distance and GM perfusion [F(1) = 0.8, p = 0.4], and no interaction between group and GM perfusion [F(1) = 0.1, p = 0.7]. Model 1 AIC = 332.2; Model 2 AIC = 331.0.

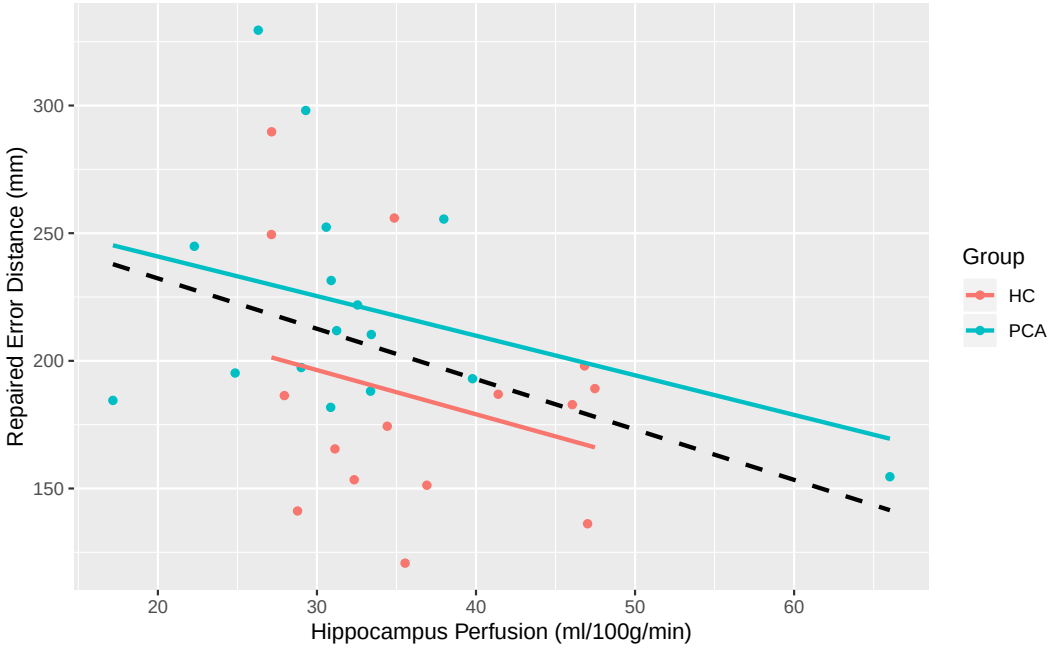

FIG. 5.4. Scatter plot of perfusion in the hippocampus for each subject in relation to repaired error distances at condition 6. The black dashed line is the line of best fit across all the subjects combined. Coloured lines indicate the line of best fit within each group (red for HC and blue for PCA).

Mean model
I also carried out a one-way ANCOVA on mean repaired error distance. In model 1, I observed no significant association between repaired error distance and grey matter perfusion [F(1) = 2.0, p = 0.2]. In model 2, I observed no significant difference in GM perfusion between the groups [F(1) = 2.1, p = 0.2], no significant association between repaired error distance and GM perfusion [F(1) = 0.9, p = 0.3], and no interaction between group and GM perfusion [F(1) = 0.0, p = 0.98]. Model 1 AIC = 302.9; Model 2 AIC = 304.4.

Mean difference model
One-way ANCOVA was also performed for the mean difference model. In model 1, I observed no significant association between repaired error distance and grey matter perfusion [F(1) = 0.01, p = 0.9]. In model 2, I observed a significant difference in GM perfusion between the groups [F(1) = 7.7, p = 0.01], but no significant association between repaired error distance and GM perfusion [F(1) = 0.5, p = 0.5], and no interaction between group and GM perfusion [F(1) = 0.006, p = 0.9]. Model 1 AIC = 297.5; Model 2 AIC = 293.2.

5.3.1.4. Caudate, condition 6

Figure 5.5 reports the relationship between the caudate and repaired error distance. In model 1, I observed no significant association between repaired error distance and grey matter perfusion [F(1) = 3.0, p = 0.1]. In model 2, I observed no significant difference in GM perfusion between the groups [F(1) = 2.9, p = 0.1], no significant association between repaired error distance and GM perfusion [F(1) = 0.1, p = 0.7], and no interaction between group and GM perfusion [F(1) = 0.2, p = 0.7]. Model 1 AIC = 331.4; Model 2 AIC = 331.8.

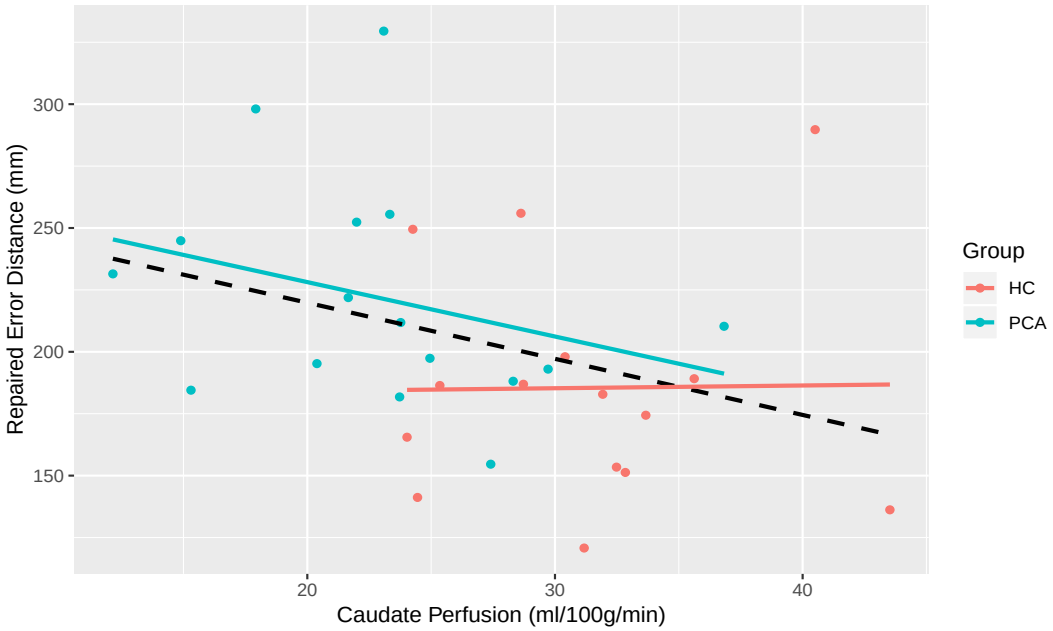

FIG. 5.5. Scatter plot of perfusion in the caudate for each subject in relation to repaired error distances at condition 6. The black dashed line is the line of best fit across all the subjects combined. Coloured lines indicate the line of best fit within each group (red for HC and blue for PCA).

Mean model

I also carried out a one-way ANCOVA on mean repaired error distance. In model 1, I observed a significant association between repaired error distance and grey matter perfusion [F(1) = 4.4, p = 0.04]. In model 2, I observed no significant difference in GM perfusion between the groups [F(1) = 0.6, p = 0.5], no significant association between repaired error distance and GM perfusion [F(1) = 1.6, p = 0.2], and no interaction between group and GM perfusion [F(1) = 2.3, p = 0.1]. Model 1 AIC = 300.4; Model 2 AIC = 301.1.

Mean difference model

One-way ANCOVA was also performed for the mean difference model. In model 1, I observed no significant association between repaired error distance and grey matter perfusion [F(1) = 4.0, p = 0.06]. In model 2, I observed no significant difference in GM perfusion between the groups [F(1) = 3.3, p = 0.08], no significant association between repaired error distance and GM perfusion [F(1) = 0.3, p = 0.6], and no interaction between group and GM perfusion [F(1) = 0.09, p = 0.8]. Model 1 AIC = 293.2; Model 2 AIC = 293.3.

5.3.1.5. Putamen, condition 6

Figure 5.6 reports the relationship between the putamen and repaired error distance. In model 1, I observed no significant association between repaired error distance and grey matter perfusion [F(1) = 2.7, p = 0.1]. In model 2, I observed no significant difference in GM perfusion between the groups [F(1) = 3.1, p = 0.09], no significant association between repaired error distance and GM perfusion [F(1) = 0.05, p = 0.8],

and no interaction between group and GM perfusion [F(1) = 0.02, p = 0.9]. Model 1 AIC = 331.7; Model 2 AIC = 332.1.

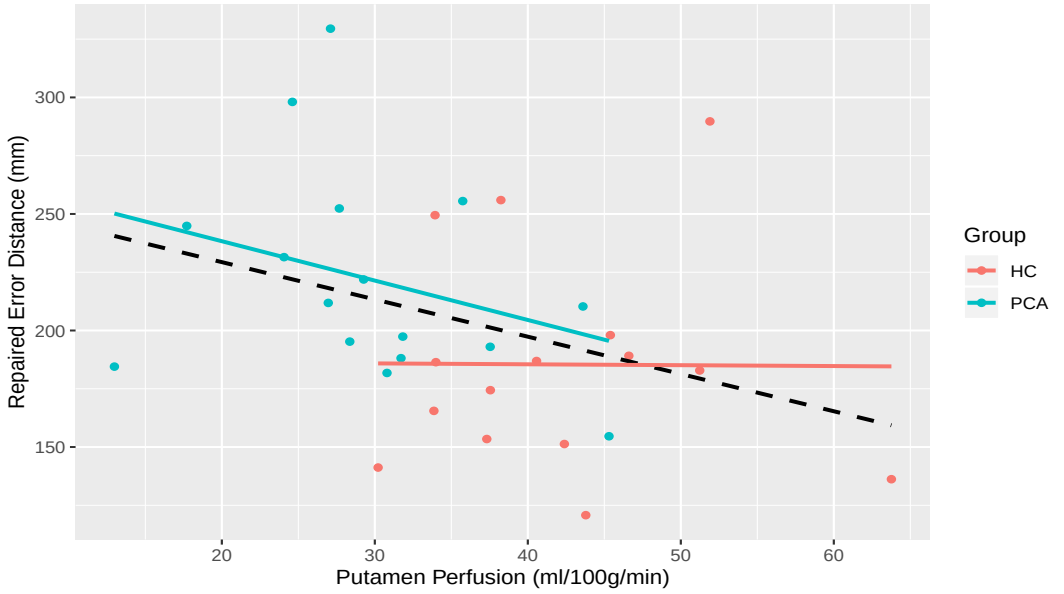

FIG. 5.6. Scatter plot of perfusion in the putamen for each subject in relation to repaired error distances at condition 6. The black dashed line is the line of best fit across all the subjects combined. Coloured lines indicate the line of best fit within each group (red for HC and blue for PCA).

Mean model

I also carried out a one-way ANCOVA on mean repaired error distance. In model 1, I observed no significant association between repaired error distance and grey matter perfusion [F(1) = 3.7, p = 0.06]. In model 2, I observed no significant difference in GM perfusion between the groups [F(1) = 0.7, p = 0.4], no significant association between repaired error distance and GM perfusion [F(1) = 1.0, p = 0.3], and no interaction between group and GM perfusion [F(1) = 1.4, p = 0.3]. Model 1 AIC = 301.1; Model 2 AIC = 302.7.

Mean difference model

One-way ANCOVA was also performed for the mean difference model. In model 1, I observed a significant association between repaired error distance and grey matter perfusion [F(1) = 4.4, p = 0.046]. In model 2, I observed no significant difference in GM perfusion between the groups [F(1) = 3.0, p = 0.1], no significant association between repaired error distance and GM perfusion [F(1) = 0.3, p = 0.6], and no interaction between group and GM perfusion [F(1) = 0.1, p = 0.8]. Model 1 AIC = 292.9; Model 2 AIC = 293.3.

5.3.2 Error Distance

5.3.2.1. Anterior cingulate cortex (ACC) and midcingulate cortex (MCC), condition 6

Figure 5.7 reports the relationship between the cingulate cortex and error distance. In model 1, I observed no significant association between error distance and grey matter perfusion [F(1) = 0.3, p = 0.6]. In model 2, I observed no significant difference in GM perfusion between the groups [F(1) = 3.4, p = 0.08], no significant association between error distance and GM perfusion [F(1) = 2.3, p = 0.1], and no interaction between group and GM perfusion [F(1) = 0.8, p = 0.4]. Model 1 AIC = 378.0; Model 2 AIC = 377.2.

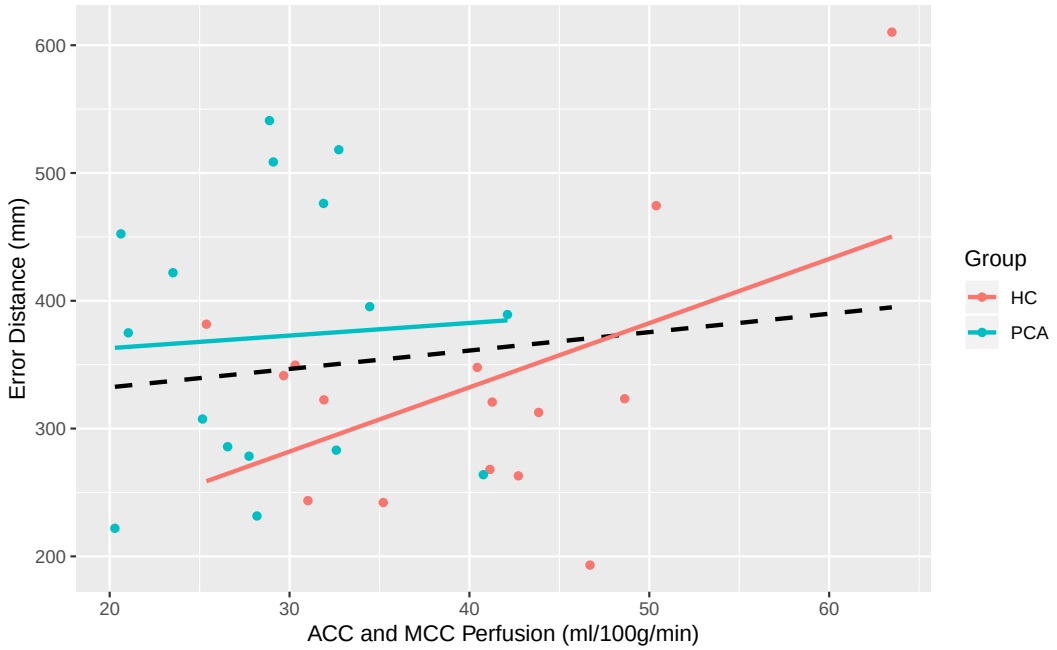

FIG. 5.7. Scatter plot of perfusion in the ACC and MCC for each subject in relation to error distances at condition 6. The black dashed line is the line of best fit across all the subjects combined. Coloured lines indicate the line of best fit within each group (red for HC and blue for PCA).

Mean model
I also carried out a one-way ANCOVA on mean error distance. In model 1, I observed no significant association between error distance and grey matter perfusion [F(1) = 0.008, p = 0.9]. In model 2, I observed no significant difference in GM perfusion between the groups [F(1) = 1.4, p = 0.2], no significant association between error distance and GM perfusion [F(1) = 0.4, p = 0.5], and no interaction between group and GM perfusion [F(1) = 1.2, p = 0.3]. Model 1 AIC = 354.8; Model 2 AIC = 355.8.

Mean difference model
One-way ANCOVA was also performed for the mean difference model. In model 1, I observed no significant association between error distance and grey matter perfusion [F(1) = 0.5, p = 0.5]. In model 2, I observed no significant difference in GM

perfusion between the groups [F(1) = 0.8, p = 0.4], no significant association between error distance and GM perfusion [F(1) = 1.2, p = 0.3], and no interaction between group and GM perfusion [F(1) = 0.9, p = 0.1]. Model 1 AIC = 358.1; Model 2 AIC = 357.8.

5.3.2.2. Middle frontal gyrus, condition 6

Figure 5.8 reports the relationship between the middle frontal gyrus and error distance. In model 1, I observed no significant association between error distance and grey matter perfusion [F(1) = 0.2, p = 0.7]. In model 2, I observed no significant difference in GM perfusion between the groups [F(1) = 1.7, p = 0.2], and no significant association between error distance and GM perfusion [F(1) = 0.4, p = 0.5], however there was a significant interaction between group and GM perfusion [F(1) = 5.2, p = 0.03]. Model 1 AIC = 378.1; Model 2 AIC = 374.5.

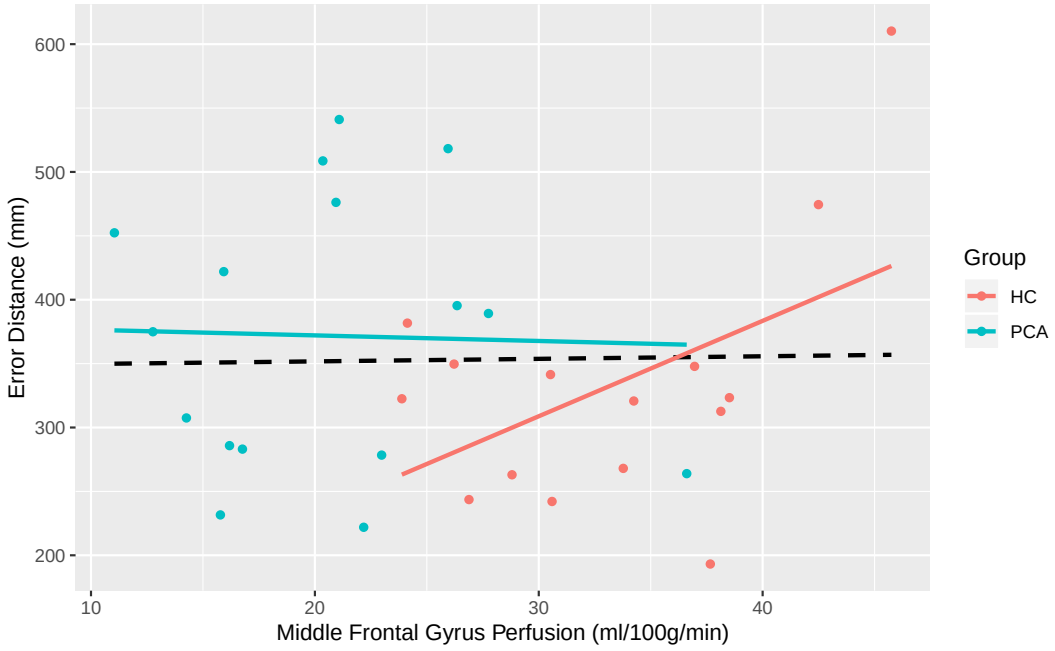

FIG. 5.8. Scatter plot of perfusion in the middle frontal gyrus for each subject in relation to error distances at condition 6. The black dashed line is the line of best fit across all the subjects combined. Coloured lines indicate the line of best fit within each group (red for HC and blue for PCA).

Mean model

I also carried out a one-way ANCOVA on mean error distance. In model 1, I observed no significant association between error distance and grey matter perfusion [F(1) = 1.2, p = 0.3]. In model 2, I observed no significant difference in GM perfusion between the groups [F(1) = 0.1, p = 0.8], no significant association between error distance and GM perfusion [F(1) = 0.3, p = 0.6], and no interaction between group and GM perfusion [F(1) = 4.0, p = 0.06]. Model 1 AIC = 353.4; Model 2 AIC = 352.7.

Mean difference model
One-way ANCOVA was also performed for the mean difference model. In model 1, I observed no significant association between error distance and grey matter perfusion [F(1) = 0.03, p = 0.9]. In model 2, I observed no significant difference in GM perfusion between the groups [F(1) = 0.09, p = 0.8], and no significant association between error distance and GM perfusion [F(1) = 0.007, p = 0.9], however there was a significant interaction between group and GM perfusion [F(1) = 7.5, p = 0.01]. Model 1 AIC = 358.6; Model 2 AIC = 354.4.

5.3.2.3. Hippocampus, condition 6

Figure 5.9 reports the relationship between the hippocampus and error distance. In model 1, I observed no significant association between error distance and grey matter perfusion [F(1) = 0.3, p = 0.6]. In model 2, I observed no significant difference in GM perfusion between the groups [F(1) = 1.9, p = 0.2], no significant association between error distance and GM perfusion [F(1) = 0.9, p = 0.4], and no interaction between group and GM perfusion [F(1) = 0.1, p = 0.8]. Model 1 AIC = 377.9; Model 2 AIC = 379.6.

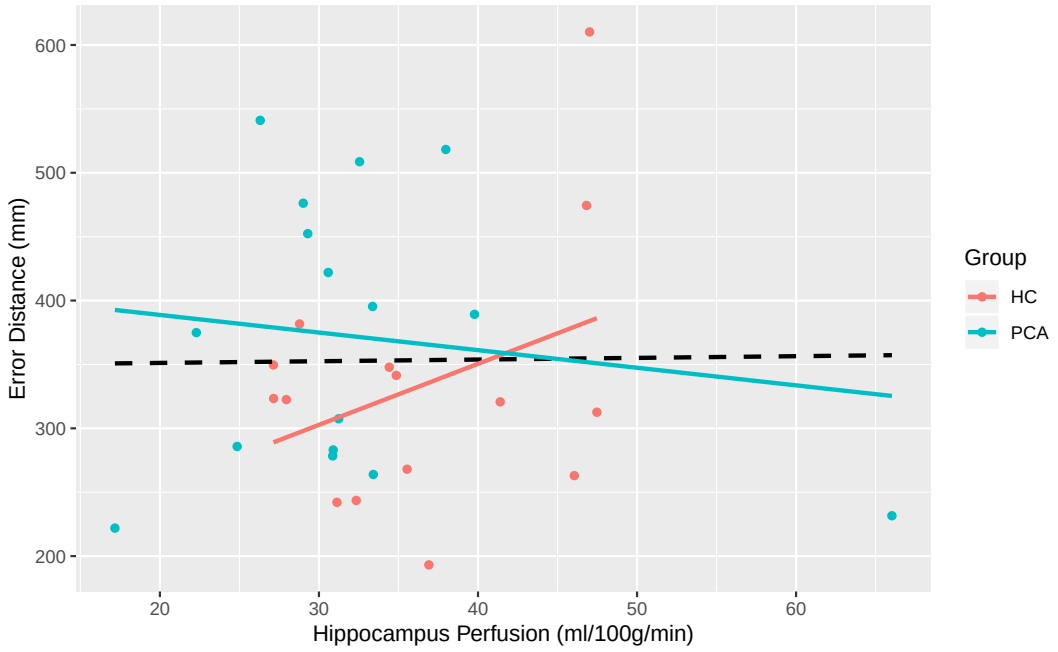

FIG. 5.9. Scatter plot of perfusion in the hippocampus for each subject in relation to error distances at condition 6. The black dashed line is the line of best fit across all the subjects combined. Coloured lines indicate the line of best fit within each group (red for HC and blue for PCA).

Mean model
I also carried out a one-way ANCOVA on mean error distance. In model 1, I observed no significant association between error distance and grey matter perfusion [F(1) = 1.2, p = 0.7]. In model 2, I observed no significant difference in GM perfusion

between the groups [F(1) = 0.8, p = 0.4], no significant association between error distance and GM perfusion [F(1) = 0.02, p = 0.9], and no interaction between group and GM perfusion [F(1) = 0.004, p = 0.9]. Model 1 AIC = 354.6; Model 2 AIC = 357.6.

Mean difference model
One-way ANCOVA was also performed for the mean difference model. In model 1, I observed no significant association between error distance and grey matter perfusion [F(1) = 0.1, p = 0.8]. In model 2, I observed no significant difference in GM perfusion between the groups [F(1) = 0.2, p = 0.7], no significant association between error distance and GM perfusion [F(1) = 0.2, p = 0.7], and no interaction between group and GM perfusion [F(1) = 0.0, p = 0.98]. Model 1 AIC = 358.5; Model 2 AIC = 362.3.

5.3.2.4. Caudate, condition 6

Figure 5.10 reports the relationship between the caudate and error distance. In model 1, I observed no significant association between error distance and grey matter perfusion [F(1) = 0.0, p = 0.995]. In model 2, I observed no significant difference in GM perfusion between the groups [F(1) = 2.2, p = 0.2], no significant association between error distance and GM perfusion [F(1) = 0.8, p = 0.4], and no interaction between group and GM perfusion [F(1) = 1.9, p = 0.2]. Model 1 AIC = 378.3; Model 2 AIC = 377.5.

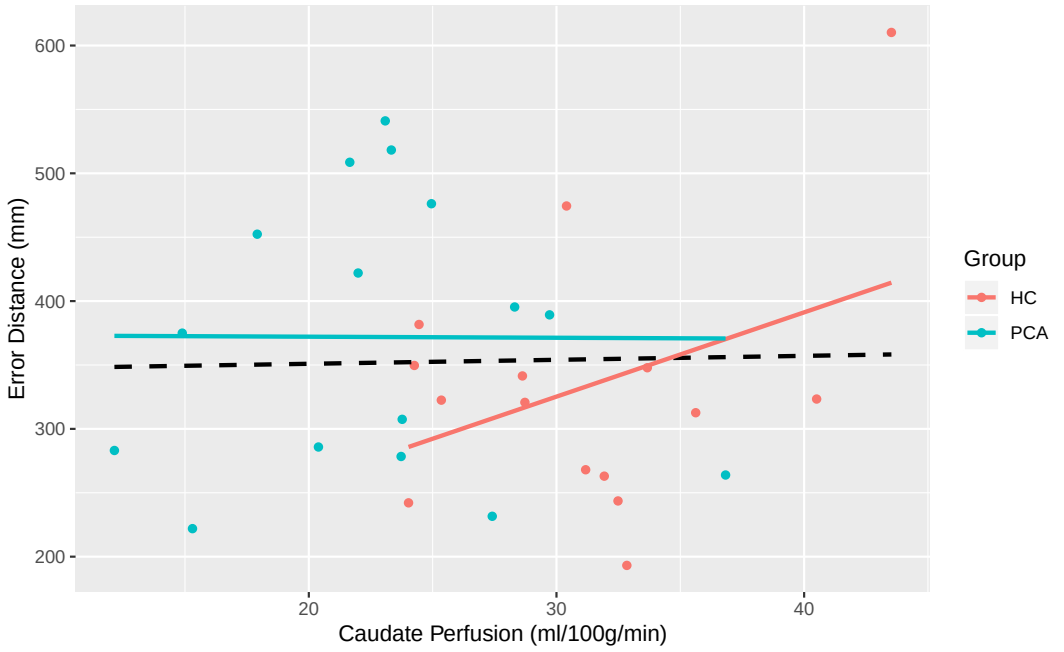

FIG. 5.10. Scatter plot of perfusion in the caudate for each subject in relation to error distances at condition 6. The black dashed line is the line of best fit across all the subjects combined. Coloured lines indicate the line of best fit within each group (red for HC and blue for PCA).

Mean model
I also carried out a one-way ANCOVA on mean error distance. In model 1, I observed no significant association between error distance and grey matter perfusion [F(1) = 0.2, p = 0.6]. In model 2, I observed no significant difference in GM perfusion between the groups [F(1) = 0.9, p = 0.3], no significant association between error distance and GM perfusion [F(1) = 0.04, p = 0.8], and no interaction between group and GM perfusion [F(1) = 3.0, p = 0.1]. Model 1 AIC = 354.6; Model 2 AIC = 354.1.

Mean difference model
One-way ANCOVA was also performed for the mean difference model. In model 1, I observed no significant association between error distance and grey matter perfusion [F(1) = 0.07, p = 0.8]. In model 2, I observed no significant difference in GM perfusion between the groups [F(1) = 0.4, p = 0.5], and no significant association between error distance and GM perfusion [F(1) = 0.3, p = 0.6], however there was a significant interaction between group and GM perfusion [F(1) = 4.5, p = 0.04]. Model 1 AIC = 358.6; Model 2 AIC = 357.0.

5.3.2.5. Putamen, condition 6

Figure 5.11 reports the relationship between the putamen and error distance. In model 1, I observed no significant association between error distance and grey matter perfusion [F(1) = 0.2, p = 0.6]. In model 2, I observed no significant difference in GM perfusion between the groups [F(1) = 3.6, p = 0.07], no significant association between error distance and GM perfusion [F(1) = 2.5, p = 0.1], and no interaction between group and GM perfusion [F(1) = 0.6, p = 0.5]. Model 1 AIC = 378.0; Model 2 AIC = 377.2.

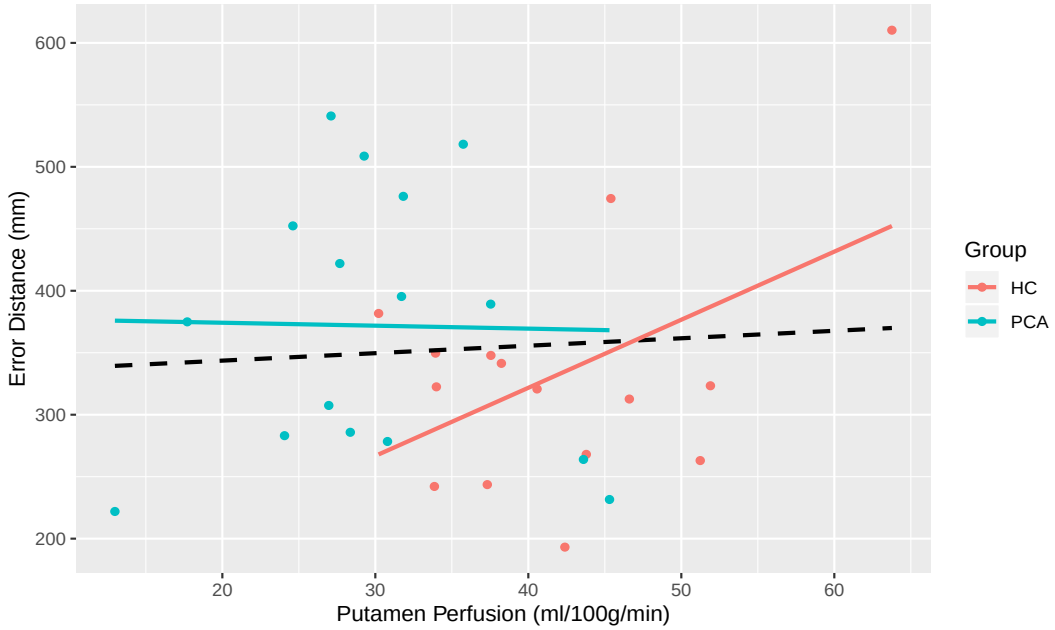

FIG. 5.11. Scatter plot of perfusion in the putamen for each subject in relation to error distances at condition 6. The black dashed line is the line of best fit across all the subjects combined. Coloured lines indicate the line of best fit within each group (red for HC and blue for PCA).

Mean model
I also carried out a one-way ANCOVA on mean error distance. In model 1, I observed no significant association between error distance and grey matter perfusion [F(1) = 0.03, p = 0.9]. In model 2, I observed no significant difference in GM perfusion between the groups [F(1) = 1.4, p = 0.3], no significant association between error distance and GM perfusion [F(1) = 0.4, p = 0.6], and no interaction between group and GM perfusion [F(1) = 1.5, p = 0.2]. Model 1 AIC = 354.8; Model 2 AIC = 355.4.

Mean difference model
One-way ANCOVA was also performed for the mean difference model. In model 1, I observed no significant association between error distance and grey matter perfusion [F(1) = 0.4, p = 0.5]. In model 2, I observed no significant difference in GM perfusion between the groups [F(1) = 0.9, p = 0.4], no significant association between error distance and GM perfusion [F(1) = 1.2, p = 0.3], and no interaction between group and GM perfusion [F(1) = 2.7, p = 0.1]. Model 1 AIC = 358.2; Model 2 AIC = 358.0.

5.4 Summary of Perfusion Findings

The CADASIL group had lower grey matter perfusion across widespread cortical and subcortical areas relative to healthy controls. At the voxel level, I observed no areas showing a significant relationship between perfusion and behavioral metrics. Regionally, the middle frontal gyrus and hippocampus showed significant repaired error correlation with cerebral blood flow in model 1. Furthermore, the middle frontal gyrus showed significant group-by-CBF interaction for the error metric. However, no significant group correlation with CBF was seen in model 2.

Generally, an AIC difference that is greater than two is taken to have substantial support that one model fits better than another (Burnham and Anderson, 2002). The AIC in this GM perfusion study suggested one of the models was better than the other, however this was not always in a consistent direction (i.e. for some regions model 1 had a higher AIC and did better, whilst model 2 was better for others). This therefore suggests that adding group as a factor does not necessarily improve the model, and may thus allude that the behavioral metrics (repaired error and error distance), GM perfusion, and group are all interlinked and tightly correlated.

Chapter 6

Discussion

This study examined executive dysfunction in CADASIL using a novel behavioral task and MRI brain scans. Participants were invited to perform the Dalmatian task, and I evaluated those results alongside their structural and perfusion MRI scans. From the behavioral results in Chapter 3, evidence suggests that working memory is affected in CADASIL, but spatial binding seems to be independent of the disease. For structural MR imaging (Chapter 4), I found a pattern of symmetrical GM atrophy in the medial and lateral frontal cortex, and temporal regions. Finally, the ASL perfusion MRI results from Chapter 5 showed that CADASIL patients had extensive hypoperfusion encompassing the frontal, pre-frontal, anterior-occipital, parietal, and temporal lobes. I found associations between the behavioral metrics (repaired error and error distances) and both MR metrics (GM volume and GM perfusion). There was some weak evidence to suggest a difference in the relationship between the healthy control group (HC) and CADASIL patient group (PCA), and MR metrics (i.e. no interaction).

6.1 Findings

6.1.1 Dalmatian Task

The novel Dalmatian task design was used as a fine-grained measure for investigating working memory, with particular focus on distinguishing between contributions from spatial working memory and the spatial binding of information. Repaired error distance was used as a measure of spatial working memory only (for location), whereas error distance was used to measure the subjects' spatial working memory and spatial binding ability of the dots (conditions 1-6) to their respective locations.

The behavioral study showed a significant group-by-repaired error distance interaction for condition. This indicates that spatial working memory was more affected in CADASIL as the task became increasingly difficult. Error distance, however, showed no significant interaction term, and no evidence of a difference between CADASIL and control subjects, suggesting that spatial binding may be independent of the disease. The behavioral results therefore suggest that executive dysfunction in CADASIL may not affect all aspects equally; spatial binding may remain unchanged, while spatial working memory deteriorates.

The post-hoc analysis for repaired error distance showed significant difference between the CADASIL group and healthy control group in conditions 4-6, but not in conditions 1-3. This created a natural divider between the easier conditions (1-3 dots), where both groups performed similarly, and the harder conditions (4-6 dots), where the CADASIL group performed worse than the healthy controls. This provided an ability to baseline each subject's performance on easier conditions in order to compare the harder conditions; this was later used to calculate the mean difference between conditions 1-3 and 4-6 as a single behavioral metric to use with MR metric analysis. The mean across conditions 1-6 was also used as a single behavioral measure for each subject. However, this was the weakest metric as the (repaired) error distance for each subject ranged greatly between the first condition (easiest) and the sixth (hardest). This led to the final single behavioral metric - using condition 6 only (with 6 dots). Condition 6 was the most difficult condition in the Dalmatian task, so it was expected to show the greatest difference in spatial working memory ability between the subjects. As such, I chose to use condition 6 as the main behavioral metric during analysis with MR metrics. However, as there is no consensus in the literature about which metric is most appropriate, I also reported results from the mean across conditions 1-6, and the mean difference between conditions 1-3 and 4-6. From this study, condition 6 and the mean difference between conditions 1-3 and 4-6 both report a significant p-value of 0.004 for repaired error distance, which corresponds with the significant interaction term between the groups and conditions. The mean across conditions 1-6 was also significantly different between groups, but to a lesser extent ($p = 0.02$). For error distance, the p-values for all three metrics used were insignificant; conditions 6 $p = 0.15$, mean difference $p = 0.46$, mean $p = 0.12$. This was expected as error distance did not have a significant interaction term between the groups and conditions, however this does not necessarily mean there is no relationship between the groups and conditions; there was merely no significant evidence for such. In this instance, it seemed condition 6 and mean across conditions 1-6 have similar results, whereas mean difference between conditions 1-3 and 4-6 was the anomaly. Condition 6 was the hardest in the Dalmatian task, the most sensitive to picking up abnormalities, and also the least likely to have a ceiling effect in terms of the level of difficulty, so I felt the most justified in choosing condition 6 as the main behavioral metric to analyse with the MR metrics.

Filley et al. (1999) reported that cognitive impairment in CADASIL was dominated by early executive dysfunction. This was corroborated by Buffon et al. (2006), where they determined particular decline in attention and working memory. Buffon et al. (2006) found significantly altered cognitive performance of visuospatial abilities for all patients, and visuospatial working memory seemed to be significantly worse in patients over 60 years old than in younger patients. Dichgans (2009) also reported executive dysfunction and compromised spatial working memory in CADASIL patients compared to healthy controls. Buffon et al. (2006) also suggested that the memory dysfunction in younger patients was more regionally located in the subcortical-frontal networks, whereas the older patients have more homogeneous and widespread cortical dysfunction as well. These studies all support my behavioral results of significantly impaired spatial working memory. However, I demonstrated that it is a specific component of spatial working memory that is disrupted. This is theoretically mediated by frontal cortical processes, in contrast to the binding of information (theoretically relying more on medial temporal lobe function).

Thus, I next explored the neural changes associated with CADASIL and spatial working memory, using T1 MRI.

6.1.2 T1 Structural MRI

Using structural MRI brain scans, I investigated how CADASIL affected grey matter volume when compared to a healthy population. Results presented here are in accord with previous work. A previous study by Rossi Espagnet et al. (2012) had a similar number of participants (14 CADASIL subjects) to my study, and also performed their analysis using voxel-based morphometry (VBM). They reported three significantly decreased GM volume clusters in the CADASIL group compared to the healthy controls: bilaterally in the middle temporal gyrus, and in the caudate nucleus. These were consistent with my findings, however I also found significant clusters of decreased GM volume in the lateral frontal and temporal regions.

Lambert et al. (2015) examined whole brain grey matter volume change in small vessel diseases, including CADASIL. In this publication they found significant subcortical GM volume decrease for CADASIL subjects in the putamen, thalamus, and caudate, as well as cortical GM volume decrease within the parietal, occipital, and temporal lobes. This is also consistent with my findings of cortical and subcortical atrophy.

De Guio et al. (2014) studied the cortical thickness of 11 CADASIL patients against 11 healthy controls; they only found significantly reduced GM volume in the right precentral gyrus. This difference to my results may be because De Guio et al. (2014) covaried for age, sex, and education, whereas I covaried for intracranial volume (ICV) instead of education. Furthermore, with only 11 participants per group, the study was most likely underpowered and may have missed regions of grey matter atrophy. The inclusion of education as a covariate may be important as education may have a protective effect on the integrity of cortical thickness (Boller et al., 2017). Furthermore, although cortical thickness and grey matter volume are both valid measurements used for cortical grey matter, they are not identical (Winkler et al., 2010). Finally, I studied grey matter atrophy in both cortical and subcortical regions, whereas De Guio et al. (2014) only considered cortical regions. As a result, it seems plausible that De Guio et al. (2014) reported fewer regions of significance compared to the nine regions in my study. The observed volumetric changes from my results were quite homogeneous and symmetrical, and is thus consistent with CADASIL being a symmetrical brain process (Stojanov et al., 2015).

There is a well-documented relationship between aging and grey matter atrophy in the normal population - the older the subjects are the more GM atrophy is expected (Giorgio et al., 2010). However, explanations for increased and early GM atrophy in CADASIL have only been speculated, but are not definitive. Jouvent et al. (2007) found significant atrophy in their study of 147 CADASIL patients, however their focus was on white matter microstructural health. They suggested that atrophy was related to lacunar lesions and widespread microstructural alterations. Rossi Espagnet et al. (2012) also suggested microstructural disorganization may be related to grey matter atrophy, as well as vascular damage, both as consequences of CADASIL. Another explanation suggested for GM atrophy was in correlation with white matter hyperintensities (WMH), a hallmark of CADASIL. Lambert et al. (2015)

reported that WMHs started from the frontal and parietal regions and expanded into the temporal and occipital cortices; this seemed to match the pattern of GM atrophy commonly seen, thus suggesting an association between WMH and GM atrophy. If CADASIL is indeed predominantly a white matter pathological process, atrophy may be expected to occur as a result of pathology affecting the axons and disrupting connectivity to cortical regions (Bohnen and Albin, 2011).

However, atrophy is an endstage change, whilst changes in perfusion may provide a more sensitive marker for underlying brain processes. In the case of CADASIL, it may be this hypoperfusion that also drives degeneration as decreased cerebral blood flow may ultimately lead to atrophy. The consistency and plausibility of my structural MRI results with previous literature gave me confidence that the methodology I used was robust, and thus allowed me to explore the more novel ASL MRI with confidence.

6.1.3 ASL Perfusion MRI

Vessel encoding pseudo-continuous arterial spin labelling (VEPCASL) was used as a novel approach to investigate how cerebral blood flow (CBF) is affected by CADASIL. Previous studies often used cerebral glucose metabolism (CMR_{Glc}) measured by ^{18}F-fluorodeoxyglucose positron emission tomography (^{18}F-FDG PET) as a measure of metabolism. In most cases, perfusion mirrors metabolism, and evidence suggests that metabolism has a good overall correlation with CBF measured by ASL (Cha et al., 2013). For example, Dolui et al. (2020) compared ^{18}F-FDG PET to ASL in Alzheimer's patients with mild cognitive impairment and found considerable overlap of measures in regions of known early AD neurodegeneration, including the bilateral and medial temporo-parietal regions, posterior cingulate cortex (PCC), inferior prefrontal cortex, and also regions in the subcortical gray matter such as caudate and thalamus. Furthermore, Tuominen et al. (2004) reported significantly correlated values between CBF and regional CMR_{Glc} when studying CBF in the grey matter of CADASIL patients. The CBF values for white matter regions did not correlate with regional CMR_{Glc} values, however ASL-derived white matter CBF is close to the noise floor and is not as robust as measures of GM perfusion. As such, I have focused on grey matter perfusion and considered my perfusion results in CADASIL in the context of previous FDG metabolic work.

Perfusion MRI brain scans revealed extensive hypoperfusion in the CADASIL group compared to the healthy controls, encompassing the frontal, pre-frontal, anterior-occipital, parietal, and temporal lobes. This is in line with Su et al. (2019), where ^{18}F-FDG PET was used to investigate metabolism in 24 CADASIL subjects and 24 matched healthy controls; in that study, CADASIL patients exhibited significantly lower metabolism in the right cerebellar posterior lobe, left cerebellar anterior lobe, bilateral thalamus, left hippocampus, and left parahippocampal gyrus. Tatsch et al. (2003) reported mean CMR_{Glc} was significantly reduced in all cortical and subcortical grey matter structures across their 11 CADASIL subjects, compared to the healthy control values. This included the frontal, temporal, parietal, and occipital lobes for the cortical regions, and also the caudate, putamen, and thalamus in the subcortical grey matter. Reports of extensive hypometabolism further agreed with my ASL study that cortical and subcortical grey matter perfusion were severely reduced in patients with CADASIL. There were no significant hyperperfusion findings in the

CADASIL group compared to healthy controls, as supported by Su et al. (2019) and Tatsch et al. (2003).

The extensive hypometabolism observed may be due to arteriopathy and tissue damage of the arteries as a result of CADASIL (Tuominen et al., 2004). It has also been suggested that ischemia further causes neuronal damage or neuronal loss, and may be a secondary contributing factor to the decreased CBF (Tatsch et al., 2003). Another explanation may be that this was related to grey matter atrophy, where morphological alterations of the cortical and subcortical regions lessened the structural support around the arterial walls/tunica externa.

The concordance between the ASL and FDG-PET results also suggests that ASL-MRI is an excellent modality to assess global and regional perfusion going forwards, with the clear advantage of being non-invasive and easily added to the clinical MRI session that most CADASIL patients would normally be receiving anyway.

6.2 CADASIL, Behaviour, and MR Imaging

One of the strongest findings in this thesis was the relationship between CADASIL, executive function, and MRI brain metrics (Figure 6.1). I identified a direct relationship between each pair of metrics. That is, the CADASIL group showed differences on the behavioral metric; the behavioral metric was associated with MRI brain metrics; and CADASIL showed differences on the MRI brain metrics. Identifying the independent contribution of any one of these domains on any other is extremely difficult given the interconnectedness of all domains.

Results showed that atrophy and hypoperfusion occurred in the dorsolateral prefrontal cortex regions, a key area underlying spatial working memory function (Fallon, Zokaei, and Husain, 2016), thus implying a tightly correlated relationship, as shown in Figure 6.1, between group, behavioral metrics (repaired error distance and error distance), and MR metrics (GM volume and GM perfusion). This suggests that MR may provide evidence for brain dysfunction underlying overt spatial working memory dysfunction in CADASIL.

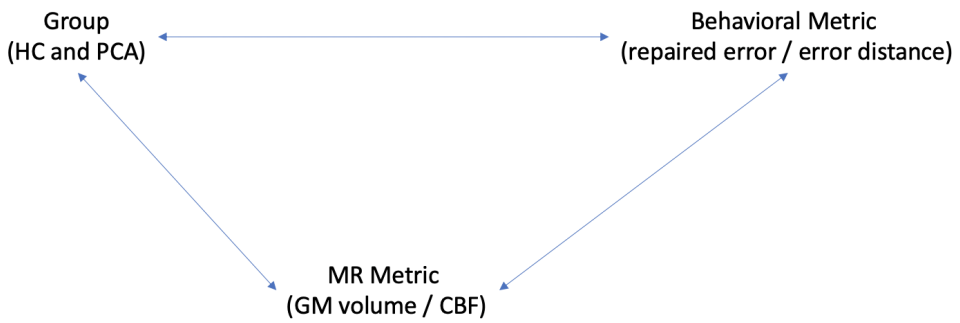

FIG. 6.1. A schematic of the relationship among executive function, MR metrics, and the two participant groups.

Given the strong relationship among the three domains, two models were used in an attempt to probe these relationships.

Model 1 investigated the relationship between the behavioral metrics and MR metrics across all subjects (CADASIL and healthy controls were combined as a single group) (Equation 6.1). This was used to establish a relationship between brain and behaviour.

$$\text{Behavioral metric} \sim \text{Age} + \text{Sex} + \text{MR metric} \qquad \textbf{Eq. 6.1.}$$

Model 2 investigated whether the association between behavior and MRI differed between the CADASIL and healthy control groups by including group and group-by-MR metric interaction terms (Eq. 6.2). Here, group captured much of the same variance captured by the MR metric. However, I specifically investigated whether there was a difference in the association between MR metric and behaviour between the groups. Across all behavioral metrics, I identified no evidence of a difference in association between controls and CADASIL participants, indicating a constant relationship between behavioral metric and brain metrics both in controls and CADASIL participants.

$$\text{Behavioral metric} \sim \text{Age} + \text{Sex} + \text{MR metric} * \text{Group} \qquad \textbf{Eq. 6.2.}$$

Significant association between structural MR and the behavioral metrics was seen in model 1. For model 2, when group was included as a covariate, the only region that indicated significant group-by-GM volume interaction was the middle frontal gyrus, with the repaired error metric. Although this was only in the mean model - all other models and regions of interest showed no significant group-by-GM volume interaction - this suggests the possibility that the middle frontal gyrus may be associated with impairment of spatial working memory in CADASIL. This was supported by the Fallon, Zokaei, and Husain (2016) study, where they reported that spatial working memory is supported by regions in the dorsolateral prefrontal cortex (DLPFC).

Perfusion MRI showed a significant GM hypoperfusion as repaired error distance increased (more impaired spatial working memory) in the middle frontal gyrus and the hippocampus for model 1. Su et al. (2019) also found lower metabolism in the hippocampus for their CADASIL group. The hypometabolism and hypoperfusion shown indicated dysfunction within the hippocampus. This suggests that the hippocampal function may be correlated with contributing to executive dysfunction in CADASIL, especially in the spatial working memory capacity. This would be very interesting as the hippocampus is more known for its spatial binding abilities of objects to their predetermined positions (Fallon, Zokaei, and Husain, 2016). For model 2, the middle frontal gyrus showed significant group-by-CBF interaction with the error metric. This was inconsistent with previous results, which may be due to the fact that ROI results did not account for multiple comparisons. Alternatively, this may suggest that the middle frontal gyrus was strongly affected in CADASIL, perhaps for both spatial working memory and spatial misbinding. This may be one of the first regions to show spatial misbinding abnormalities as executive functioning deteriorates in CADASIL patients. However, and more likely, as the error distance

metric accounts for both spatial working memory and spatial misbinding, this observation may just be reflecting the impaired spatial working memory, independent of spatial misbinding.

I observed extensive perfusion and GM volume loss in the CADASIL group, relative to healthy controls, yet their global cognitive ability was not severely impaired. This suggests, perhaps, some sort of compensation or maintenance of performance, at least on the global level. However, more subtle changes, specifically within executive function, were identified using the novel behavioral task (the 'Dalmatian task'), in which the CADASIL participants performed progressively worse as the Dalmatian task increased in difficulty. Taken together, these results suggest underlying CADASIL-associated brain changes may manifest as executive dysfunction, prior to more global cognitive issues. The novel behavioral task may therefore help assess cognitive severity in CADASIL; however, longitudinal studies are needed to confirm this.

6.3 Limitations

This study has a number of limitations. First, the sample size was relatively small. This was due to the relatively rare nature of CADASIL and the availability of CADASIL participants willing to participate. This small sample size hindered my ability to acquire more statistically meaningful results, especially for the regression analysis sections. This was also a cross-sectional study with no follow-up assessments conducted. It would be very interesting to determine if the novel behavioral task is capable of tracking the progression of executive dysfunction. Specifically, as the disease progresses, is spatial mis-binding ever affected, or is executive dysfunction confined to spatial working memory? At the time of testing and imaging, all of the CADASIL patients were not severely cognitively compromised. This resulted in a relatively small range of impairments. Even at this early stage, I identified dysfunction in spatial working memory, but more extensive association with MRI metrics may have been affected by the restricted range of behavioral metrics. As the disease progresses, it is likely that more extensive associations would emerge. Lastly, although only used to improve segmentation of GM in this thesis, white matter hyperintensity (WMH) volume was inflated in the control group. As previously mentioned, the BIANCA algorithm was maximized to capture WMH in the CADASIL group. As a consequence of using the same parameters for the control group, the algorithm was over-inclusive and WMH volume was inflated in healthy controls. Recently released updates to the BIANCA algorithm will most likely improve WMH identification across a wide range of volumes, and future work would benefit from these recent updates. However, for my purposes, the current WMH maps facilitated acceptable GM segmentation, with minimal influence of mis-classified WMHs. More broadly this emphasizes the importance of pre-processing stages of MRI analysis, particularly when there are significant changes in the underlying brain anatomy (such as in CADASIL). In fact, one possible, and important explanation for different results across different studies may be a methodological one. Given recent problems with reproducibility in many realms of neuroscience, such methodological considerations are crucial for patient-related studies.

6.4 Future Work

Future work should include a longitudinal study to track both global and domain-specific cognitive decline of CADASIL patients with both neuropsychological and behavioral assessments. Additionally, replication in a larger cohort would lend confidence to the current findings. It would also be interesting to see if the behavioral metrics will significantly correlate with grey matter atrophy and cerebral blood flow when the patients become progressively more cognitively compromised. From a national perspective, I would also be interested in investigating the incidence and prevalence of CADASIL in a New Zealand context, especially given our unique ethnic makeup (e.g., across Māori, Pasifika, Asian, and Pakeha). Furthermore, additional MR modalities should be used to investigate CADASIL, specifically resting state, diffusion tensor imaging (DTI), quantitative susceptibility mapping (QSM), and newer vascular techniques such as 4D flow and water exchange imaging to investigate the blood brain barrier (BBB) breakdown.

Chapter 7

Conclusion

In this thesis, I investigated cognitive processing and brain integrity in CADASIL using a number of different methods. First, working memory in CADASIL was investigated using the novel behavioral task to dissociate components underlying the working memory process; namely, spatial working memory and spatial binding. Using the Dalmatian task, I found a significant interaction term for conditions (number of dots to remember, which is an indication of the difficulty of the task) between the CADASIL group and the healthy controls in repaired error distance; the CADASIL group was equivalent to controls during the first 3 conditions (the easier trials), but was significantly more impaired during the three harder trials. This interaction effect was not observed for error distance metric. This suggests that spatial working memory was impaired in CADASIL, but the spatial binding of information was not affected.

Second, I investigated structural and perfusion differences associated with CADASIL using MRI. Structural MR showed regional grey matter atrophy in CADASIL patients compared to the healthy controls in the medial and lateral frontal, and temporal regions. ASL MRI displayed widespread hypoperfusion in the CADASIL group compared to the healthy controls, encompassing the frontal, pre-frontal, anterior-occipital, parietal, and temporal lobes. Results from these two imaging modalities suggest both structural and functional (perfusion) deficits in CADASIL patients.

Finally, I investigated whether the aforementioned changes in the imaging metrics can predict working memory performance in CADASIL, both globally and within specific regions of interest. Whole-brain analysis identified two small regions of significant association between grey matter volume and behavioral metrics – in the right frontal and left occipital poles. Within specific regions of interest, the anterior and midcingulate cortex (ACC and MCC) and the middle frontal gyrus showed significant behavioral correlation with GM volume. Furthermore, the hippocampus and putamen also showed significant group correlation with GM volume, whereas significant group-by-GM volume interaction was identified in the middle frontal gyrus. Whole-brain perfusion correlation analysis identified no regions that survived correction for multiple comparisons, suggesting there were no significant associations between cerebral blood flow (CBF) and the behavioral metrics. Within specific regions of interest, the middle frontal gyrus and hippocampus showed significant repaired error correlation with CBF. The middle frontal gyrus further showed significant group-by-CBF interaction for the error metric.

Taken together, the behavioral and imaging results suggest impaired brain structure, perfusion, and spatial working memory in CADASIL patients. While some areas exhibited a strong relationship between working memory performance and brain changes - suggesting that these brain changes may underlie executive dysfunction - not all executive dysfunction was directly explainable by volume or perfusion deficits. In the future, longitudinal studies with serial behavioral assessments, additional MRI modalities, and larger samples may help extend the results presented here. In conclusion, techniques used, and results obtained in this thesis provide additional insight into the underlying brain changes and specific cognitive dysfunctions that occur in CADASIL.

References

Alexander, Andrew L. et al. (2007). "Diffusion tensor imaging of the brain". In: *Neurotherapeutics* 4.3, pp. 316–329. ISSN: 1933-7213. DOI: 10.1016/j.nurt.2007.05.011.

Alsop, David C. et al. (2015). "Recommended implementation of arterial spin-labeled perfusion MRI for clinical applications: A consensus of the ISMRM perfusion study group and the European consortium for ASL in dementia". In: *Magnetic Resonance in Medicine* 73.1, pp. 102–116. ISSN: 07403194. DOI: 10.1002/mrm.25197.

Amberla, Kaarina et al. (2004). "Insidious cognitive decline in CADASIL". In: *Stroke* 35.7, pp. 1598–1602. ISSN: 00392499. DOI: 10.1161/01.STR.0000129787.92085.0a.

Anstey, K. J. and J. J. Maller (2003). "The role of volumetric MRI in understanding mild cognitive impairment and similar classifications". In: *Aging and Mental Health* 7.4, pp. 238–250. ISSN: 13607863. DOI: 10.1080/1360786031000120732.

Ashburner, John and Karl J. Friston (2000). "Voxel-based morphometry - The methods". In: *NeuroImage* 11.6 I, pp. 805–821. ISSN: 10538119. DOI: 10.1006/nimg.2000.0582.

Baird, Alison E. (2010). "Genetics and genomics of stroke: Novel approaches". In: *Journal of the American College of Cardiology* 56.4, pp. 245–253. ISSN: 07351097. DOI: 10.1016/j.jacc.2010.02.051.

Basser, Peter J. et al. (2000). "In vivo fiber tractography using DT-MRI data". In: *Magnetic Resonance in Medicine* 44.4, pp. 625–632. ISSN: 07403194. DOI: 10.1002/1522-2594(200010)44:4<625::AID-MRM17>3.0.CO;2-O.

Battaglini, Marco, Mark Jenkinson, and Nicola De Stefano (2012). "Evaluating and reducing the impact of white matter lesions on brain volume measurements". In: *Human Brain Mapping* 33.9, pp. 2062–2071. ISSN: 10659471. DOI: 10.1002/hbm.21344.

Bohnen, Nicolaas I. and Roger L. Albin (2011). "White matter lesions in Parkinson disease". In: *Nature Reviews Neurology* 7.4, pp. 229–236. ISSN: 17594758. DOI: 10.1038/nrneurol.2011.21.

Boller, Benjamin et al. (2017). "Relationships between years of education, regional grey matter volumes, and working memory-related brain activity in healthy older adults". In: *Brain Imaging and Behavior* 11.2, pp. 304–317. ISSN: 19317565. DOI: 10.1007/s11682-016-9621-7.

Bottino, Cássio M.C. et al. (2002). "Volumetric MRI measurements can differentiate Alzheimer's disease, mild cognitive impairment, and normal aging". In: *International Psychogeriatrics* 14.1, pp. 59–72. ISSN: 10416102. DOI: 10.1017/S1041610202008281.

Buffon, F. et al. (2006). "Cognitive profile in CADASIL". In: *Journal of Neurology, Neurosurgery and Psychiatry* 77.2, pp. 175–180. ISSN: 00223050. DOI: 10.1136/jnnp.2005.068726.

Burnham, Kenneth P. and David R. Anderson (2002). *Model Selection and Inference: A Practical Information-Theoretic Approach*. Ed. by Kenneth P. Burnham and David R. Anderson. 2nd. New York, NY: Springer-Verlag New York, p. 488. ISBN: 978-0-387-95364-9.

Calamante, Fernando (2013). "Arterial input function in perfusion MRI: A comprehensive review". In: *Progress in Nuclear Magnetic Resonance Spectroscopy* 74, pp. 1–32. ISSN: 00796565. DOI: 10.1016/j.pnmrs.2013.04.002.

Cantril, Hadley (1965). *The Pattern of Human Concern*. 1st. Rutgers University Press, pp. 22–24.

Cha, Yoon Hee K. et al. (2013). "Regional correlation between resting state FDG PET and pCASL perfusion MRI". In: *Journal of Cerebral Blood Flow and Metabolism* 33.12, pp. 1909–1914. ISSN: 0271678X. DOI: 10.1038/jcbfm.2013.147.

Chabriat, H. et al. (1995). "Clinical spectrum of CADASIL: a study of 7 families". In: *The Lancet* 346.8980, pp. 934–939. ISSN: 01406736. DOI: 10.1016/S0140-6736(95)91557-5.

Chabriat, H. et al. (1999). "Clinical severity in CADASIL related to ultrastructural damage in white matter: In vivo study with diffusion tensor MRI". In: *Stroke* 30.12, pp. 2637–2643. ISSN: 00392499. DOI: 10.1161/01.STR.30.12.2637.

Chabriat, Hugues et al. (2009). "Cadasil". In: *The Lancet Neurology* 8.7, pp. 643–653. ISSN: 14744422. DOI: 10.1016/S1474-4422(09)70127-9.

Chan, Raymond C.K. et al. (2008). "Assessment of executive functions: Review of instruments and identification of critical issues". In: *Archives of Clinical Neuropsychology* 23.2, pp. 201–216. ISSN: 08876177. DOI: 10.1016/j.acn.2007.08.010. arXiv: 1511.04103.

Chavoshi Tarzjani, Seyedeh Parisa et al. (2018). "Genetic study of the NOTCH3 gene in CADASIL patients". In: *Egyptian Journal of Medical Human Genetics* 19.4, pp. 425–427. ISSN: 20902441. DOI: 10.1016/j.ejmhg.2018.05.001.

Chutinet, Aurauma and Natalia S. Rost (2014). "White matter disease as a biomarker for long-term cerebrovascular disease and dementia topical collection on cerebrovascular disease and stroke". In: *Current Treatment Options in Cardiovascular Medicine* 16.3, p. 292. ISSN: 10928464. DOI: 10.1007/s11936-013-0292-z.

Dadar, Mahsa et al. (2019). "White matter in different regions evolves differently during progression to dementia". In: *Neurobiology of Aging* 76, pp. 71–79. ISSN: 15581497. DOI: 10.1016/j.neurobiolaging.2018.12.004.

De Guio, François et al. (2014). "In vivo high-resolution 7 tesla MRI shows early and diffuse cortical alterations in CADASIL". In: *PLoS ONE* 9.8. ISSN: 19326203. DOI: 10.1371/journal.pone.0106311.

De Guio, François et al. (2015). "White matter edema at the early stage of cerebral autosomal-dominant arteriopathy with subcortical infarcts and leukoencephalopathy". In: *Stroke* 46.1, pp. 258–261. ISSN: 15244628. DOI: 10.1161/STROKEAHA.114.007018.

Di Donato, Ilaria et al. (2017). "Cerebral Autosomal Dominant Arteriopathy with Subcortical Infarcts and Leukoencephalopathy (CADASIL) as a model of small vessel disease: Update on clinical, diagnostic, and management aspects". In: *BMC Medicine* 15.1, p. 41. ISSN: 17417015. DOI: 10.1186/s12916-017-0778-8.

Diamond, Adele (2013). "Executive Functions". In: *Annual Review of Psychology* 64.1, pp. 135–168. ISSN: 0066-4308. DOI: 10.1146/annurev-psych-113011-143750.

Dichgans, Martin (2009). "Cognition in CADASIL". In: *Stroke* 40.3 SUPPL. 1, S45–S47. ISSN: 00392499. DOI: 10.1161/STROKEAHA.108.534412.

Dolui, Sudipto et al. (2020). "Arterial spin labeling versus 18F-FDG-PET to identify mild cognitive impairment". In: *NeuroImage: Clinical* 25.December 2019, p. 102146. ISSN: 22131582. DOI: 10.1016/j.nicl.2019.102146.

Douaud, Gwenaëlle et al. (2007). "Anatomically related grey and white matter abnormalities in adolescent-onset schizophrenia". In: *Brain* 130.9, pp. 2375–2386. ISSN: 00068950. DOI: 10.1093/brain/awm184.

Duchesnay, Edouard et al. (2018). "Different types of white matter hyperintensities in CADASIL". In: *Frontiers in Neurology* 9.JUL, pp. 1–8. ISSN: 16642295. DOI: 10.3389/fneur.2018.00526.

Duering, Marco et al. (2011). "Strategic role of frontal white matter tracts in vascular cognitive impairment: A voxel-based lesion-symptom mapping study in CADASIL". In: *Brain* 134.8, pp. 2366–2375. ISSN: 00068950. DOI: 10.1093/brain/awr169.

Fallon, Sean James, Nahid Zokaei, and Masud Husain (2016). "Causes and consequences of limitations in visual working memory". In: *Annals of the New York Academy of Sciences* 1369.1, pp. 40–54. ISSN: 17496632. DOI: 10.1111/nyas.12992.

Filley, Christopher M. et al. (1999). "White matter dementia in CADASIL". In: *Journal of the Neurological Sciences* 163.2, pp. 163–167. ISSN: 0022510X. DOI: 10.1016/S0022-510X(99)00038-6.

Gavazzi, Gioele et al. (2019). "Functional magnetic resonance imaging of inhibitory control reveals decreased blood oxygen level dependent effect in cerebral autosomal dominant arteriopathy with subcortical infarcts and leukoencephalopathy". In: *Stroke* 50.1, pp. 69–75. ISSN: 15244628. DOI: 10.1161/STROKEAHA.118.022923.

Giorgio, Antonio et al. (2010). "Age-related changes in grey and white matter structure throughout adulthood". In: *NeuroImage* 51.3, pp. 943–951. ISSN: 10538119. DOI: 10.1016/j.neuroimage.2010.03.004.

Glover, Gary H. (2011). "Overview of functional magnetic resonance imaging". In: *Neurosurgery Clinics of North America* 22.2, pp. 133–139. ISSN: 10423680. DOI: 10.1016/j.nec.2010.11.001.

Good, Catriona D. et al. (2001). "A voxel-based morphometric study of ageing in 465 normal adult human brains". In: *NeuroImage* 14.1 I, pp. 21–36. ISSN: 10538119. DOI: 10.1006/nimg.2001.0786.

Grade, M. et al. (2015). "A neuroradiologist's guide to arterial spin labeling MRI in clinical practice". In: *Neuroradiology* 57.12, pp. 1181–1202. ISSN: 14321920. DOI: 10.1007/s00234-015-1571-z.

Griffanti, Ludovica et al. (2016). "BIANCA (Brain Intensity AbNormality Classification Algorithm): A new tool for automated segmentation of white matter hyperintensities". In: *NeuroImage* 141, pp. 191–205. ISSN: 10959572. DOI: 10.1016/j.neuroimage.2016.07.018.

Groth-Marnat, Gary (2012). *Neuropsychological Assessment in Clinical Practice: A Guide to Test Interpretation and Integration*. Vol. 159.

Hsieh, Sharpley et al. (2013). "Validation of the Addenbrooke's Cognitive Examination III in Frontotemporal Dementia and Alzheimer's Disease". In: *Dementia and Geriatric Cognitive Disorders* 36.3-4, pp. 242–250. ISSN: 14219824. DOI: 10.1159/000351671.

Huettel, Scott A., Allen W. Song, and Gregory McCarty (2008). *Functional Magnetc Resonance Imaging Textbook*. 2nd ed. Massachusetts, USA: Sinauer Associates, p. 559. ISBN: 9780878932863.

Jenkinson, Mark et al. (2012). "Review FSL". In: *NeuroImage* 62.2, pp. 782–790. ISSN: 10538119. DOI: 10.1016/j.neuroimage.2011.09.015. arXiv: NIHMS150003.

Jiménez-Balado, Joan et al. (2019). "Cognitive Impact of Cerebral Small Vessel Disease Changes in Patients with Hypertension". In: *Hypertension* 73.2, pp. 342–349. ISSN: 15244563. DOI: 10.1161/HYPERTENSIONAHA.118.12090.

Jouvent, Eric et al. (2007). "Brain atrophy is related to lacunar lesions and tissue microstructural changes in CADASIL". In: *Stroke* 38.6, pp. 1786–1790. ISSN: 00392499. DOI: 10.1161/STROKEAHA.106.478263.

Lambert, Christian et al. (2015). "Characterising the grey matter correlates of leukoaraiosis in cerebral small vessel disease". In: *NeuroImage: Clinical* 9, pp. 194–205. ISSN: 22131582. DOI: 10.1016/j.nicl.2015.07.002.

Le Heron, Campbell et al. (2018). "Dysfunctional effort-based decision-making underlies apathy in genetic cerebral small vessel disease". In: *Brain* 141.11, pp. 3193–3210. ISSN: 14602156. DOI: 10.1093/brain/awy257.

Logothetis, N. K. et al. (2001). "Neurophysiological investigation of the basis of the fMRI signal". In: *Nature* 412.6843, pp. 150–157. ISSN: 00280836. DOI: 10.1038/35084005.

Lohner, Valerie et al. (2017). "Apathy, but not depression, is associated with executive dysfunction in cerebral small vessel disease". In: *PLoS ONE* 12.5. Ed. by Josef Priller, e0176943. ISSN: 19326203. DOI: 10.1371/journal.pone.0176943.

Martinkovic, Lukas et al. (2014). "Modern techniques of epileptic focus localization". In: *International Review of Neurobiology*. 1st ed. Vol. 114. Elsevier Inc., pp. 245–278. ISBN: 9780124186934. DOI: 10.1016/B978-0-12-418693-4.00010-8.

Mascalchi, Mario et al. (2017). "Diffusion Tensor Imaging to Map Brain Microstructural Changes in CADASIL". In: *Journal of Neuroimaging* 27.1, pp. 85–91. ISSN: 15526569. DOI: 10.1111/jon.12374.

McAleese, Kirsty E. et al. (2016). "Post-mortem assessment in vascular dementia: Advances and aspirations". In: *BMC Medicine* 14.1, p. 129. ISSN: 17417015. DOI: 10.1186/s12916-016-0676-5.

Memarian, Negar et al. (2013). "Quantitative analysis of structural neuroimaging of mesial temporal lobe epilepsy". In: *Imaging in Medicine* 5.3, pp. 219–235. ISSN: 17555191. DOI: 10.2217/iim.13.28.

Molko, N. et al. (2001). "Diffusion tensor imaging study of subcortical gray matter in CADASIL". In: *Stroke* 32.9, pp. 2049–2054. ISSN: 00392499. DOI: 10.1161/hs0901.094255.

Moreton, Fiona C. et al. (2015). "Cerebral hyperperfusion on arterial spin labeling MRI during CADASIL migrainous encephalopathy". In: *Neurology* 85.24, pp. 2177–2179. ISSN: 1526632X. DOI: 10.1212/WNL.0000000000002214.

Moreton, Fiona C. et al. (2018). "Vasoreactivity in CADASIL: Comparison to structural MRI and neuropsychology". In: *Journal of Cerebral Blood Flow and Metabolism* 38.6, pp. 1085–1095. ISSN: 15597016. DOI: 10.1177/0271678X17710375.

Mori, Susumu and Jiangyang Zhang (2006). "Principles of Diffusion Tensor Imaging and Its Applications to Basic Neuroscience Research". In: *Neuron* 51.5, pp. 527–539. ISSN: 08966273. DOI: 10.1016/j.neuron.2006.08.012.

Nasreddine, Ziad S. et al. (2005). "The Montreal Cognitive Assessment, MoCA: A brief screening tool for mild cognitive impairment". In: *Journal of the American Geriatrics Society* 53.4, pp. 695–699. ISSN: 15325415. DOI: 10.1111/j.1532-5415.2005.53221.x.

Okell, Thomas W. et al. (2013). "Cerebral blood flow quantification using vessel-encoded arterial spin labeling". In: *Journal of Cerebral Blood Flow and Metabolism* 33.11, pp. 1716–1724. ISSN: 0271678X. DOI: 10.1038/jcbfm.2013.129.

Okell, Thomas W. et al. (2019). "Measurement of collateral perfusion in acute stroke: a vessel-encoded arterial spin labeling study". In: *Scientific Reports* 9.1, p. 8181. ISSN: 20452322. DOI: 10.1038/s41598-019-44417-7.

Opherk, Christian et al. (2004). "Long-term prognosis and causes of death in CADASIL: A retrospective study in 411 patients". In: *Brain* 127.11, pp. 2533–2539. ISSN: 00068950. DOI: 10.1093/brain/awh282.

Opherk, Christian et al. (2006). "Heritability of MRI lesion volume in CADASIL: Evidence for genetic modifiers". In: *Stroke* 37.11, pp. 2684–2689. ISSN: 00392499. DOI: 10.1161/01.STR.0000245084.35575.66.

Pantoni, Leonardo (2010). "Cerebral small vessel disease: from pathogenesis and clinical characteristics to therapeutic challenges". In: *The Lancet Neurology* 9.7, pp. 689–701. ISSN: 14744422. DOI: 10.1016/S1474-4422(10)70104-6.

Peters, N. et al. (2006). "Brain volume changes in CADASIL: A serial MRI study in pure subcortical ischemic vascular disease". In: *Neurology* 66.10, pp. 1517–1522. ISSN: 00283878. DOI: 10.1212/01.wnl.0000216271.96364.50.

Peters, Nils et al. (2005). "The pattern of cognitive performance in CADASIL: A monogenic condition leading to subcortical ischemic vascular dementia". In: *American Journal of Psychiatry* 162.11, pp. 2078–2085. ISSN: 0002953X. DOI: 10.1176/appi.ajp.162.11.2078.

Rossi Espagnet, Maria Camilla et al. (2012). "Grey matter volume alterations in CADASIL: A voxel-based morphometry study". In: *Journal of Headache and Pain* 13.3, pp. 231–238. ISSN: 11292377. DOI: 10.1007/s10194-012-0418-9.

Salmenpera, T. M. and John S. Duncan (2005). "Imaging in epilepsy". In: *Neurology in Practice* 76.3, pp. iii2–iii10. ISSN: 14737086. DOI: 10.1136/jnnp.2005.075135.

Schoemaker, Dorothee et al. (2019). "Clinical and research applications of magnetic resonance imaging in the study of CADASIL". In: *Neuroscience Letters* 698.January, pp. 173–179. ISSN: 18727972. DOI: 10.1016/j.neulet.2019.01.014.

Shen, Qian et al. (2011). "Volumetric and visual rating of magnetic resonance imaging scans in the diagnosis of amnestic mild cognitive impairment and Alzheimer's disease". In: *Alzheimer's and Dementia* 7.4, e101–e108. ISSN: 15525260. DOI: 10.1016/j.jalz.2010.07.002.

Smith, Stephen M. et al. (2004). "Advances in functional and structural MR image analysis and implementation as FSL". In: *NeuroImage* 23.SUPPL. 1, S208–S219. ISSN: 10538119. DOI: 10.1016/j.neuroimage.2004.07.051.

Smith, Tasha, Nadia Gildeh, and Clive Holmes (2007). "The Montreal cognitive assessment: Validity and utility in a memory clinic setting". In: *Canadian Journal of Psychiatry* 52.5, pp. 329–332. ISSN: 14970015. DOI: 10.1177/070674370705200508.

Sourbron, Steven P. and David L. Buckley (2013). "Classic models for dynamic contrast-enhanced MRI". In: *NMR in Biomedicine* 26.8, pp. 1004–1027. ISSN: 09523480. DOI: 10.1002/nbm.2940.

Stojanov, Dragan et al. (2015). "Imaging characteristics of cerebral autosomal dominant arteriopathy with subcortical infarcts and leucoencephalopathy (CADASIL)". In: *Bosnian Journal of Basic Medical Sciences* 14.3, pp. 1–8. ISSN: 18404812. DOI: 10.17305/bjbms.2015.247.

Su, Jingjing et al. (2019). "Altered Brain Glucose Metabolism Assessed by 18F-FDG PET Imaging Is Associated with the Cognitive Impairment of CADASIL". In: *Neuroscience* 417, pp. 35–44. ISSN: 18737544. DOI: 10.1016/j.neuroscience.2019.07.048.

Tatsch, Klaus et al. (2003). "Cortical hypometabolism and crossed cerebellar diaschisis suggest subcortically induced disconnection in CADASIL: An 18F-FDG PET study". In: *Journal of Nuclear Medicine* 44.6, pp. 862–869. ISSN: 01615505.

Tombaugh, Tom N. (2004). "Trail Making Test A and B: Normative data stratified by age and education". In: *Archives of Clinical Neuropsychology* 19.2, pp. 203–214. ISSN: 08876177. DOI: 10.1016/S0887-6177(03)00039-8.

Topp, Christian Winther et al. (2015). "The WHO-5 well-being index: A systematic review of the literature". In: *Psychotherapy and Psychosomatics* 84.3, pp. 167–176. ISSN: 14230348. DOI: 10.1159/000376585.

Tosto, Giuseppe et al. (2014). "Predicting aggressive decline in mild cognitive impairment: The importance of white matter hyperintensities". In: *JAMA Neurology* 71.7, pp. 872–877. ISSN: 21686149. DOI: 10.1001/jamaneurol.2014.667.

Tucha, Lara et al. (2012). "The Five-Point Test: Reliability, Validity and Normative Data for Children and Adults". In: *PLoS ONE* 7.9. Ed. by Gabriel Alejandro de Erausquin, e46080. ISSN: 19326203. DOI: 10.1371/journal.pone.0046080.

Tuominen, Susanna et al. (2004). "Positron emission tomography examination of cerebral blood flow and glucose metabolism in young CADASIL patients". In: *Stroke* 35.5, pp. 1063–1067. ISSN: 00392499. DOI: 10.1161/01.STR.0000124124.69842.2d.

Van Den Boom, Rivka et al. (2003). "Cerebral Autosomal Dominant Arteriopathy with Subcortical Infarcts and Leukoencephalopathy: MR Imaging Findings at Different Ages - 3rd-6th Decades". In: *Radiology* 229.3, pp. 683–690. ISSN: 00338419. DOI: 10.1148/radiol.2293021354.

Winkler, Anderson M. et al. (2010). "Cortical thickness or grey matter volume? The importance of selecting the phenotype for imaging genetics studies". In: *NeuroImage* 53.3, pp. 1135–1146. ISSN: 10538119. DOI: 10.1016/j.neuroimage.2009.12.028.

Winkler, Anderson M. et al. (2014). "Permutation inference for the general linear model". In: *NeuroImage* 92, pp. 381–397. ISSN: 10959572. DOI: 10.1016/j.neuroimage.2014.01.060.

Yoshita, Mitsuhiro, Evan Fletcher, and Charles DeCarli (2005). "Current concepts of analysis of cerebral white matter hyperintensities on magnetic resonance imaging". In: *Topics in Magnetic Resonance Imaging* 16.6, pp. 399–407. ISSN: 08993459. DOI: 10.1097/01.rmr.0000245456.98029.a8.